HHS Public Access

Author manuscript

Cell. Author manuscript; available in PMC 2023 July 07.

Published in final edited form as:

Cell. 2022 July 07; 185(14): 2523–2541.e30. doi:10.1016/j.cell.2022.05.024.

Generating human artery and vein cells from pluripotent stem cells highlights the arterial tropism of Nipah and Hendra viruses

Lay Teng Ang[1,11,*], **Alana T. Nguyen**[1,2,11], **Kevin J. Liu**[1,11], **Angela Chen**[1,2,12], **Xiaochen Xiong**[1,2,12], **Matthew Curtis**[7], **Renata M. Martin**[1,3], **Brian C. Raftry**[1,4,5], **Chun Yi Ng**[8,9], **Uwe Vogel**[10], **Angelika Lander**[10], **Benjamin J. Lesch**[1,3], **Jonas L. Fowler**[1,2], **Alyssa R. Holman**[1,2], **Timothy Chai**[1,2], **Siva Vijayakumar**[1,2], **Fabian P. Suchy**[1,6], **Toshinobu Nishimura**[1,6], **Joydeep Bhadury**[1,6], **Matthew H. Porteus**[1,3], **Hiromitsu Nakauchi**[1,6], **Christine Cheung**[8,9], **Steven C. George**[7], **Kristy Red-Horse**[1,4,5], **Joseph B. Prescott**[10,*], **Kyle M. Loh**[1,2,13,*]

[1]Stanford Institute for Stem Cell Biology & Regenerative Medicine, Stanford University, Stanford, CA 94305 USA

[2]Department of Developmental Biology, Stanford Cardiovascular Institute, Stanford University, Stanford, CA 94305 USA

[3]Department of Pediatrics, Stanford University, Stanford, CA 94305 USA

[4]Department of Biology, Stanford University, Stanford, CA 94305 USA

[5]Howard Hughes Medical Institute, Stanford University, Stanford, CA 94305 USA

[6]Department of Genetics, Stanford University, Stanford, CA 94305 USA

[7]Department of Biomedical Engineering, University of California-Davis, Davis, CA, USA 95616

[8]Lee Kong Chian School of Medicine, Nanyang Technological University, Singapore 308232

[9]Institute of Molecular and Cell Biology, A*STAR, Singapore 138673

[10]Center for Biological Threats and Special Pathogens, Robert Koch Institute, Berlin, Germany 13353

SUMMARY

[*]Correspondence: layteng@stanford.edu (L.T.A.); prescottj@rki.de (J.B.P.); kyleloh@stanford.edu (K.M.L.).

[11]Equal contribution

[12]Equal contribution

[13]Lead Contact

AUTHOR CONTRIBUTIONS

L.T.A., A.T.N., A.C., K.J.L., X.X., J.L.F., A.R.H. and K.M.L. differentiated hPSCs and, with M.C., B.C.R., C.Y.N., C.C., S.C.G and K.R.H., performed functional assays. L.T.A., K.J.L., X.X., J.L.F., S.V. and K.M.L. performed genomics analyses. R.M.M., B.J.L., M.H.P., F.P.S., T.N., J.B. and H.N. provided reagents. U.V., A.L. and J.B.P. performed BSL4 experiments. L.T.A., J.B.P. and K.M.L. supervised the study.

DECLARATION OF INTERESTS

K.M.L., L.T.A., A.C., A.T.N. and J.L.F. have filed patent applications related to endothelial differentiation.

Stem cell research endeavors to generate specific subtypes of classically-defined “cell-types”. Here we generate >90% pure human artery or vein endothelial cells from pluripotent stem cells within 3–4 days. We specified artery cells by inhibiting vein-specifying signals and *vice versa*. These cells modeled viral infection of human vasculature by Nipah and Hendra viruses, which are extraordinarily deadly (~57–59% fatality rate) and require biosafety-level-4 containment. Generating pure populations of artery and vein cells highlighted that Nipah and Hendra viruses preferentially infected arteries; arteries expressed higher levels of their viral-entry receptor. Virally-infected artery cells fused into syncytia containing up to 23 nuclei, which rapidly died. Despite infecting arteries and occupying ~6–17% of their transcriptome, Nipah and Hendra largely eluded innate-immune detection, minimally eliciting interferon signaling. We thus efficiently generate artery and vein cells, introduce stem-cell-based toolkits for biosafety-level-4 virology, and explore the arterial tropism and cellular effects of Nipah and Hendra viruses.

In Brief:

Pure populations of human artery and vein cells are rapidly generated from pluripotent stem cells. This provides a BSL4-compatible *in vitro* model to study how the deadly Nipah and Hendra viruses infect blood vessels.

Graphical Abstract

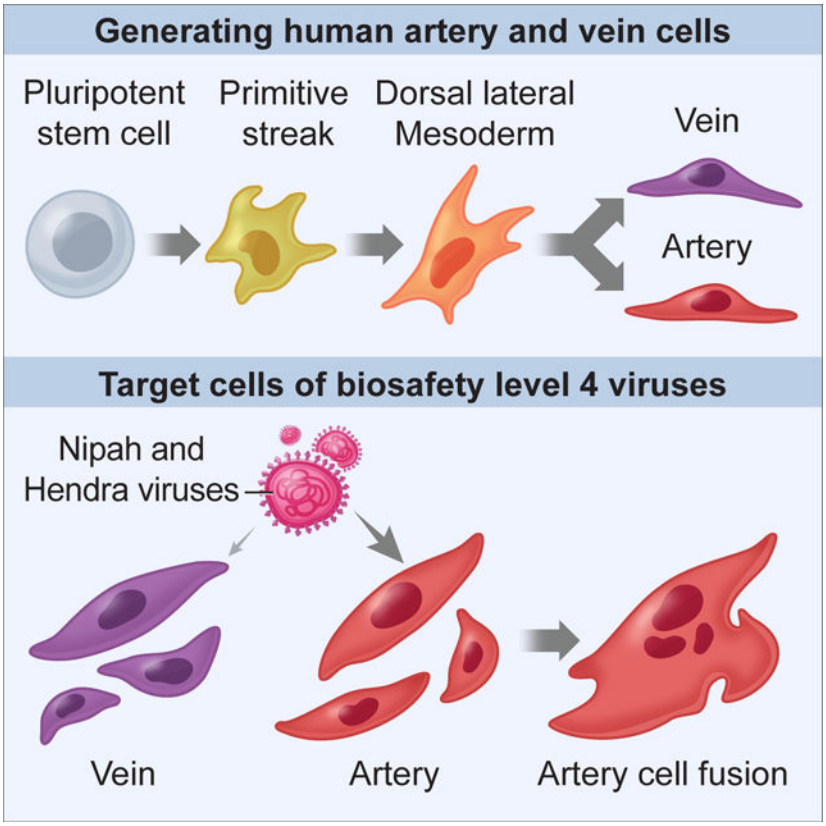

INTRODUCTION

Endothelial cells (ECs)—the innermost constituents of blood vessels—pervade all tissues and have manifold roles in health and disease. In health, they control entry and exit of bloodborne nutrients, wastes and immune cells to and from their client tissues (Augustin and Koh, 2017; Coultas et al., 2005; Potente and Mäkinen, 2017; Rafii et al., 2016). In disease, ECs contribute to atherosclerosis and other afflictions that account for over half of human deaths (Augustin and Koh, 2017; Carmeliet, 2005), including viral diseases of the vasculature.

Many Risk Group-4 viruses cause deadly vascular diseases, are among the most lethal human pathogens known, and require biosafety-level-4 (BSL4) containment (CDC and NIH, 2020). Here we focus on Nipah and Hendra viruses, which respectively cause outbreaks throughout Asia (~59% fatality rate) and Australia (~57% fatality rate), and are Risk Group-4 paramyxoviruses in the genus *Henipavirus* (Ang et al., 2018; Chua et al., 2000; Mahalingam et al., 2012; Murray et al., 1995). Individual Nipah virus outbreaks epidemiologically vary due to viral variants and other factors: the 1999 Malaysian and 2018 Indian outbreaks respectively exhibited fatality rates of ~40% and ~91% (Ang et al., 2018; Arunkumar et al., 2019). Of exigent concern, no treatments or vaccines for either Nipah or Hendra are presently approved for human use, and these diseases are thus classified Priority Diseases by the World Health Organization (Gomez Roman et al., 2021; Mehand et al., 2018). Nipah and Hendra viruses engender severe vascular disease (multiorgan vasculitis), which can culminate in respiratory and neurological failure (Baseler et al., 2015; Geisbert et al., 2010; Murray et al., 1995; Wong et al., 2002). To understand the enigmatic vascular diseases caused by Risk Group-4 viruses, we must precisely map their target cells and effects on such cells. This pursuit has been complicated by unique constraints of BSL4 experimentation and inadequate experimental systems.

A challenge in studying ECs is that they encompass multiple subtypes—including artery, vein, capillary and lymphatic ECs—which are molecularly distinct and subserve different physiological functions (De Val and Black, 2009; Fish and Wythe, 2015; Potente and Mäkinen, 2017). ECs are well known to be targets of Nipah and Hendra *in vitro* (Aljofan et al., 2009; Erbar et al., 2008; Lo et al., 2010; Mathieu et al., 2012; Monaghan et al., 2014; Schountz et al., 2019) and *in vivo* (Baseler et al., 2015; Geisbert et al., 2010; Murray et al., 1995; Wong et al., 2002). However, whether different EC subtypes harbor distinct functions in viral diseases remains enigmatic. Artery ECs express higher levels of *EFNB2* (Chong et al., 2011; Wang et al., 1998)—an entry receptor for Nipah and Hendra viruses (Bonaparte et al., 2005; Negrete et al., 2005)—leading to the hypothesis that these viruses might preferentially infect artery ECs. Nevertheless, both artery and vein ECs can reportedly be infected by Nipah and Hendra *in vitro* (Aljofan et al., 2009; Lo et al., 2010; Mathieu et al., 2012; Monaghan et al., 2014). Yet, an important proviso is that current systems to culture ECs do not preserve arteriovenous identity: primary ECs originally isolated from arteries or veins rapidly relinquish their arteriovenous subtype identity *in vitro* (Aranguren et al., 2013). This technical limitation has obscured viral tropism for, and their effects on, specific EC subtypes.

Generating well-defined populations of human artery vs. vein ECs *en masse* would empower us to explore viral infection of the vasculature, and in particular which EC subtype(s) are infected. Differentiation of human pluripotent stem cells (hPSCs, including embryonic and induced pluripotent stem cells) into specific cell-types (e.g., ECs) is rapidly advancing, yet generating pure populations of desired cellular *subtypes* (e.g., artery and vein ECs) remains quite challenging (Fowler et al., 2019). Starting from pluripotent cells, we must map the branching lineage choices through which they differentiate into cellular subtypes and the extracellular signals that control each step in their journey. Extant protocols often differentiate hPSCs towards mesoderm using BMP, FGF, TGFβ and/or WNT, and then bias differentiation towards ECs using VEGF and other signals. However, these signals are also permissive for the formation of other mesodermal lineages; consequently, a heterogeneous population containing a subset of ECs usually arises (e.g., Halaidych et al., 2018; Kurian et al., 2012; Lian et al., 2014; McCracken et al., 2019; Nguyen et al., 2016; Olmer et al., 2018; Paik et al., 2018; Patsch et al., 2015; Zhang et al., 2017). hPSC-derived ECs sometimes lack (reviewed by Lin et al., 2017) or coexpress (Halaidych et al., 2018; Olmer et al., 2018) arterial and venous markers. On the other hand, overexpression of pan-endothelial transcription factor (TF) *ETV2* efficiently differentiates hPSCs into ECs, but they are also apparently bereft of arterial or venous identity (Ng et al., 2020; Wang et al., 2020).

Inspired by our developmental understanding of how VEGF and NOTCH specify artery vs. vein subtypes of ECs *in vivo* (Coultas et al., 2005; De Val and Black, 2009; Fang and Hirschi, 2019; Fish and Wythe, 2015; Lin et al., 2007; Potente and Mäkinen, 2017), recent protocols manipulated these two signals to bias hPSC-derived ECs towards artery or vein identity with partial efficiency *in vitro* (Ditadi et al., 2015; Gage et al., 2020; Park et al., 2018; Rosa et al., 2019; Sriram et al., 2015; Zhang et al., 2017), which constituted an important step forward. However, the challenges in generating artery and vein ECs *in vitro* indicate gaps in our understanding of how these subtypes developmentally arise and intimate that additional signals for arteriovenous specification may exist.

Here we chart a developmental roadmap for the stepwise diversification of hPSCs into primitive streak, lateral mesoderm, and subsequently into artery and vein ECs. At each step of differentiation, we reveal the extracellular signals that need to be *activated*, and those that must be simultaneously *inhibited* to prevent emergence of undesired cell-types. We created >90% pure populations of either human artery or vein ECs within 3–4 days of hPSC differentiation. We then applied these well-defined artery and vein EC populations to BSL4 virology: Nipah and Hendra viruses preferentially targeted hPSC-derived artery ECs. More broadly, hPSC-derived cell-types will provide a powerful platform to explore the biology of, and countermeasures against, Risk Group-4 viruses under BSL4 containment.

RESULTS

Efficient differentiation of hPSCs into primitive streak and lateral mesoderm by repressing paraxial mesoderm and endoderm

Starting from hPSCs *in vitro*, we sought to emulate the stepwise *in vivo* development of pluripotent cells (corresponding to day 5.5 of mouse embryonic development [~E5.5]) into primitive streak (~E6.5), lateral mesoderm (~E7–7.5), and finally artery (~E8.25) and vein

ECs (~E9.0) (Fig. 1a) (Chong et al., 2011). First, activating BMP, FGF, TGFβ and WNT for 24 hours differentiated hPSCs into 97.3±0.3% pure MIXL1-GFP$^+$ mid primitive streak while suppressing ectoderm formation (Fig. 1b) (Loh et al., 2016).

Second, we further differentiated hPSC-derived day 1 mid primitive streak into day 2 lateral mesoderm, which contains endothelial progenitors *in vivo* (Ciau-Uitz et al., 2013). We induced lateral mesoderm markers *SCL*, *LMO2* and *FLI1* by *1*) activating BMP, VEGF and PKA, while *2*) simultaneously inhibiting WNT, TGFβ and PI3K to repress formation of unwanted paraxial mesoderm and endoderm (Loh et al., 2014; Loh et al., 2016) (Fig. 1c, Fig. S1a–e). We thus generate lateral mesoderm prior to generating ECs.

Efficient differentiation of hPSC-derived lateral mesoderm into artery ECs by repressing vein and heart fates

Subsequently, we identified the signals that controlled the further segregation of hPSC-derived day 2 lateral mesoderm into artery, vein or heart lineages (Fig. 2a). To differentiate lateral mesoderm towards ECs, we activated VEGF, while simultaneously inhibiting BMP and WNT, which respectively induced NKX2.5$^+$ heart precursors (Loh et al., 2016) and CDX2$^+$ non-ECs (Fig. S2a–c). Having inhibited formation of non-ECs, next we screened for signals that induce arterial marker SOX17 (Corada et al., 2013; Sakamoto et al., 2007) using *SOX17-mCherry* knock-in reporter hPSCs (Loh et al., 2014).

Additional signals (TGFβ and PI3K) controlled the bifurcation of day-2 lateral mesoderm into artery vs. vein fates: TGFβ specified arteries, whereas PI3K conversely induced veins (Fig. 2b, Fig. S2bii–iv). Consequently, we efficiently generated artery ECs by *1*) inducing arterial fate through TGFβ activation, while *2*) repressing vein formation by simultaneously inhibiting PI3K (Ditadi et al., 2015; Hong et al., 2006; Park et al., 2018). While previous protocols to putatively generate hPSC-derived artery ECs inhibited TGFβ (Zhang et al., 2017), we found that TGFβ inhibition in fact blocked artery specification and instead induced venous marker *NR2F2* (Fig. 2b, Fig. S2bii). This thus disclosed a temporally-dynamic role for TGFβ signaling in specifying arterial fate, changing every 24 hours across 3 days of hPSC differentiation. TGFβ had to be initially activated (inducing primitive streak, day 1), then inhibited (specifying lateral mesoderm, day 2) and later re-activated (to induce arterial fate, day 3) (Fig. 2c).

Taken together, activation of TGFβ (to specify arteries) and VEGF (to specify ECs) together with simultaneous blockade of BMP, WNT and PI3K for 24 hours differentiated day-2 lateral mesoderm into day-3 artery ECs, while inhibiting unwanted differentiation into either heart or vein lineages (Fig. S2d). This delineates a complex signaling code for arterial specification beyond activation of VEGF and NOTCH (reviewed by Coultas et al., 2005; Fang and Hirschi, 2019; Fish and Wythe, 2015). We generated SOX17$^+$ CD144$^+$ artery ECs within 3 days of hPSC differentiation (Fig. 2c), which were >90% pure, as assayed using newly-engineered *SOX17–2A-mPlum* reporter hPSCs (Fig. 2d) and *SOX17-mCherry* hPSCs (Fig. S2e). Artery differentiation was reproducible across 4 hESC and hiPSC lines, generating 97.9±2.4% pure CD144$^+$ DLL4$^+$ arterial ECs within 3 days, and was more efficient and rapid than 4 published differentiation protocols (Lian et al., 2014; Patsch et al., 2015; Sriram et al., 2015; Zhang et al., 2017) (Fig. 2e, Fig. S2f,g).

Identity and uniformity of hPSC-derived artery cells, and similarities with *in vivo* artery cells

scRNAseq reaffirmed the efficiency of artery differentiation. After 3 days of differentiation, 91.9% of the population formed a predominant artery EC cluster that expressed artery-specific (*SOX17*, *CXCR4* and *DLL4*) and pan-EC (*VE-CADHERIN*, *CD31* and *CD34*) markers (Fig. 2f), which was confirmed by qPCR (Fig. S2h,i). Nevertheless, individual artery ECs varied in their cell-cycle status, as shown by *MKI67* expression (Fig. 2f). ECs were artery-specific: they did not express venous marker *NR2F2* (Fig. 2f), consistent with our inhibition of vein-specifying signals (e.g., PI3K). This thus contrasts with past hPSC-derived ECs that co-expressed both arterial and venous markers (Olmer et al., 2018; Paik et al., 2018). However, 8.1% of cells were non-ECs that expressed mesenchymal markers (Fig. 2f). Taken together, activation of artery-inducing signals with simultaneous inhibition of vein-specifying signals efficiently generated hPSC-derived artery ECs, with scarce mesenchyme-like cells.

Attesting to their lineage fidelity, hPSC-derived artery ECs showed overall transcriptional similarity (R=0.74) with *in vivo* artery ECs within 4-week-old human fetuses (Zeng et al., 2019), and expressed comparable levels of pan-EC and arterial markers (Fig. 2g). This was promising, given that *in vivo* vs. *in vitro* cells were not precisely matched in their genetic background or developmental stage. Genes that were differentially expressed by artery ECs *in vivo* and *in vitro* largely related to metabolism and protein translation (Fig. S2j, Table S1), and as such, may reflect metabolic adaptation to cell culture. Additionally, *ESM1*—a VEGF-induced gene (Shin et al., 2008)—was higher *in vitro* (Fig. S2j), perhaps reflecting VEGF levels in the media. Overall, hPSC-derived artery ECs are transcriptionally similar, but are not identical, to fetal artery ECs.

Efficient differentiation of hPSC-derived lateral mesoderm into veins by repressing artery and heart fates

Having defined artery-specifying signals, next we asked what signals confer vein identity (Fig. 3a). Starting from day 2 hPSC-derived lateral mesoderm, we dually inhibited the artery-specifying signals TGFβ and NOTCH to block arterial differentiation (Fig. 3b). While NOTCH inhibition promotes venous fate (Ditadi et al., 2015; Duarte et al., 2004; Gage et al., 2020; Gale et al., 2004; Krebs et al., 2004; Lawson et al., 2001; Park et al., 2018), we found that NOTCH inhibition was not sufficient to efficiently induce vein ECs *in vitro*. We thus explored additional signals for vein specification.

We discovered that VEGF/ERK signaling had a temporally-dynamic role in vein EC specification *in vitro*: on day 3, it had to be *activated* to generate ECs, whereas on day 4, it had to be *inhibited* to generate vein ECs (Fig. 3c). ERK blockade on day 3 prevented EC specification (Fig. 3c). Yet, after cells acquired EC identity by day 3, subsequently inhibiting ERK on day 4 did not impair EC identity but rather was critical to instruct vein fate (Fig. 3c). Prolonged activation or inhibition of VEGF for 48 hours did not yield vein ECs, illustrating the importance of temporal VEGF/ERK modulation *in vitro* (Fig. 3c). Modulating VEGF/ERK signaling with such dynamism is also crucial for vein specification *in vivo* (Casie Chetty et al., 2017; Lawson et al., 2002; Shalaby et al., 1995), but was not

fully appreciated by earlier vein differentiation protocols (Ditadi et al., 2015; Gage et al., 2020; Park et al., 2018; Rosa et al., 2019; Sriram et al., 2015; Zhang et al., 2017). Taken together, manipulating VEGF/ERK and WNT in a temporally-dynamic way, along with inhibiting artery-specifying signals, differentiated hPSCs into vein ECs (Fig. 3a, Fig. S3a,b).

Through this approach, we could efficiently generate >88% pure NR2F2$^+$ CD144$^+$ vein ECs, as shown using newly-engineered *NR2F2–2A-GFP* knock-in reporter hPSCs (Martin et al., 2019) (Fig. 3d, Fig. S3c,d) and wild-type hPSCs (Fig. 3e, Fig. S3e). scRNAseq reaffirmed the efficiency of vein differentiation: 89.3% of cells formed a vein EC cluster that expressed vein (*NR2F2*, *FLRT2* and *APLNR*) and pan-EC (*VE-CADHERIN*, *CD31* and *CD34*) markers (Fig. 3f). ECs were vein-specific: they minimally expressed arterial markers (Fig. 3f), consistent with our inhibition of artery-specifying signals (e.g., NOTCH, TGFβ and VEGF/ERK). There was a small fraction (10.7%) of contaminating, mesenchyme-like non-ECs (Fig. 3f). Taken together, we efficiently generated hPSC-derived vein ECs, with a minority of mesenchyme-like cells. hPSC-derived vein ECs showed high overall transcriptional similarity with *in vivo* artery ECs within the 4-week-old CS13 human fetus (Zeng et al., 2019) (R = 0.83); both expressed venous markers (Fig. 3g, Fig. S3f). Genes that were differentially expressed by vein ECs *in vivo* and *in vitro* largely related to metabolism and protein translation and trafficking (Fig. S3g,h, Table S2). Taken together, hPSC-derived vein ECs are transcriptionally similar to fetal vein ECs, although they are not identical.

In summary, we generate enriched populations of either artery (Fig. 2) or vein ECs (Fig. 3) within 3 or 4 days of hPSC differentiation, respectively. We find that artery ECs arise earlier than vein ECs from hPSCs, mirroring how artery ECs (~E8.25) precede vein ECs (~E9.0) in mouse embryos (Chong et al., 2011).

Transcriptional and functional differences between hPSC-derived artery and vein cells

There were stark transcriptome-wide differences between hPSC-derived artery and vein ECs, including disparate expression of known arteriovenous subtype markers (Fig. 4a, Fig. S4a, Table S3). Certain EC attraction and repulsion signals showed arterial- or venous-biased expression, suggesting potential bidirectional signaling between these two EC subtypes to coordinate their spatial positions. First, hPSC-derived artery ECs expressed the chemokine *APELIN*, whereas vein ECs expressed its cognate receptor (*APLNR*; Fig. 4a, Fig. S4a), which is investigated below. *In vivo*, artery-secreted APELIN chemoattracts APLNR$^+$ veins, thus positioning arteries and veins in parallel (Kidoya et al., 2015). Second, hPSC-derived vein ECs expressed *FLRT2*, a repulsive ligand for the arterially-expressed netrin receptor *UNC5B* (Fig. 4a, Fig. S4a) (Lu et al., 2004; Tai-Nagara et al., 2017), potentially contributing to why arteries and veins do not intermix. However, hPSC-derived artery and vein ECs did not express markers of organ-specific ECs (Kalucka et al., 2020) (Fig. S4b): hence, they may correspond to the earliest ECs arising during development prior to their entry into various organs (Chong et al., 2011). An interactive browser to explore scRNAseq profiles of Hpsc-derived artery and vein ECs is available at https://anglab.shinyapps.io/arteryveinscrna/.

Importantly, both hPSC-derived artery and vein ECs executed hallmark EC functions. First, both EC subtypes formed 3-dimensional vascular networks *in vitro* when cocultured with

mesenchymal cells within fibrin hydrogels for 1 week (Fig. 4b, Fig. S4c,d) (Kurokawa et al., 2017). Second, artery and vein ECs likewise formed vascular networks *in vivo* upon subcutaneous transplantation into adult immunodeficient NOD-SCID *Il2rg*$^{-/-}$ mice for 1 month (Fig. 4c–e). Third, artery and vein ECs also incorporated LDL and acetylated LDL (Fig. 4f, Fig. S4e) and sealed a deliberate gap in monolayer cultures (Fig. S4f).

Nevertheless hPSC-derived artery and vein ECs functionally differed in various properties: *1*) responses to shear stress, *2*) sprouting ability, *3*) responses to inflammation, and *4*) migration towards chemokines, revealing differences between these two EC subtypes. First, upon 24 hours of exposure to fluid flow, both artery and vein ECs aligned themselves to the flow axis and upregulated flow-induced TF *KLF2* (Fig. 4g, Fig. S4g). However, shear stress preferentially upregulated *AQP1* and *CX37* in artery ECs (Fig. 4g, Fig. S4g), evincing different transcriptional responses to shear stress by these two EC subtypes. Second, vein (not artery) ECs coated on beads formed vascular sprouts that protruded into fibrin gels within 24 hours (Fig. 4h). This is consistent with the notion that vein ECs preferentially sprout *in vivo* (Red-Horse and Siekmann, 2019; Xu et al., 2014). Third, ECs respond to inflammation by upregulating adhesion molecules to recruit immune cells (e.g., Halaidych et al., 2018; Patsch et al., 2015; Zhang et al., 2017). Upon treatment with inflammatory cytokine TNFα for 4 hours, both artery and vein ECs upregulated the immune-cell adhesion molecule ICAM1 and physically adhered to monocyte-like cells (Fig. 4i,j). Nevertheless, artery and vein ECs partially differed in their responses to inflammation: immune-cell adhesion molecules VCAM1 and ESELECTIN were specifically upregulated in artery ECs (Fig. 4i, Fig. S4h). Fourth, we found that artery and vein ECs migrated towards different chemokines. Vein ECs preferentially migrated across a porous membrane towards the endothelial chemokine APELIN (Fig. 4k). This is consistent with how vein ECs express higher levels of *APLNR* (Fig. 4a, Fig. S4a), which is critical for vein migration *in vivo* (Kidoya et al., 2015). Collectively, hPSC-derived artery and vein ECs exhibited important transcriptional and functional differences, reifying that they have acquired distinct subtype identities.

Nipah and Hendra viruses preferentially induce multinucleated syncytia from artery cells

Next we applied hPSC-derived artery and vein ECs to study the tropism of Nipah and Hendra viruses, which must be handled under BSL4 containment (CDC and NIH, 2020). Thus hPSC-derived artery and vein ECs were cryopreserved, and then thawed and briefly cultured and expanded prior to viral infection under BSL4 containment. To expand vein ECs, it was critical to continuously inhibit the artery-specifying signals TGFβ and NOTCH (Fig. S5a,b). In these conditions, artery and vein ECs could be cultured for at least 6 days, while retaining their respective subtype identities and the ability to activate interferon signaling (Fig. S5a–d).

Upon infecting artery ECs, Nipah and Hendra viruses induced them to fuse into multinucleated syncytia, including prodigious syncytia harboring up to 23 nuclei per cell (Fig. 5a). Within 24 hours, Nipah virus extensively induced arterial syncytia (accounting for 44.5% of ECs), whereas vein ECs were minimally fused (1.3% of ECs; P=0.0013, Fig. 5b). Likewise, Hendra virus preferentially induced syncytia among artery ECs (P=0.0041, Fig.

5b). Nipah virus reduced artery EC numbers by 71.0% within 24 hours of infection; vein ECs were significantly less affected (P=0.0002, Fig. S5e).

By implementing live imaging in BSL4 containment, we confirmed that Nipah and Hendra viruses preferentially induced syncytia formation in artery ECs. Cocultures of GFP^+ and wild-type hPSC-derived ECs were infected and cell fusion was continuously quantified by live imaging (Fig. S5f,g; Movie S1). Nipah-infected artery ECs were progressively consumed into several massive syncytia over tens of hours and eventually eliminated (Fig. 5c). Again, Nipah and Hendra viruses preferentially induced cell fusion in artery ECs, as opposed to vein ECs (Fig. 5d). Cell fusion was rapid, occurring in minutes (Fig. 5d). Strikingly, after virally-induced cell fusion, nuclei subsequently aggregated together within syncytia, forming large clusters of nuclei (Fig. 5e, Movie S1) akin to a “bunch of grapes” (Fig. 5a). This contrasts with healthy syncytia (e.g., skeletal muscle), wherein nuclei are randomly distributed across the cell (Metzger et al., 2012). Taken together, Nipah and Hendra viruses preferentially induce artery ECs to fuse together, as opposed to vein ECs.

Nipah and Hendra viruses preferentially target artery cells in an EFNB2-dependent fashion

Consistent with how Nipah virus preferentially induced syncytia among artery ECs, Nipah-infected artery ECs produced 11.2-fold higher levels of Nipah viral RNA relative to vein ECs, as assayed by viral RNA levels in the culture media (P=0.01, Fig. 6a). Likewise, artery ECs produced 17.4-fold higher levels of Hendra viral RNA compared to vein ECs, (P=0.01, Fig. 6a). Intracellular viral RNA levels similarly disclosed an arterial tropism of these viruses, with the proviso that at later timepoints, Nipah RNA levels in artery ECs declined due to destruction of the cells (Fig. S6a).

Why do Nipah and Hendra viruses preferentially infect artery ECs, as opposed to vein ECs? EFNB2—a known receptor for these viruses (Bonaparte et al., 2005; Negrete et al., 2005)—is expressed more highly by artery ECs *in vivo*, in both mice (Chong et al., 2011; Wang et al., 1998) and humans (Fig. 6b) (Travaglini et al., 2020). hPSC-derived ECs faithfully reproduced this arteriovenous difference in *EFNB2* expression. hPSC-derived artery ECs expressed 8.8- and 10.4-fold higher levels of EFNB2 surface protein and mRNA, respectively, compared to vein ECs (Fig. 6c, Fig. S6b,c). By contrast, primary human artery and vein ECs expanded in conventional media relinquished arteriovenous differences (Aranguren et al., 2013): they expressed similar *EFNB2* levels (Fig. S6d). In sum, hPSC-derived cell-types afford advantages (e.g., preserved subtype identity) relative to previous cellular models used in BSL4 virology.

Preferential Nipah virus entry into artery ECs was principally driven by EFNB2. Genetically deleting *EFNB2* using Cas9 (Fig. S6e) (Martin et al., 2019) led to a substantial 430.3- to 6289.2-fold reduction of Nipah and Hendra virus replication in $EFNB2^{-/-}$ artery ECs, respectively (Fig. 6d). To precisely assay viral *entry*, we employed Nipah pseudoviruses, which enter cells but do not replicate or inflict virus-specific cellular derangements (Palomares et al., 2013). Indeed, Nipah pseudoviruses entered artery ECs 3.2±0.2 times more efficiently than vein ECs (Fig. 6e, Fig. S6f). Ablating *EFNB2* completely abrogated Nipah pseudovirus entry into artery ECs, but did not impair entry of an unrelated vesicular stomatitis virus (VSV)-based pseudovirus (Fig. 6e, Fig. S6g). Therefore EFNB2 is *necessary*

for Nipah and Hendra virus entry, complementing the longstanding findings that EFNB2 is *sufficient* for entry of these viruses (Bonaparte et al., 2005; Negrete et al., 2005).

In sum, the developmental bifurcation between artery vs. vein ECs is important for viral infection, as it culminates in differential expression of viral-entry receptors (i.e., EFNB2) between these two EC subtypes and thus differing susceptibility to Nipah and Hendra infection. Beyond EFNB2, artery and vein ECs also differ in the expression of other genes, which may contribute to preferential viral entry and replication efficiencies in artery ECs.

Nipah and Hendra viruses minimally alter gene expression in artery cells, largely eluding the antiviral program

Finally, we used RNA-seq to discover how artery ECs transcriptionally react to Nipah virus, Hendra virus or a related non-pathogenic paramyxovirus, Sendai virus (Cantell strain) (López et al., 2006). Cells were infected with a high viral titer (multiplicity of infection [MOI] ≈ 5), and RNA-seq was performed at 5, 10 or 15 hours post-infection (Fig. 7a, Table S4). All three paramyxoviruses exhibited the expected 3'-to-5' gene transcriptional gradient along their genomes (Fig. S7a,b), authenticating our RNA-seq analysis.

Between 5 and 15 hours post-infection, Nipah and Hendra virus RNA replicated extensively in artery ECs (114.5-fold and 93.2-fold increase, respectively), relative to Sendai virus, which achieved limited (2.9-fold) RNA replication (Fig. 7a). After 15 hours, Nipah occupied 17.2% of the transcriptome (~1 in 6 mRNAs encoding Nipah genes) and Hendra occupied 6.4% of the transcriptome (Fig. 7a). Therefore, Nipah and Hendra viruses replicate significantly more efficiently than the non-pathogenic Sendai virus in artery ECs.

Despite immense viral replication and cell fusion, Nipah and Hendra viruses led to surprisingly minimal host gene expression changes: they were remarkably effective at suppressing interferon production. Nipah virus massively replicated in artery ECs, yet it did not upregulate or downregulate a single gene across the entire transcriptome to a statistically significant extent, at 5–10 hours post-infection (Fig. 7b, Fig. S7c). Similar results were observed for Hendra virus (Fig. 7b, Fig. S7c). Even when Nipah and Hendra virus RNA achieved extremely high levels at later timepoints (6.4–17.2% of the transcriptome, at 15 hours post-infection), artery ECs minimally upregulated *IFNβ1*, *IFNλ1* and interferon target genes *IFIT2* and *IFIT3* (all less than 6-fold upregulation; Fig. 7c,d). Despite high viral loads, Nipah- or Hendra-infected artery ECs did not secrete the antiviral cytokine IFNβ to a statistically-significant degree at 12 or 24 hours post-infection (Fig. 7e). This starkly differed from Sendai virus, which induced a 100.8-fold elevation in IFNβ secretion within 24 hours (Fig. 7e). Despite low viral loads (<0.8% of the transcriptome), Sendai potently induced antiviral genes, including type I/III interferons (López et al., 2006) and interferon response genes that restrict viral replication (Shaw et al., 2017) (Fig. 7c,d). Additionally, Sendai-infected artery ECs elaborated immune cytokines, chemokines and immune-cell adhesion molecules known to recruit immune cells; these antiviral and inflammatory genes were minimally induced by Nipah or Hendra infection (Fig. 7c,d). Normalizing to viral loads, Nipah and Hendra viruses induced *IFNλ1* to a much lower extent (69.5-fold and 45.1-fold, respectively) than Sendai virus (Fig. 7d). Likewise, Nipah and Hendra viruses

upregulated interferon target gene *IFIT2* much less effectively (109.2-fold and 23.2-fold, respectively) than Sendai virus (Fig. 7d).

DISCUSSION

To precisely induce desired cellular subtypes, here we chart a stepwise roadmap for hPSC differentiation into artery vs. vein subtypes of ECs. We mapped the temporally-dynamic extracellular signals that drive or inhibit each step of differentiation. At the bifurcation between artery vs. vein subtypes, we precisely induced artery ECs by repressing vein-specifying signals and *vice versa*. This approach generated >90% pure populations of artery- vs. vein-specific ECs within 3–4 days of hPSC differentiation. The ability to efficiently and rapidly generate artery and vein ECs "on demand" should avail regenerative medicine, tissue engineering and modelling of human vascular diseases. Importantly, these hPSC-derived artery and vein ECs were distinguished by clear transcriptional and functional differences. Here we emphasize a pivotal distinction between artery and vein ECs: Nipah and Hendra viruses preferentially target artery ECs *in vitro*. In turn, this subtype-specific viral tropism emphasizes the importance of producing specific cellular subtypes *in vitro* and provides a vista on the target cells of deadly viruses.

A roadmap for human artery vs. vein development

First, we differentiated hPSCs into $MIXL1^+$ primitive streak and then SCL^+ $HAND1^+$ lateral mesoderm within 1 and 2 days, respectively. Subsequently, hPSC-derived lateral mesoderm bifurcated into >90% pure $SOX17^+$ artery ECs (day 3) or, alternatively, >90% pure $NR2F2^+$ vein ECs (day 4). Thus, artery ECs arise *prior* to vein ECs *in vitro*, consistent with *in vivo* findings (Chong et al., 2011)—these two cellular subtypes do not arise synchronously.

Inducing cellular subtypes: blocking the formation of alternative subtypes

As opposed to generating "generic" cell-types of ambiguous subtype identity, we hypothesized it should be possible to produce desired cellular subtypes by explicitly *inhibiting* the signals that induce the opposing cellular subtype. At the bifurcation between artery and vein subtypes, TGFβ and NOTCH specify artery fate, whereas PI3K instructs vein identity. We induced artery ECs through a two-pronged approach: *activating* artery-inducing signal TGFβ, while *repressing* vein-specifying signal PI3K. The converse signals —TGFβ and NOTCH inhibition (together with PI3K activation)—instead induced vein ECs. This signaling logic enabled the exclusive generation of either artery or vein ECs in the absence of the opposing lineage, as quantified by scRNAseq and other means. Our findings thus reveal a more complex signaling code for artery vs. vein specification, extending beyond the current manipulation of VEGF and/or NOTCH (reviewed by Coultas et al., 2005; Fang and Hirschi, 2019; Fish and Wythe, 2015) to bias hPSCs towards arterial or venous fates (Ditadi et al., 2015; Gage et al., 2020; Park et al., 2018; Rosa et al., 2019; Sriram et al., 2015; Zhang et al., 2017). Explicitly *inhibiting* the signals that specify alternate subtype identities may be a general approach to precisely engineer desired cellular subtypes from stem cells.

Inducing cellular subtypes: temporally-dynamic signaling

hPSCs swiftly traverse alternating lineage paths every 24 hours and consequently, extracellular signals must be rapidly activated or inhibited to precisely guide differentiation down desired paths in preference to unwanted ones. Indeed, in the mouse embryo, cells rapidly segue between different states every 12–24 hours: E5.5 pluripotent cells → E6.5 primitive streak → ~E7-E7.5 lateral mesoderm → ~E8.25 artery ECs and ~E9.0 vein ECs (Chong et al., 2011). We found the same extracellular signal specified 3 different cell-types over the course of 3 days. For instance, TGFβ initially *induced* mid primitive streak on day 1; then *repressed* lateral mesoderm on day 2; and finally *induced* arterial ECs on day 3. By contrast, VEGF *induced* lateral mesoderm on day 2, and then *induced* and eventually *inhibited* vein ECs on days 3 and 4, respectively. Temporally-dynamic activation and repression of extracellular signals was required to efficiently transition cells from one state to the next, with two consecutive cell-types sometimes sharing diametrically opposed requirements for the same signal (e.g., VEGF) *in vitro*, consistent with VEGF's temporally-dynamic role *in vivo* (Casie Chetty et al., 2017; Lawson et al., 2002; Shalaby et al., 1995). Consequently, prolonged activation or inhibition of a given signal generates a heterogeneous cell population. The previously-overlooked requirement for temporally-dynamic TGFβ and VEGF signals likely complicated past efforts to generate artery and vein ECs from hPSCs. It is therefore critical to map the temporal dynamics with which these signals operate, and to manipulate them with equal dynamism to precisely effect differentiation.

Artery ECs are target cells of Nipah and Hendra viruses

By virtue of their high fatality rates and a general dearth of approved treatments, Risk Group-4 viruses imperil global health: mapping their human target cells and their effects on such cells is crucial. Arteries and veins have largely been regarded synonymously in viral diseases. However, we found Nipah and Hendra viruses preferentially targeted artery ECs and fused them into multinucleated arterial ECs *in vitro*. This is consonant with a past study of Syrian hamsters, which suggested that Nipah primarily infected arteries *in vivo*, as morphologically inferred by elastic membrane staining (Baseler et al., 2015). Hence, as opposed to promiscuously targeting all ECs, we demonstrate that certain viruses may preferentially target specific endothelial subtypes. Mechanistically, this arterial tropism was driven at least in part by higher expression of viral-entry receptor *EFNB2* (Bonaparte et al., 2005; Negrete et al., 2005) in artery ECs, which we demonstrated was required for viral entry, as shown by genetic deletion. The developmental diversification of artery vs. vein ECs may thus hold hitherto-unappreciated significance in viral diseases.

Past studies infected various ECs sourced from a range of species and organs with Nipah and Hendra viruses *in vitro* (Aljofan et al., 2009; Erbar et al., 2008; Lo et al., 2010; Mathieu et al., 2012; Monaghan et al., 2014; Schountz et al., 2019). However, these ECs were cultured in conditions wherein arteriovenous subtype identity was lost (Aranguren et al., 2013), often unbeknownst to researchers. This thus accentuates the importance of being able to generate and maintain well-defined populations of hPSC-derived artery and vein ECs *in vitro* to study whether viruses preferentially target specific EC subtypes and exert subtype-specific effects.

Having identified artery ECs as preferential target cells of Nipah and Hendra viruses, we systematically detailed the effects of these viruses on artery ECs using live-imaging and RNA-seq. One of the greatest surprises was that Nipah and Hendra viruses inflicted surprisingly minor transcriptional effects on artery ECs, despite extensive viral replication and prodigious cell fusion. Indeed, both viruses were “stealthy” to the innate immune system of artery ECs. Despite occupying an impressive fraction (6.4–17.2%) of an artery cell’s transcriptome, both Nipah and Hendra viruses minimally induced interferon signaling or antiviral genes. This minimal interferon response correlated with the ability of these lethal viruses to massively replicate and achieve high viral loads, in stark contrast with the non-pathogenic Sendai virus. Indeed, Nipah virus P, V and W proteins are known to silence interferon production and signaling (Childs et al., 2007; Ciancanelli et al., 2009; Rodriguez et al., 2002). Past studies reached diverging conclusions regarding whether Nipah virus activates (Elvert et al., 2020; Lo et al., 2010; Mathieu et al., 2012), or fails to elicit (Schountz et al., 2019; Virtue et al., 2011), interferon signaling *in vitro*. Here, we re-investigate this question using well-defined populations of artery and vein ECs. Additionally, we quantify the extent of interferon suppression *relative* to respective viral RNA loads, using RNA-seq. Our work also illuminates the cellular effects of Hendra virus, which hitherto were generally understudied compared to, and assumed to be similar to, Nipah virus.

A platform to study Risk Group 4 viruses using hPSC-derived cell-types

More broadly, we introduce hPSC-derived cell-types as enhanced model systems to study the target cells and cellular effects of Risk Group-4 viruses. Due to BSL4 experimental constraints, *in vitro* studies of Risk Group-4 viruses have hitherto exploited cancer cells (which poorly reflect native physiology) or primary cells (which are difficult to expand long-term and to genetically edit, and often relinquish features of their *in vivo* counterparts), neither of which may harbor clear subtype identities (e.g., arteriovenous identity). hPSC-derived cell-types can be rapidly generated in large numbers, are genetically manipulatable, and retain certain properties of their *in vivo* counterparts (e.g., subtype identity) (Drubin and Hyman, 2017). These decisive advantages of hPSC-derived cell-types have already been exploited to provide new insights into Risk Group 2 and 3 viruses (Harschnitz and Studer, 2021; Simoneau and Ott, 2020). Indeed, hPSC-derived ECs exemplify many of these advantages: they exhibit arteriovenous differences in *EFNB2* expression (which are otherwise obscured in primary ECs cultured in conventional conditions) and are genetically tractable (as evinced by our genetic deletion of *EFNB2* to confirm its role in viral entry).

Beyond Nipah and Hendra viruses, hPSC-derived artery and vein ECs could provide a powerful platform to delineate the target cells and cellular effects of additional Risk Group-4 viruses—including arenaviruses, filoviruses, flaviviruses and nairoviruses—that cause lethal and enigmatic vascular diseases. Eventually hPSC-derived cell-types could enable therapeutic and genetic screens to discover countermeasures against currently-incurable Risk Group-4 viruses, using cell-types that are more physiologically relevant than the cancer cells often used in BSL4 experiments.

Limitations of the study

The endothelial roadmap described here remains incomplete: it focuses on artery and vein ECs, but does not encompass generation of capillaries, lymphatics or organ-specific ECs (Augustin and Koh, 2017; Nguyen et al., 2021; Potente and Mäkinen, 2017). Creating an increasingly diverse array of ECs *in vitro* will, in turn, avail virology. Nipah and Hendra viruses infect ECs across multiple organs *in vivo* (Baseler et al., 2015; Geisbert et al., 2010; Murray et al., 1995; Wong et al., 2002), but how organ-specific ECs respond to these viruses remains a mystery. Finally, while we find Nipah and Hendra viruses preferentially target human artery ECs *in vitro*, *in vivo* verification is of paramount import. In this regard, it is critical to appreciate that cells *in vivo* and *in vitro* are not equivalent (Fowler et al., 2019): hPSC-derived artery and vein ECs are transcriptionally similar, but are not identical to, their respective *in vivo* counterparts. Going forward, we envision that hPSC-derived cell-types will provide a powerful *in vitro* platform to explore the tropism and biology of Risk Group-4 viruses, generating hypotheses that can then be tested in *de rigueur* animal models *in vivo*.

STAR METHODS

RESOURCE AVAILABILITY

Lead Contact—Requests for further information should be directed to and will be fulfilled by the Lead Contact, Kyle M. Loh (kyleloh@stanford.edu).

Materials Availability—Multiple human pluripotent stem cell lines were developed as part of this study: H1 *NR2F2–2A-GFP* hESCs, H1 *SOX17–2A-mPlum* hESCs, H1 *EFNB2*$^{-/-}$ hESCs, SUN004.1.9 *CAG-eGFP* hiPSCs, SUN004.2 *CAG-mScarlet* hiPSCs, and SUN003.1 *CAG-AkaLuciferase-tdTomato* hiPSCs. All cell lines will be made freely available upon request and the completion of applicable Material Transfer Agreements.

Data and Code Availability—Bulk-population RNA-seq and single-cell RNA-seq datasets generated as part of this study are available at the NCBI Sequence Read Archive, accession number PRJNA837932. Single-cell RNAseq datasets of hPSC-derived artery and vein ECs that were generated as part of this study can be interactively browsed at a custom web portal: https://anglab.shinyapps.io/arteryveinscrna/. Computational scripts used for genomics analyses conducted as part of this study are available at Github: https://github.com/LayTengAngLab/ArteryVeinEndothelial.

EXPERIMENTAL MODEL AND SUBJECT DETAILS

Cell culture—All cells in this study were cultured in standard incubator conditions (20% O_2, 5% CO_2 and 37 °C).

Human pluripotent stem cell lines—The following human pluripotent stem cell (hPSC) lines were used in this study: wild-type H1, H7 and H9 hESCs (WiCell); H9 *SOX17-mCherry* knock-in reporter hESCs (Loh et al., 2014); H1 *NR2F2–2A-GFP* knock-in reporter hESCs (generated in this study); H1 *SOX17–2A-mPlum* knock-in reporter hESCs (generated in this study); SUN004.1.9 hiPSCs carrying a constitutively-expressed *CAG-GFP* PiggyBac transgene (generated in this study); SUN004.2 hiPSCs carrying

a constitutively-expressed *CAG-mScarlet* lentiviral transgene (generated in this study); and SUN003.1 hiPSCs carrying a constitutively-expressed *CAG-AkaLuciferase-tdTomato* lentiviral transgene (generated in this study). SUN004.1.9, SUN004.2 and SUN003.1 hiPSCs represent three clonal hiPSC lines originally obtained from two different individuals (SUN003 and SUN004). H1, SUN004.1.9, SUN004.2 and SUN003.1 hPSCs are of a XY genotype, whereas H7 and H9 hPSCs are of a XX genotype.

Undifferentiated hPSCs were propagated in mTeSR1 medium (StemCell Technologies) + 1% penicillin/streptomycin (Thermo Fisher) or alternatively, mTeSR Plus medium (StemCell Technologies) + 1% penicillin/streptomycin in monolayer cultures, on Geltrex basement membrane matrix-coated plates (described below). For mTeSR1, media was changed daily and for mTeSR Plus, media was changed every other day as per the manufacturer's recommendations. For the sake of brevity, we refer to mTeSR1 and mTeSR Plus interchangeably as "mTeSR" for the remainder of these Methods. In order to maintain cultures of undifferentiated hPSCs, when they became partially confluent, undifferentiated hPSCs were passaged by treating them for 7 minutes with EDTA (Versene, Thermo Fisher) at room temperature. Subsequently, EDTA was removed, mTeSR was added, and then hPSCs were manually scraped off the plate to generate clumps. hPSC clumps were then seeded onto new plates that had been precoated with Geltrex basement membrane matrix (described below) in mTeSR medium + 1% penicillin/streptomycin. To reiterate, during EDTA-based maintenance passaging of undifferentiated hPSCs as clumps, ROCK inhibitor was not added.

Human pluripotent stem cell-derived endothelial cells—After differentiation of hPSCs into artery cells (within 3 days, as described below) or vein cells (within 4 days, as described below), the resultant hPSC-derived artery and vein cells could be expanded for up to 6 additional days. Day 3 hPSC-derived artery cells were expanded in EGM2 (Endothelial Cell Growth Medium 2, Lonza CC-3162), which was refreshed every 24 hours. Day 4 hPSC-derived vein cells were expanded in EGM2 + SB505124 (2 μM) + RO4929097 (2 μM), which was refreshed every 24 hours. Expansion of hPSC-derived artery and vein cells was performed in monolayer cultures on Geltrex-coated cell culture plates. Expanded hPSC-derived artery and vein cells were used for certain functional assays as well as viral infection experiments. The biological sex of hPSC-derived artery and vein cells corresponds to the biological sex of the parental hPSC line used to generate them.

Human umbilical artery and vein endothelial cells—Human umbilical artery endothelial cells (HUAEC, Sigma-Aldrich, 202–05N) and human umbilical vein endothelial cells (HUVEC, Sigma-Aldrich, 200–05N) were both propagated on Geltrex-coated plates in EGM2 (Lonza CC-3162) media, which was refreshed every 1–2 days. The biological sex of these primary human endothelial cells was not determined.

Human lung fibroblast cells—Primary human adult lung fibroblasts (normal human lung fibroblasts [NHLF], Lonza, CC-2512) were propagated in Fibroblast Growth Medium-2 (Lonza, CC-3132), with media changes every 2–3 days. Once confluent, fibroblasts were washed twice with DPBS without ions (Thermo Fisher, 14190144) and exposed to 0.05% Trypsin-EDTA (Thermo Fisher, 25300062) for 2 min. Trypsin was

neutralized using fresh FGM2, and the cell solution was centrifuged at 300g in order to pellet cells for additional culture or experiments. Human fibroblasts were cocultured with endothelial cells to generate 3-dimensional vascular networks (described below). For all relevant experiments, fibroblasts between passages 3–7 were used. Where indicated, NHLFs obtained from different donors were used in experiments. The biological sex of these primary human lung fibroblasts was not determined.

THP1 cells—THP1 cells (ATCC, TIB-202) were propagated in RPMI-1640 + 10% fetal bovine serum (FBS) in suspension cultures, and were passaged every 2–3 days by adding fresh media and diluting their concentration to 3×10^5 cells/mL. THP1 cells were used to assess the ability of immune cells to adhere to endothelial cells (described below). THP1 cells represent a transformed human monocyte-like cell line of a XY genotype.

HEK293T/17 cells—HEK293T/17 cells (ATCC, CRL-11268) were propagated in DMEM + 10% fetal bovine serum (FBS) and were passaged every 3–4 days at a 1:10 ratio through trypsinization. HEK293 cells were used to package pseudotyped lentivirus particles (described below). HEK293T/17 cells represent a transformed human cell line that is an easily-transfected derivative of the parental HEK293T line, and are of a XX genotype.

Vero E6 cells—Vero C1008 (Vero 76, clone E6, Vero E6) cells (European Collection of Authenticated Cell Cultures (ECACC), 85020206) were propagated in DMEM containing 2% FBS, 2 mM glutamine, and 1% penicillin/streptomycin and passaged at a 1:10 ratio through trypsinization. Vero E6 cells were used to propagate Nipah and Hendra viruses in order to generate viral stocks and to quantitatively titrate infectious virus from the supernatant of virally-infected cell cultures (described below). Vero E6 cells represent a transformed African green monkey (*Chlorocebus sabaeus*) cell line of a XX genotype.

Mouse models—Immunodeficient NOD-SCID *Il2rg*$^{-/-}$ (NSG) mice, obtained from The Jackson Laboratory, were housed in the Lokey Stem Cell Research Building's Barrier Mouse Facility. Adult NSG mice were transplanted with hPSC-derived artery and vein ECs (described below). NSG mice were 2–4 months old and both male and female mice were used.

Nipah virus, Malaysia variant—Nipah virus, Malaysia variant (Nipah virus/human/MY/1999/CDC; genomic sequence reported in NCBI accession number NC_002728) was originally isolated by the CDC from the cerebrum of an infected human in Malaysia in 1999, and was passaged on Vero E6 cells (Harcourt et al., 2000). We previously demonstrated the ability of Nipah virus, Malaysia variant to cause fatal disease in African green monkeys (Prescott et al., 2015) and Syrian hamsters (DeBuysscher et al., 2013), thus verifying its pathogenicity. Nipah virus is a member of the species *Nipah henipavirus*; genus *Henipavirus*; family *Paramyxoviridae*; order *Mononegavirales*. Nipah virus, Malaysia variant was obtained from CDC Viral Special Pathogens Branch reference stocks.

Hendra virus, Brisbane variant—Hendra virus, Brisbane variant (Hendra virus/horse/AU/1994/Hendra; genomic sequence reported in NCBI accession number NC_001906) was originally isolated from an infected horse in Hendra, a suburb of Brisbane,

Australia, in 1994 (Murray et al., 1995). Hendra virus is a member of the species *Hendra henipavirus*; genus *Henipavirus*; family *Paramyxoviridae*; order *Mononegavirales*. Hendra virus, Brisbane variant was obtained from CDC Viral Special Pathogens Branch reference stocks.

Sendai virus, Cantell strain—The original provenance of Sendai virus, Cantell strain is unknown, but it was passaged over 100 times in chicken embryonated eggs at the Central Public Health Laboratory in Helsinki, Finland (Cantell and Hirvonen, 1981). Sendai virus, Cantell strain is known to induce interferon-β signaling *in vivo* and *in vitro*: it does not cause severe disease in mice, nor is it presently known to cause human disease (López et al., 2006; Yoshida et al., 2018). Sendai virus is a member of the species *Murine respirovirus*; genus *Respirovirus*; family *Paramyxoviridae*; order *Mononegavirales*. Sendai virus, Cantell strain was obtained from ATCC (VR-907).

METHOD DETAILS

Data visualization—Standard plots were prepared with Microsoft Excel, Microsoft PowerPoint or GraphPad Prism. Heatmaps were constructed in Heatmapper (Babicki et al., 2016) or, alternatively, the HeatMapViewer function of the online GenePattern platform (Reich et al., 2006). Flow cytometry data were visualized with FlowJo. Other types of data visualization were prepared as described in the respective sections below.

Basement membrane matrices—hPSCs were maintained and differentiated on cell culture plates that been pre-coated with either Geltrex or vitronectin basement membrane matrices. Geltrex (Thermo Fisher) was diluted 1:100–1:200 in DMEM/F12 (Thermo Fisher) and was used to coat tissue culture plastics for at least 1 hour at 37 °C. Recombinant human truncated vitronectin (Gibco, A14700; “VTN-N”) was diluted to a 10 μg/mL stock in PBS (lacking Ca^{2+} or Mg^{2+}) and was used to coat tissue culture plastics for at least 1 hour at 37 °C. After coating with either Geltrex or vitronectin, the basement membrane solution was aspirated, leaving behind a thin film; subsequently, cells were plated on the Geltrex- or vitronectin-coated cell culture plastics.

Preparing CDM2 basal media—hPSCs were differentiated into artery and vein cells as described below in Chemically Defined Medium 2 (CDM2). The composition of CDM2 has been described previously (Loh et al., 2014; Loh et al., 2016): 50% IMDM + GlutaMAX (Thermo Fisher, 31980–097) + 50% F12 + GlutaMAX (Thermo Fisher, 31765–092) + 1 mg/mL polyvinyl alcohol (Sigma, P8136–250G) + 1% v/v chemically defined lipid concentrate (Thermo Fisher, 11905–031) + 450 μM 1-thioglycerol (Sigma, M6145–100ML) + 0.7 μg/mL recombinant human insulin (Sigma, 11376497001) + 15 μg/mL human transferrin (Sigma, 10652202001) + 1% v/v penicillin/streptomycin (Thermo Fisher, 15070–063). Polyvinyl alcohol was brought into suspension by gentle warming and magnetic stirring, and the media was sterilely filtered (through a 0.22 μm filter) prior to use.

hPSC differentiation into artery and vein cells

- Seeding hPSCs for differentiation (Step 0). In contrast to passaging hPSCs for maintenance, a different passaging procedure was used to plate hPSCs for

differentiation; notably, sparse seeding of hPSCs as single cells is paramount for efficient differentiation. To seed hPSCs for differentiation, undifferentiated hPSCs were dissociated into single cells (Accutase, Thermo Fisher) and plated into recipient wells in mTeSR supplemented with thiazovivin (1 μM, Tocris; a ROCK inhibitor, to enhance hPSC survival after passaging) onto plates precoated with either Geltrex basement membrane matrix or recombinant Vitronectin (described above), thus plating 25,000–50,000 hPSCs/cm^2 (i.e., ~95,000–190,000 hPSCs/well of a 12-well plate). Freshly-seeded hPSCs were allowed to adhere and recover for 24 hours in mTeSR + 1 μM thiazovivin prior to initiating differentiation, during which the hPSCs re-formed small clumps. All subsequent differentiation steps were performed in defined, serum-free CDM2 basal media (Loh et al., 2014; Loh et al., 2016). To reiterate, hPSCs are maintained by passaging as clumps (to maintain normal karyotype) but are seeded for differentiation as single cells (to enable efficient differentiation).

- Day 1 (mid primitive streak induction, 24 hours [Step 1]). Day 0 hPSCs were briefly washed (DMEM/F12, Thermo Fisher) to remove all traces of mTeSR + thiazovivin. Then, they were differentiated towards mid primitive streak in CDM2 media supplemented with Activin A (30 ng/mL, R&D Systems), BMP4 (40 ng/mL, R&D Systems), CHIR99021 (6 μM, Tocris), FGF2 (20 ng/mL, Thermo Fisher) for 24 hours, as previously described (Loh et al., 2016) (with the optional addition of PIK90 (100 nM, Calbiochem)).
- Day 2 (lateral mesoderm induction, 24 hours [Step 2]). Day 1 mid primitive streak cells were briefly washed (DMEM/F12) and then differentiated towards lateral mesoderm in CDM2 media supplemented with BMP4 (40 ng/mL), GDC-0941 (2.5 μM, Cellagen Technology), Forskolin (10 μM, Tocris), SB-505124 (2 μM, Tocris), VEGF (100 ng/mL, R&D Systems), XAV939 (1 μM, Tocris) and ascorbic acid-2-phosphate (AA2P; 200 μg/mL, Sigma) for 24 hours. Subsequently, lateral mesoderm was used for artery induction (Step 3a; below) or vein induction (Step 3b; below).
- Day 3 (artery induction, 24 hours [Step 3a]). Day 2 lateral mesoderm cells were briefly washed (DMEM/F12) and then differentiated towards artery ECs in CDM2 media supplemented with Activin A (15 ng/mL), DMH1 (250 nM, Tocris), GDC-0941 (2.5 μM), VEGF (100 ng/mL), XAV939 (1 μM) and AA2P (200 μg/mL) for 24 hours, thereby yielding day 3 artery ECs.
- Days 3–4 (vein induction, 24 hours [Step 3b]). Day 2 lateral mesoderm cells were briefly washed (DMEM/F12) and then differentiated in CDM2 media supplemented with SB505124 (2 μM), DMH1 (250 nM), RO4929097 (2 μM, Cellagen Technology), VEGF (100 ng/mL), XAV939 (1 μM) and AA2P (200 μg/mL) for 24 hours. Subsequently, day 3 cells were briefly washed (DMEM/F12) and then differentiated in CDM2 media supplemented with SB505124 (2 μM), RO4929097 (2 μM), PD0325901 (500 nM, Tocris), CHIR99021 (1 μM) and AA2P (200 μg/mL) for 24 hours, thereby yielding day 4 vein ECs.

In most experiments, hPSCs were plated and then differentiated into artery and vein ECs using the aforementioned media with respective media changes every 24 hours (without dissociating and replating cells at intermediate timepoints). However, we subsequently found that the efficiency of vein EC differentiation was enhanced when, at the end of day 2 of differentiation, lateral mesoderm cells were dissociated and re-plated at high density (~79,000 cells/cm^2, i.e., 300,000–400,000 cells/well of a 12-well plate) in day-3 vein induction media (Fig. S3b). No ROCK inhibitor was used when replating lateral mesoderm cells. After 24 hours, day-3 cells were then differentiated into vein ECs using the aforementioned day-4 vein induction media without any additional resplitting.

Maintenance of hPSC-derived artery and vein cells—After hPSC differentiation into artery cells (within 3 days) or vein cells (within 4 days) as described above, they could be maintained for at least 6 additional days *in vitro* on Geltrex-coated cell culture plates. Day 3 hPSC-derived artery cells were expanded in EGM2 (Endothelial Cell Growth Medium 2, Lonza CC-3162), which was refreshed every 24 hours. Day 4 hPSC-derived vein cells were expanded in EGM2 + SB505124 (2 μM) + RO4929097 (2 μM), which was refreshed every 24 hours.

Cryopreservation and thawing of hPSC-derived artery and vein cells—After hPSC differentiation into artery cells (within 3 days) or vein cells (within 4 days) as described above, they were dissociated using either Accutase (Thermo Fisher) or TrypLE Express (Thermo Fisher). hPSC-derived artery cells were of sufficient purity to be frozen directly, whereas in certain experiments, hPSC-derived vein cells were first magnetically enriched for $CD34^+$ cells using CD34 microbead-based Magnetically Activated Cell Sorting (MACS, Miltenyi Biotec 130–046-703) prior to freezing. MACS was performed generally as per the manufacturer's recommendations, with slight modifications: after dissociation, hPSC-derived vein cells were counted using a hemocytometer, and then resuspended in FACS buffer (PBS + BSA + EDTA) with a 6- to 7-fold excess of CD34 microbeads and Fc blocking reagent (Miltenyi Biotec 130–046-703) compared to the manufacturer's recommendation. Vein cells were stained on ice for 30 minutes with CD34 microbeads and Fc blocking reagent, washed, and then magnetically bound to a MACS LS column (Miltenyi Biotech 130–042-401). Unbound cells were then magnetically bound to a second MACS LS column to recover any residual $CD34^+$ cells that were not captured in the first enrichment. Subsequently, $CD34^+$ vein cells were collected, pelleted, and frozen. Flow cytometry was performed prior to and after magnetic enrichment (both bound and unbound cell fractions) to assess the precision of cell enrichment, which yielded >95% pure $CD144^+$ cells throughout all MACS experiments. Both hPSC-derived artery and vein cells were frozen in freezing media (90% FBS + 10% DMSO, which was sterilely filtered before use) in cryopreservation vials, and were transferred to liquid N_2 for long-term storage.

When desired, hPSC-derived artery and vein cells were rapidly thawed in a 37 °C water bath, washed to remove freezing media, and then thawed onto Geltrex-coated plates. As described above, hPSC-derived artery cells were maintained in EGM2, whereas hPSC-derived vein cells were maintained in EGM2 + SB505124 (2 μM) + RO4929097 (2 μM).

For the first 24 hours post-thawing, ROCK inhibitor (thiazovivin, 1 μM) was added to both artery and vein cells to enhance cell survival, and was subsequently removed.

Alternate endothelial differentiation protocols for hPSCs—hPSCs were differentiated towards ECs using the artery EC differentiation protocol developed in this study, or alternatively, 4 published methods for EC differentiation (Lian et al., 2014; Patsch et al., 2015; Sriram et al., 2015; Zhang et al., 2017) in a side-by-side comparison. As per above, hPSCs were dissociated into single cells (using Accutase) and plated at a density of 25,000–50,000 hPSCs/cm^2 onto Geltrex-coated plates, in mTeSR media supplemented with thiazovivin (1 μM, Tocris). Freshly-seeded hPSCs were allowed to adhere and recover for 24 hours in mTeSR + 1 μM thiazovivin prior to initiating differentiation. Immediately before differentiation, cells were briefly washed (DMEM/F12) to remove all traces of mTeSR media, and then the following differentiation media was added:

- Lian et al., 2014. As described previously (Lian et al., 2014), hPSCs were treated with CHIR99021 6 μM, Tocris) for 2 days in LaSR basal medium (Advanced DMEM/F12 [Thermo Fisher] + GlutaMAX [2.5 mM, Gibco] + AA2P [60 μg/ml, Sigma]) for 2 days. Then, cells were briefly washed (DMEM/F12) to remove all traces of CHIR99021-containing medium and cells were maintained in LaSR basal medium for 3–4 additional days.
- Patsch et al., 2015. As described previously (Patsch et al., 2015), hPSCs were treated with BMP4 (25 ng/ml, R&D Systems) and CP21R7 (1 μM, Selleckchem) in Priming Medium (50% DMEM/F12 with Glutamax media + 50% Neurobasal media + N2 + B27 [all from Thermo Fisher]). After 3 days, the cells were briefly washed (DMEM/F12) to remove all traces of Priming Medium and were cultured in EC Induction Medium (StemPro-34 SFM medium [Life Technologies] + VEGF [200 ng/ml, R&D Systems] + Forskolin [2 μM, Tocris]). EC Induction Medium was renewed after one day and was maintained for an additional 2–3 days.
- Sriram et al., 2015. As described previously (Sriram et al., 2015), hPSCs were treated with CHIR99021 (5 μM, Tocris) in STEMdiff APEL basal medium (StemCell Technologies) for 1 day. After 24 hours, cells were briefly washed (DMEM/F12) to remove all traces of CHIR99021-containing medium and were treated with FGF2 (50 ng/mL, R&D Systems) in STEMdiff APEL basal medium for 1 day. Then, cells were briefly washed (DMEM/F12, Thermo Fisher) to remove all traces of FGF2-containing medium and were cultured in STEMdiff APEL basal medium + BMP4 (25 ng/mL, R&D Systems) + VEGF (50 ng/mL, R&D Systems) for 3 additional days.
- Zhang et al., 2017. As described previously (Zhang et al., 2017), hPSCs were cultured in E8BAC media (E8 media [Thermo Fisher] + BMP4 [5 ng/mL, R&D Systems] + Activin A [25 ng/mL, R&D Systems] + CHIR99021 [1 μM, Tocris]) for 2 days. Subsequently, cells were briefly washed (DMEM/12), and then from day 2 to day 6, cells were differentiated in E5 media + FGF2 (100 ng/ml, R&D

Systems) + VEGF (50 ng/ml, R&D Systems) + SB431542 (10 μM, Tocris) + Resveratrol (10 μM, R&D Systems) + L690 (10 μM, R&D Systems).

Flow cytometry to quantify the efficiency of EC differentiation was performed on days 0, 3, 5 and 6 of differentiation.

Generation of hiPSC lines—Human peripheral blood mononuclear cells (PBMCs) obtained from two different healthy adult human volunteers (SUN003 and SUN004) were reprogrammed using non-integrating, replication-deficient Sendai viruses encoding the iPSC reprogramming factors (Nishimura et al., 2017). This yielded SUN004.1.9 hiPSCs (referring to donor 4, line 1, subclone 9), SUN004.2 hiPSCs (referring to donor 4, line 2) and SUN003.1 hiPSCs (referring to donor 3, line 1) used in this study.

Ficoll was used to isolate PBMCs from the whole blood of healthy human adult volunteers (SUN003 and SUN004), whose identities were kept anonymous. 2 million PBMCs from each donor were split between two wells of a 24-well plate, with each well containing 1 million cells in 1 mL of PBMC media (RPMI + 10% FBS + GM-CSF (10 ng/mL) + IL-3 (10 ng/mL) + IL-6 (10 ng/mL) + FLT3L (10 ng/mL) + TPO (10 ng/mL) + SCF (10 ng/mL)) for PBMC expansion; cultures were kept in standard incubator conditions (37 °C and 5% CO_2). After 6 days of PBMC expansion, cells were dissociated and combined into a single well of a 24-well plate in fresh PBMC media and expansion cytokines.

Subsequently, PBMCs were inoculated with replication-deficient, auto-erasing Sendai virus encoding *KLF4*, *OCT4* (*POU5F1*), *SOX2* and *C-MYC* (a gift from Dr. Mahito Nakanishi, at the National Institute of Advanced Industrial Science and Technology, Tsukuba, Japan (Nishimura et al., 2017)) at multiplicity of infection (MOI) = 2 to initiate iPSC reprogramming. This recombinant Sendai virus has been described previously: it encodes *1*) modified versions of the *NP* and *P/C/V/W* genes of Sendai virus (Nagoya strain), followed by *2*) *KLF4*, *OCT4*, *SOX2* and *C-MYC* genes, and finally *3*) a modified version of the *L* gene of Sendai virus (C1.151 strain) whose 3' UTR contains 4x repeats of the *miR-302* target sequence (Nishimura et al., 2017; Nishimura et al., 2011). This recombinant Sendai virus does not encode the structural genes *M*, *F* or *HN* and thus is replication-deficient: after infecting a cell, it does not produce progeny virions (Nishimura et al., 2011). Moreover, after infected cells have become reprogrammed into iPSCs and upregulate *miR-302*, this recombinant Sendai virus becomes auto-erased, as it contains 4x repeats of the *miR-302* target sequence (Nishimura et al., 2017).

2 days after inoculation with Sendai virus, cells were again dissociated, pelleted and resuspended in 12 mL of 50% PBMC media and 50% hiPSC media (DMEM/F12, 20% KnockOut Serum Replacement [KOSR], 1% non-essential amino acids [NEAA], 1% penicillin/streptomycin [P/S], 100 μM 2-mercaptoethanol, and 5 ng/ml FGF2) supplemented with GM-CSF (10 ng/mL), IL-3 (10 ng/mL), IL-6 (10 ng/mL), FLT3L (10 ng/mL), TPO (10 ng/mL) and SCF (10 ng/mL). The cell suspension was split among three wells of a 6-well plate that contained mouse embryonic fibroblasts (MEFs). MEFs had been seeded on the previous day by first coating wells with 0.1% porcine gelatin (which had been pre-coated for 1 hour at 37 °C), after which mitomycin-C-treated, mitotically-inactivated C57BL/6 MEFs

were plated at 15,000 cells/cm^2 in MEF media (DMEM with 10% FBS). After plating hiPSCs on MEFs in 50% PBMC media + 50% hiPSC media, half-media changes were performed for the next 7–10 days with hiPSC media, thereby gradually shifting the overall media composition towards hiPSC media.

Morphologically-conspicuous hiPSC colonies were then manually picked, mechanically separated by pipette trituration and placed in hiPSC media on a new MEF-coated plate with 10 μM Y-27632 (ROCK inhibitor, to enhance cell survival) for first 24 hours. After 5 days of daily media changes (using hiPSC media), hiPSCs were dissociated into single cells with TrypLE and transitioned onto a vitronectin-coated plate in E8 media supplemented with 10 μM Y-27632 for 24 hours. Undifferentiated hiPSCs were routinely passaged every 4–6 days by re-seeding them at a density of 5,000–10,000 cells/cm^2. Subsequently, hiPSCs were adapted to culture on Geltrex-coated plates in mTeSR media. This procedure was used to generate three distinct, clonal hiPSC lines referred to as SUN003.1, SUN004.1 and SUN004.2 (see next section).

Fluorescent labelling of hiPSC lines—SUN003.1, SUN004.1 and SUN004.2 hiPSC lines were engineered to carry constitutively-expressed reporter transgenes to enable the tracking of differentiated progeny cells.

SUN003.1 hiPSCs carry a constitutively-expressed *CAG-AkaLuciferase-tdTomato* lentiviral transgene. The *pCS-CAG-AkaLuciferase-tdTomato* lentiviral plasmid was generated by cloning *AkaLuciferase* (Iwano et al., 2018) into the *pCS-CAG-tdTomato* plasmid (Masaki et al., 2016), such that AkaLuciferase and tdTomato are expressed together as an in-frame fusion protein. Lentivirus was then generated using the LV-MAX Lentiviral Production System (Gibco, A35684) as per the manufacturer's protocol. SUN003.1 hiPSCs were transduced with the *CAG-AkaLuciferase-tdTomato* lentivirus, cultured for 7–10 days, and then tdTomato+ hiPSCs were isolated by FACS, thus yielding *CAG-AkaLuciferase-tdTomato*$^+$ SUN003.1 hiPSCs (referring to referring to donor 3, line 1).

SUN004.1.9 hiPSCs carry a constitutively-expressed *CAG-eGFP* PiggyBac transgene. To integrate the PiggyBac transposon, SUN004.1 hiPSCs were seeded into 1 well of a 6-well plate at a density of 20,000 cells/cm^2, and the following day, they were then transfected with 250 μL of transfection mixture, which contained 1.25 μg of donor plasmid (*CAG-GFP* PiggyBac donor plasmid), 1.25 μg of helper plasmid (*CMV-PBase*, encoding the PiggyBac transposase enzyme) and 7.5 μL of Lipofectamine 3000 (L3000001, Thermo Fisher). 5 to 10 days post-transposition, GFP$^+$ hiPSCs that had been successfully transposed were isolated by fluorescence-activated cell sorting (FACS). The *CAG-GFP*$^+$ SUN004.1.9 hiPSC subclonal line (referring to donor 4, clone 1, subclone 9) was isolated by manually picking and expanding a single GFP$^+$ colony.

SUN004.2 hiPSCs carry a constitutively-expressed *CAG-mScarlet* lentiviral transgene. The *pCS-CAG-mScarlet* lentiviral plasmid was generated by cloning *mScarlet* into the *pCS-CAG-eGFP* plasmid (Masaki et al., 2016). Lentivirus production and transduction of SUN004.2 hiPSCs was performed as described above, and then 7–10 days post-transduction,

mScarlet^{+} hiPSCs were isolated by FACS, thus yielding *CAG-mScarlet*$^{+}$ SUN004.2 hiPSCs (referring to referring to donor 4, line 2).

Flow cytometry—Undifferentiated and differentiated hPSCs were dissociated by incubation in TrypLE Express (Gibco) for 5 minutes at 37°C. Subsequently, dissociated cells in TrypLE Express were diluted 1:5–1:10 in DMEM/F12 and centrifuged (pelleted) at 500g for 5 minutes. Each cell pellet was resuspended in FACS buffer (PBS + 1 mM EDTA [Invitrogen] + 2% v/v FBS [Atlanta Bio] + 1% Penicillin/Streptomycin [Gibco]) supplemented with fluorescently-conjugated primary antibodies, and antibody staining occurred for 30 minutes on ice protected from light. After staining, cells were washed twice with FACS buffer and resuspended in 200 μL FACS buffer with DAPI (1:10,000, Biolegend) for live/dead discrimination. Flow cytometry was performed on a BD Biosciences FACSAria II flow cytometer or a Beckman Coulter CytoFlex analyzer (Stanford Stem Cell Institute FACS Core). For data analysis, cells were gated based on forward and side scatter with height and width used for doublet discrimination. Subsequently, live cells that were negative for DAPI were gated for all marker analyses and calculations of population frequency.

Quantitative PCR—Undifferentiated or differentiated hPSCs were lysed in 350 μL of RLT Plus Buffer and RNA was extracted using the RNeasy Plus Mini Kit (Qiagen) according to the manufacturer's protocol. 300 ng of total RNA was reverse transcribed into cDNA for qPCR using the High-Capacity cDNA Reverse Transcription Kit (Applied Biosystems) according to the manufacturer's protocol. qPCR was performed in 384-well format as previously described (Loh et al., 2016), using gene-specific forward and reverse primers on a QuantStudio 5 qPCR machine (Thermo Fisher). qPCR primer sequences are provided in Table S5. Expression of all genes was normalized to the levels of the reference gene *YWHAZ*. This qPCR procedure was only used for biosafety level 2 (BSL2) cell cultures. A separate qPCR procedure was used for biosafety level 4 (BSL4) materials, and is detailed further below.

Immunostaining—Cultured monolayer cells were fixed, permeabilized and immunostained as previously described (Loh et al., 2016). Imaging was conducted using an FV3000 confocal microscope (Olympus).

Genome editing to create knock-in fluorescent reporter hPSCs—H1 *NR2F2–2A-GFP* knock-in hPSCs and H1 *SOX17–2A-mPlum* knock-in hPSCs were genetically engineered using the Cas9/AAV6 system (Martin et al., 2019). This genomic knock-in strategy entails the electroporation of hPSCs with a Cas9-sgRNA ribonucleoprotein (RNP) complex (to create a double-stranded break at a desired genomic locus), and delivery of a donor template for homologous recombination, supplied by AAV6 (Martin et al., 2019).

In brief, hPSCs were treated with 10 μM ROCK inhibitor (Y-27632) 24 hours prior to genome editing. hPSCs at 70–80% confluence were then dissociated using Accutase (Life Technologies) followed by neutralization with ROCK inhibitor-supplemented mTeSR1 media. Prior to electroporation, RNP complex was formed by combining 5 μg of HiFi SpCas9 (Integrated DNA Technologies) and 1.75 μg of sgRNA for 10 minutes at room temperature, which was then diluted with 20 μL of P3 Primary Cell Solution buffer

(Lonza). For each electroporation reaction, 500,000 hPSCs were mixed with the Cas9/sgRNA RNP-containing nucleofection solution. Nucleofection was performed using a 16-well Nucleocuvette Strip with the 4D Nucleofector system (Lonza) using the CA137 electroporation code. Following electroporation, cells were transferred into one well of a Matrigel-coated 24-well plate containing 500 μL of mTeSR1 media supplemented with 10 μM Y-27632. AAV6 donor vector (encoding *NR2F2–2A-GFP* and *SOX17–2A-mPlum* donor templates for homologous recombination) was added at 100,000 multiplicity of infection (MOI) directly to hPSCs immediately after plating. Cells were then incubated at 37°C for 24 hours. Media was changed 24 hours post-editing and 10 μM Y-27632 was removed 48 hours after.

The *NR2F2* and *SOX17* synthetic sgRNAs were purchased from Synthego with chemically-modified nucleotides at the three terminal positions at both the 5′ and 3′ ends. Modified nucleotides contained 2′-O-methyl 3′-phosphorothioate:

- *NR2F2* sgRNA: AUUUAUUGAAUUGCCAUAUA
- *SOX17* sgRNA: CUGCAGGCUGGGGCGGAUCA

Genome editing to create *EFNB2*-knockout hPSCs—The *EFNB2* gene was deleted in H1 hPSCs using the aforementioned Cas9 protocol (section “Genome editing to create knock-in fluorescent reporter hPSCs” (Martin et al., 2019)), with the exception that Cas9 RNPs were used to generate indels in the *EFNB2* locus, but no templates for homologous recombination were provided. This procedure was repeated twice: the initial round of gene targeting produced $EFNB2^{+/-}$ hPSCs, which were then re-electroporated with Cas9 RNP targeting *EFNB2*, thereby generating $EFNB2^{-/-}$ hPSCs.

sgRNAs targeting the *EFNB2* locus were designed using CHOPCHOP (Labun et al., 2019) and verified using the COSMID program (Cradick et al., 2014). The *EFNB2* synthetic sgRNAs was purchased from Synthego with chemically-modified nucleotides at the three terminal positions at both the 5' and 3' ends. Modified nucleotides contained 2'-O-methyl 3'-phosphorothioate. The genomic sgRNA target sequence was:

- *EFNB2* sgRNA: AGGCUCUAAAACUAUCGAUU

3D network formation from hPSC-derived endothelial cells—Three different types of endothelial cells were used in the formation of *in vitro* vascular networks in fibrin hydrogels. Where indicated, *1*) hPSC-derived artery endothelial cells, *2*) hPSC-derived vein endothelial cells, or *3*) umbilical cord blood-derived endothelial colony forming cells (CB-ECFC, a positive control (Kurokawa et al., 2017)) were utilized.

hPSC-derived artery and vein cells were frozen and thawed (as described above), and after thawing, were cultured in EGM2 medium for 3 days (supplemented with 2 μM Thiazovivin for the first 24 hours). EGM2 media was refreshed every 24 hours for the 3-day period. After 3 days of expansion, hPSC-derived artery and vein endothelial cells and normal human lung fibroblasts (NHLFs) were used to produce 3D endothelial networks as described previously (Kurokawa et al., 2017). In brief, hPSC-derived endothelial cells and normal human lung fibroblasts (NHLFs) were respectively dissociated using 0.05% Trypsin-EDTA (Thermo

Fisher, 25300062). The cells were then mixed at a ratio of 1 endothelial cell:2 fibroblasts. The resultant cell mixture was centrifuged at 300g for 5 min, and resuspended in 10 mg/mL of bovine fibrinogen (Sigma-Aldrich, F8630). 50 μL of the cell-fibrinogen solution was then placed inside of a small chamber consisting of cured polydimethylsiloxane (Sylgard 184) on glass, and clotted using thrombin from bovine plasma (Sigma-Aldrich T4648). The final thrombin concentration in the 10 mg/mL fibrin hydrogel was 2 unit/mL (which allowed for clotting of the fibrinogen into fibrin). After complete clotting of the hydrogels, the resultant fibrin hydrogels were submerged in 500 μL EGM2 and cultured in a 37 °C, 5% CO2 humidified incubator. EGM2 media changes occurred every 1–2 days with fresh, warm EGM2. After 7 days of culture to allow for network formation in EGM2, hydrogels were fixed using 10% formalin (Sigma F5554) in order to undergo immunofluorescent analysis. Briefly, hydrogels were blocked using 2% BSA (Sigma A2153) in PBS+0.1% Tween-20 (Sigma P9416), after which antibodies were used to stain the tissues overnight at 4 °C. Images were then taken on a fluorescent inverted microscope (Olympus IX83). Resultant image analysis and image preparation was performed using Fiji.

hPSC-derived endothelial cell migration *in vitro* in scratch assay—hPSCs were differentiated into artery and vein endothelial cells as described above. Then, hPSC-derived artery cells were cultured in EGM2 for 1 day while vein endothelial cells were cultured in EGM2 + SB505124 (2 μM) + RO4929097 (2 μM) for 1 day, until they formed a confluent monolayer. Then, media was removed and cells were washed with DMEM/F12 before being scratched with a P200 pipette tip affixed to the end of a P200 pipette. After cells were scratched, floating cells were washed away with DMEM/F12. Then, artery expansion media (EGM2) was added to artery endothelial cells and vein expansion media (EGM2 + SB505124 (2 μM) + RO4929097 (2 μM)) was added to vein endothelial cells. Media was replaced every 24 hours. Cells were imaged 0, 6, 12, 24 and 48 hours after scratching, using the Leica Paula Microscope. For image acquisition, tape was used on the microscope stage to mark the perimeter of the cell culture plate after scratching such that for images taken at different timepoints, the image was acquired at the same location every time. To quantify the closure of the gap, each image was set to scale using ImageJ. Then, using the ImageJ measurement tool, the length of the gap between both borders of the closing cell monolayer were measured at 6 different locations.

Shear stress-induced polarization of hPSC-derived endothelial cells—hPSC-derived day-3 artery endothelial cells were cultured in a 6-well plate with EGM2 medium for 24 hours, either in static culture (standard conditions) or a rotator (shear stress conditions). hPSC-derived day-4 vein endothelial cells were magnetically enriched for $CD34^+$ cells (Miltenyi Biotec) and cultured for 1 week in EGM2 media prior to exposure to shear stress for 24 hours as per above. Shear stress conditions were described previously and entailed culturing cells on a 6-well plate on an orbital shaker (Poduri et al., 2017). After 24 hours of static or shear stress conditions, both immunostaining and qPCR was performed.

After exposure to static media or shear stress for 24 hours, immunostaining was performed to quantify the degree of cell alignment. To this end, cells were fixed in 4% paraformaldehyde (PFA) for 15 minutes at 4 °C. Then, the cells were washed with PBS

for three times, waiting 5 minutes between each wash. After washing, cells were incubated in 4 °C overnight with primary antibody in 0.5% Triton X-100/PBS solution. Next, cells were washed with PBS for three times, waiting 15 minutes between each wash. Afterwards, the cells were incubated with secondary antibody in 0.5% Triton X-100/PBS solution. Secondary antibody was removed and DAPI in PBS was added and incubated for 5 minutes. Then, the cells were washed with 0.5% Triton X-100/PBS three times, waiting 15 minutes between each wash. Finally, PBS was added to the cells, and imaging was conducted using a Keyence BZ-9000 microscope.

After imaging, quantification of cell alignment was performed using ImageJ. Cell directionality analysis was done using the “Directionality” plugin, using Fourier components analysis with Nbins=90, producing a directionality histogram which starts at −90 degrees and ends at +90 degrees.

LDL and acetylated LDL uptake assay—hPSC-derived day 3 artery and day 4 vein endothelial cells were washed with DMEM/F12 (Thermo Fisher) and incubated at 37°C for 4 hours with either a 1:25 concentration of low-density lipoprotein (LDL) conjugated with DyLight550 (Cayman) or a 5 μg/mL concentration of acetylated LDL conjugated to Alexa Fluor 488 (Fisher Scientific) in their respective differentiation media. As a negative control, hPSC-derived day 3 artery and day 4 vein endothelial cells were incubated in their respective differentiation media without LDL DyLight 550 or acetylated LDL Alexa 488. After incubation, cells were dissociated by incubating them in TrypLE Express (Gibco) for 5 minutes at 37 °C. Subsequently, the dissociated cells were diluted 1:10 in DMEM/F12 and centrifuged at 500g for 5 minutes. Each cell pellet was then resuspended in FACS buffer (DPBS + 5 mM EDTA [Invitrogen] + 0.5% BSA) supplemented with anti-CD144 antibody conjugated to Alexa Fluor 647 (BD Biosciences) and incubated on ice for 30 minutes, while being protected from light. After antibody staining, cells were washed twice with FACS buffer and resuspended in 300 μL FACS buffer containing DAPI (1:10,000, Biolegend). Then the resuspended cells were passed through a 100 μm strainer (BD Biosciences) and analyzed using a FACSAria II flow cytometer (Stanford Stem Cell Institute FACS Core). During flow cytometry data analysis, we gated on $CD144^{+}$ endothelial cells before quantifying fluorescent LDL or acetylated LDL uptake by endothelial cells.

Immune cell adhesion to TNFα-treated endothelial cells—The THP1 human monocyte-like cell line was fluorescently labelled with CFSE and then cocultured with hPSC-derived endothelial cells to assess immune cell adhesion to endothelial cells. Methods to assess adhesion of immune cells to endothelial cells were modified from previously-published protocols (Rosa et al., 2019; Zhang et al., 2017).

First, THP1 cells were fluorescently labelled with CFSE, largely as per the manufacturer’s recommendations. THP1 cells were resuspended in DMEM/F12 at a concentration of 1 million cells/mL and then incubated with 5 μM of CellTrace CFSE (Thermo Fisher Scientific, C34554) for 20 minutes at room temperature, protected from light, and with occasional pipetting to keep cells resuspended during the staining process. After 20 minutes of incubation, the cell suspension was diluted 1:5 in RPMI1640 + 10% FBS for 5 minutes.

Then, cells were centrifuged at 300g for 5 minutes, the supernatant was aspirated, and then fresh RPMI1640 + 10% FBS was added.

Separately, hPSC-derived artery and vein endothelial cells cultured in 12-well plates were stimulated with the inflammatory cytokine TNFα (10 ng/mL) for 4 hours in their respective culture media (EGM2 for artery cells and EGM2 + RO4929097 (2μM) + SB505124 (2μM) for vein cells) at 37 °C. As a negative control, artery and vein cells were cultured in their respective culture media in the absence of TNFα.

Subsequently, Hoechst dye (1 μg/mL) was added in the dark for 5 minutes to fluorescently label the nuclei of live artery and vein cells. Then, cells were washed with DMEM/F12. After washing, CFSE-labelled THP-1 immune cells (described above) were added to each well in a 12-well plate at 1 million cells/well in EGM2 media for 30 minutes at 37 °C. After this 30-minute coculture of THP1 and endothelial cells, the wells were washed 3 times with DMEM/F12 to remove any non-adhered THP1 cells. Images were taken using a Keyence BZ-9000 fluorescence microscope and quantification of the number of adhered THP1 cells was performed using ImageJ/Fiji.

Endothelial sprouting assay—The sprouting assay was performed as previously described (Nakatsu et al., 2007), with modifications. First, *CAG-GFP*$^{+}$ SUN004.1.9 hPSC-derived artery or vein ECs were thawed and respectively maintained in artery or vein expansion media (EGM2 for artery ECs and EGM2 + RO4929097 (2 μM) + SB505124 (2 μM) for vein ECs) for 24 hours until they were fully confluent. Second, ECs were cultured with EGM2 + 10% heat-inactivated FBS for 24 hours, prior to dissociating them for the sprouting assay. Third, hPSC-derived artery and vein ECs were dissociated using trypsin and counted. In parallel, Cytodex-3 beads (Sigma Aldrich, C3275) were allowed to settle for 5 minutes, and were washed briefly in 1 mL of warm EGM2 media before removing the media. Fourth, Cytodex-3 beads were coated with hPSC-derived ECs by incubating them at a concentration of ~400 cells/bead in 1.5 mL of warm EGM2 media. The bead/cell suspension was incubated for 4 hours at 37°C, with gentle pipetting every 20 minutes. After 4 hours, the EC-coated beads were transferred to a well of a non-tissue-culture-treated 24-well plate and left overnight in EGM2 + 10% heat-inactivated FBS. The EC-coated beads were then transferred to a 15 mL conical tube and left to settle for 5 minutes, followed by three washes with warm EGM2, and then the beads were counted on a coverslip.

To embed EC-coated beads in a 3D fibrin gel, beads were resuspended in sterilely-filtered fibrinogen solution (2.0 mg/mL, Sigma Aldrich, F8630) at a concentration of ~500 beads/mL, and 0.5 mL of the fibrinogen/bead suspension was added to each well of a 24-well plate. Then, 0.5 mL of thrombin (0.625 units/mL, Sigma Aldrich, T3399) was added and the bead-fibrinogen-thrombin mixture was triturated ~4–5 times, with care to avoid the formation of bubbles. The plate was left in the hood for 5 minutes, and then incubated at 37° C for 10 minutes to generate fibrin gels. After the gels formed, 1 mL of EGM2 media + 10% FBS was added dropwise. Gels were incubated at 37°C for 24 hours in order for GFP^{+} endothelial sprouts to emerge. At the end of the assay, EGM2 was removed and the gels were washed with DPBS prior to overnight fixation in 4% paraformaldyde. Gels were

imaged using a fluorescence microscope. The number of sprouts per bead and the length of each sprout was quantitated on at least five beads using MetaMorph software.

Endothelial chemotaxis towards Apelin-13—The chemotaxis assay was performed as previously reported (Kälin et al., 2007), with modifications. The polycarbonate membrane of a Transwell filter (with 8 μm pores; Corning, 3422) was coated with 0.1% gelatin overnight. Separately, *CAG-GFP*$^{+}$ SUN004.1.9 hPSC-derived artery or vein ECs were respectively maintained in artery or vein expansion media (EGM2 for artery ECs and EGM2 + RO4929097 (2 μM) + SB505124 (2 μM) for vein ECs) until they were fully confluent. hPSC-derived artery or vein ECs were then dissociated using trypsin and resuspended in Endothelial Basal Media 2 media (EBM2, Lonza) at concentration of 1.5×10^5 cells/mL. Then, 100 μL of the cell suspension was added to the upper chamber of the gelatin-coated Transwell filter, and 600 μL of EBM2 media + Apelin-13 (100 ng/mL, Tocris, 2420) was added to the lower chamber. Cells were incubated at 37°C for 4 hours to allow for cell migration towards the lower chamber. Then, non-migratory cells were removed with a cotton swab. Migratory cells on the bottom of the Transwell membrane were fixed and stained with DAPI. Cells were imaged under a fluorescence microscope and counted using ImageJ software.

Subcutaneous transplantation of hPSC-derived endothelial cells—SUN003.1 *CAG-AkaLuciferase-tdTomato* hPSC-derived ECs were subcutaneously transplanted into adult, immunodeficient NOD-SCID *Il2rg*$^{-/-}$ (NSG) mice. In brief, hPSC-derived endothelial cells were suspended in a 1:1 mixture of Matrigel (phenol-free, growth factor reduced) + F12 medium (supplemented with 100 ng/mL FGF2 and 50 ng/mL VEGF). NSG mice were then anesthetized with 2% isoflurane and 100% oxygen flowing at 2 liters/minute until they were unconscious and unresponsive to stimuli (i.e., a toe pinch). A fold of skin directly lateral to the spine and near the neck was swabbed with ethanol in order to disinfect it, and then was gently pinched. A volume of 50–200 μL containing ~10^6 cells suspended in the Matrigel + F12 + FGF2 + VEGF solution was then injected under the skin flap using a 27-gauge syringe. Anesthesia was then discontinued, and mice were allowed to recover in a warm cage until they became alert and awake.

1 month post-transplantation, NSG mice were sacrificed, and subcutaneous gels containing hPSC-derived ECs were recovered and then fixed in 4% formaldehyde overnight at 4 °C. Fixed gels were then placed in PBT buffer (PBS with 0.5% Triton-X) with primary antibodies and incubated overnight at 4 °C on a shaker. The next day, samples were washed every 1.5 hours in PBT buffer for approximately 8 hours at room temperature, and with gentle agitation. Subsequently, Alexa Fluor 488-conjugated secondary antibodies (Life Technologies) were then added in PBT buffer at a 1:250 concentration and incubated overnight at 4 °C on a shaker. Finally, the stained samples were washed every 1.5 hours with PBT buffer for approximately 8 hours and cleared using Vectashield (Vector Labs, H-1000). Samples were then placed in a microscope chamber and imaged using a Zeiss LSM-700 confocal microscope. Image processing was done in ImageJ.

Single-cell RNA-sequencing—We executed single-cell RNA-seq on H1 hPSC-derived day 3 artery ECs and day 4 vein ECs using the 10x Genomics Chromium v3 platform

(Zheng et al., 2017). Libraries were prepared using the 10x Genomics Chromium 3' Kit v3 following the manufacturer's guidelines. Libraries were prepared with i7 indices (compatible with Illumina sequencers) and then multiplexed. Multiplexed libraries were sequenced across multiple lanes of an Illumina HiSeq 4000 sequencer by Novogene. Unique sequences in each i7 index were used for demultiplexing. Cell Ranger (10x Genomics) was used to perform read alignment to the hg38 reference genome, filtering, barcode counting and UMI counting.

Cell matrix files generated from Cell Ranger were imported into RStudio using the function "Read10x_h5" in Seurat v3 (Stuart et al., 2019). We then implemented well-established quality control procedures to exclude dying/dead cells that *1*) expressed low numbers of genes, *2*) displayed too low or too high mitochondrial counts, or *3*) did not express reference/housekeeping genes *ACTB* or *YWHAZ*; additionally, we also *4*) computationally excluded doublets by removing cells that had expressed markedly higher numbers of genes. Only high-quality single-cell transcriptomes that passed these quality control metrics were used for subsequent analyses. scRNAseq data were normalized using the "LogNormalized" function and scaled using a linear transformation in Seurat v3 (Stuart et al., 2019). Expression of marker genes was denoted by different color shades and superimposed over the entire cell population, as visualized on a Uniform Manifold Approximation and Projection (UMAP) projection (Becht et al., 2018). Importantly, all cells within the entire day 3 and day 4 differentiated populations were shown on the UMAP projection, without any pre-selection of ECs.

An interactive web portal (Ouyang et al., 2021) to explore scRNAseq profiles of hPSC-derived artery and vein ECs is available at https://anglab.shinyapps.io/arteryveinscrna/.

Comparing *in vivo* vs. *in vivo* artery and vein cells using single-cell RNA-seq—We used scRNAseq to quantify the degree of transcriptional similarity between hPSC-derived artery and vein ECs (*in vitro*; described above) as well as human artery and vein ECs obtained from a Carnegie Stage 13 (CS13) human fetus (*in vivo*). scRNAseq data of CS13 human fetal artery and vein ECs were generated previously (Zeng et al., 2019) and were downloaded from the Gene Expression Omnibus (GSE135202). Importantly, both *in vivo* and *in vitro* EC datasets were generated using the 10x Genomics Chromium platform (Zheng et al., 2017), thus mitigating concerns that would otherwise arise from a cross-platform comparison.

We performed quality control and normalization for CS13 human fetal scRNAseq data using the methods described above for hPSC-derived artery and vein ECs (section "Single-cell RNA-sequencing"). In brief, dead/dying cells as well as doublets were computationally excluded and then CS13 human fetal scRNAseq data were normalized using the "LogNormalized" function and scaled using a linear transformation in Seurat v3 (Stuart et al., 2019).

To decompose the CS13 human fetal scRNAseq dataset into its constituent cell-types, we used Seurat v3 (Stuart et al., 2019) to perform Louvain clustering (resolution 0.05), which separated the fetal cell population into 4 subsets: artery ECs (*CDH5+, PECAM1+, DLL4+,*

CXCR4+, HEY1+); vein ECs (*CDH5+, PECAM1+, NT5E+, APLNR+, NR2F2+, NRP2+*); mesenchymal (*TWIST2+ CXCL12+ DLK1+ HAND1+ FBLN5+ WT1+*), and epithelial cells (*EPCAM+, CDX2+*). The existence of these 4 clusters—and the marker genes used to discriminate them—are consistent with what was reported in the original report that described these scRNAseq data (Zeng et al., 2019). Next, we focused our analysis only on the fetal ECs: we selected cells that expressed pan-endothelial genes (*PECAM1* and *CDH5*) at a level of UMI > 1.221 (i.e., UMI $e^{0.2}$) in both the CS13 artery and CS13 vein subpopulations for downstream analyses.

In parallel, we computationally isolated ECs from our scRNAseq datasets of hPSC-derived day 3 artery and day 4 vein ECs *in vitro*. Louvain clustering (resolution = 0.1) was applied using Seurat v3 (Stuart et al., 2019), which decomposed the day 3 population into artery ECs (*CDH5+, PECAM1+, CD34+, SOX17+, CXCR4+, DLL4+*) vs. non-ECs; similarly, this procedure decomposed the day 4 population into vein ECs (*CDH5*+, *PECAM1*+, *CD34*+, *NR2F2*+, *NT5E*+, *FLRT2*+) vs. non-ECs. The hPSC-derived artery ECs and vein ECs were computationally isolated and then used for subsequent analyses.

We then merged our *in vitro* scRNAseq dataset—composed of hPSC-derived day 3 artery ECs and day 4 vein ECs, in addition to other *in vitro* cell-types—with the CS13 human fetal artery and vein EC dataset. The combined scRNAseq dataset was normalized and scaled using SCTransform (Hafemeister and Satija, 2019) to remove technical variation while retaining biological variation. Next, we calculated the average expression of each gene in the SCTransform-normalized dataset (containing both *in vivo* and *in vitro* ECs) using the "AverageExpression" function in Seurat v3 (Stuart et al., 2019). We then identified the top 6000 variable genes in this merged dataset using the "CellScatter" function.

On the basis of the expression of these 6000 variable genes, we calculated the Pearson correlation coefficient *1*) between our hPSC-derived artery ECs vs. CS13 human fetal artery ECs and *2*) between our hPSC-derived vein ECs vs. CS13 human fetal vein ECs.

To find differentially-expressed genes between hPSC-derived vs. CS13 fetal artery and vein ECs, we used the function "FindMarkers" in Seurat v3 (Stuart et al., 2019), with parameters set to only identify genes that were expressed in at least 25% of cells within that subcluster. This identified the most differentially-expressed genes between *1*) hPSC-derived vs. human fetal artery ECs and *2*) hPSC-derived vs. human fetal vein ECs. Of these genes that strongly differed in expression levels between *in vitro*-derived vs. *in vivo* ECs, we manually annotated those that had been previously linked to ribosome translation (*GNB2L1*, *EEF1G*, *RPL17*, *RPS17*) and mitochondrial respiration (*ATP5G2*, *ATP5E*, *ATP5L*, *MT-ND2*, *MT-ND1*, *MT-ND4*, *MT-CTB*, *MT-CO1*, *MT-ATP6*, *MT-CO2*, *MT-CO3*, *MT-CTB).* Finally, we performed gene ontology analysis on the lists of genes differentially expressed between hPSC-derived vs. CS13 fetal ECs using the online Enrichr platform (Chen et al., 2013; Kuleshov et al., 2016).

Bulk-population RNA-seq of uninfected cells—We performed bulk-population RNA-seq on H1 hPSC-derived day 3 artery ECs and day 4 vein ECs, both of which were FACS purified for $CD144^+$ ECs to exclude any spurious gene expression from contaminating

non-ECs. Cells were lysed using Zymo RNA lysis buffer and RNA was extracted using the Zymo Quick RNA kit according to the manufacturer's instructions. We determined the RNA integrity number (RIN) of each sample using Agilent Bioanalyzer on-chip electrophoresis, and high-quality RNA samples with RIN ≥ 8 were enriched for poly(A) sequences and used to construct RNA-seq libraries, which were then ligated to adaptors for multiplexing. RNA-seq libraries were then sequenced on the DNBSEQ-G400 sequencer using DNA nanoball and combinational probe anchor synthesis technology by BGI Global Genomic Services to generate 150-bp paired-end reads. To minimize batch effects, all libraries were pooled together into a single sample, which was then sequenced on multiple lanes.

After obtaining RNA-seq reads, we performed quality control using FastQC (Andrews, 2010). Next, we used Trim Galore (Krueger, 2012) to remove index adaptors, low-quality base-calls or reads less than 20bp, using a read quality cutoff Phred score of 33. Trimmed and filtered reads from each single library (which was originally sequenced on multiple lanes) were then merged into a pooled file, each representing a single library. Subsequently reads were aligned with the GRCh38 (hg38) *Homo sapiens* reference genome and gene-level RNA-seq counts were quantified using Kallisto (Bray et al., 2016). We then filtered and $\log_2$ normalized counts per million (Tidyverse, BaseR, and EdgeR) (Robinson et al., 2010; Wickham et al., 2019). Then, we performed dimensional reduction and differential gene expression analyses (Limma and EdgeR) (Law et al., 2014; Ritchie et al., 2015; Robinson et al., 2010) to identify genes differentially expressed between hPSC-derived artery vs. vein ECs. These data were visualized on volcano plots: genes that showed a $\log_2$ fold differences less than 3 (i.e., less than 8-fold differential expression) were represented in gray, while differentially expressed genes (i.e., those with greater than 8-fold expression differences) were highlighted in distinct colors.

Generation of Nipah-pseudotyped lentivirus—Non-replicating, *GFP*-expressing lentiviruses pseudotyped to solely display Nipah or vesicular stomatitis virus (VSV) envelope proteins were generated from HEK293T/17 packaging cells using a 3rd generation lentiviral packaging system. In brief, cell-culture plates were coated with poly-L-lysine (R&D Systems, 3438–200-01) for 5 minutes at room temperature, which was then aspirated. Then 1 million HEK293T/17 cells (ATCC, CRL-11268) were seeded onto each poly-L-lysine-coated well of a 6-well plate. 24 hours after seeding, HEK293T/17 cells were ~80–90% confluent and they were transfected using FuGENE HD (Promega, E2311).

The following lentiviral packaging plasmids encoding Nipah or VSV envelope proteins were used:

- pCAGGS-coNiV-G-HA: Encodes a codon-optimized *NiV-G* gene whose amino acid product is identical to the protein encoded by the *NiV-G* reference gene (NC_002728.1: 8710–11255 nucleotides, from Nipah virus/human/MY/1999/CDC), and additionally carries a hemagglutinin (HA) tag (Palomares et al., 2013). Provided by Dr. Benhur Lee's laboratory (Icahn School of Medicine).
- pcDNA3.1-coNiV-F T5F-Au1: Encodes a codon-optimized *NiV-F* gene whose amino acid product is a truncated version of the protein encoded by the *NiV-F* reference gene (NC_002728.1: 6370–8706 nucleotides, from Nipah virus/

human/MY/1999/CDC). However *1*) the cytoplasmic tail of NiV-F was truncated to only carry 5 amino acid residues (a change that improves the production of pseudotyped lentiviruses) and *2*) additionally it carries an AU1 tag (Palomares et al., 2013). Provided by Dr. Benhur Lee's laboratory (Icahn School of Medicine).

- VSV-G: Encodes vesicular stomatitis virus envelope protein (VSV-G). Provided by Dr. Owen Witte's laboratory (University of California Los Angeles) (Goldstein et al., 2011).

HEK293T/17 cells were transfected using FuGENE HD with the following amounts of lentiviral packaging plasmids per well of a 6-well plate: 1.38 μg pMDL plasmid + 0.53 μg pREV plasmid + 0.76 μg envelope protein-encoding plasmid(s) + 2.13 μg pRS348 *EF1A-GFP* plasmid. For the envelope protein-encoding plasmid(s), the following amounts were used for: *1*) VSV pseudovirus (0.76 μg VSV-G plasmid) or *2*) Nipah pseudovirus (0.37 μg NiV-G plasmid + 0.37 μg NiV-F plasmid). For transfection, room temperature DMEM medium was first mixed with FuGENE, and then mixed with plasmid DNA; after 15 minute incubation at room temperature, the transfection solution was added dropwise to HEK293T/17 cells.

16–20 hours post-transfection, the culture media was replaced with 1mL of pre-warmed DMEM + 10% FBS media. 24 hours media later, the media (containing pseudotyped lentivirus particles encoding a constitutively-expressed *EF1A-GFP* reporter) was harvested and either immediately used for transduction experiments or frozen at −80 °C.

Transduction of endothelial cells with Nipah-pseudotyped lentivirus—After Nipah- and VSV-pseudotyped lentiviruses were generated as described above, they were used to transduce hPSC-derived artery and vein endothelial cells. First, wells in a 96-well, flat-bottom plate were coated with Geltrex (50–100 μL/well), which was then aspirated. Subsequently, hPSC-derived artery or vein cells (generated from either wild-type or *EFNB2*$^{-/-}$ hPSCs) were thawed and 16,800–67,200 cells were seeded per Geltrex-coated well of a 96-well plate in 100 μL of respective artery or vein expansion media supplemented with the ROCK inhibitor thiazovivin for 24 hours. Artery or vein expansion media was changed every 24 hours, and thiazovivin was withheld after the initial 24 hour seeding period.

72 hours post-seeding, media was removed from artery and vein cells, and then 100 μL of fresh artery or vein expansion media was added, in addition to 0.3–100 μL of viral supernatant containing pseudotyped lentiviruses (or control media lacking pseudotyped viruses). Pseudotyped lentiviruses were added for 24 hours prior to removal of culture media, and subsequently, media was replaced with fresh artery and vein media every 24 hours.

6 days post-seeding (i.e., 3 days post-transduction), each well of artery or vein cells was dissociated through the addition of 50 μL TrypLE Express (incubated at 37 °C, 3–6 minutes) and trituration. Then, 150 μL of FACS buffer was added per well, and cells were transferred into a 96-well V-bottom plate before centrifugation (at 4 °C, 5 minutes). Subsequently, supernatant was aspirated to remove the dissociation buffer, and cells were resuspended in

150 μL of FACS buffer + DAPI per well. Flow cytometry was performed using a CytoFLEX flow cytometer (Beckman Coulter Life Sciences) to enumerate the percentage of GFP^+ (i.e., virally-transduced) viable cells in each well.

The percentage of GFP^+ cells was used to quantify the relative efficiency with which a given pseudotyped lentivirus transduces artery vs. vein endothelial cells (i.e., the arteriovenous tropism of a given pseudotyped lentivirus). In brief, artery and vein cells were inoculated with an *equal* volume of lentiviral supernatant containing Nipah- or VSV-pseudotyped lentivirus and the percentage of GFP^+ cells were quantified by flow cytometry, as described above. In parallel, wells of artery and vein cells were dissociated and counted to determine cell numbers, in order to correct for any differences in transduction efficiency attributable to the use of different numbers of artery vs. vein cells.

Next, the multiplicity of infection (i.e., after inoculation with a given volume of pseudotyped lentiviruses, the *number* of pseudotyped lentiviruses per each single cell) was calculated using Poisson statistics as follows. Assuming that, after viral inoculation, the number of viruses that transduces a single cell follows a Poisson distribution (Ellis and Delbrück, 1939), then: $P(n) = (m^n * e^{-m})/n!$, where P(n) is the probability that a cell will be transduced by n number of viruses and m is the multiplicity of infection.

The frequency of non-transduced cells in a given cell population is described by $P(n = 0) = e^{-m}$. The frequency of transduced cells is described by $P(n > 0) = 1 – P(0)$. Consequently, $P(n > 0) = 1 – e^{-m}$. In this case, after transduction with *GFP*-encoding lentiviruses, P(n > 0) is equivalent to the percentage of GFP^+ cells in a given cell population (henceforth "GFP^+"). In summary, the multiplicity of infection (m) can be described by: $m = –\ln(1 – GFP^+)$. In this study, the percentage of GFP^+ cells was always than 60% (i.e., the multiplicity of infection was always less than 0.916), thereby enabling the multiplicity of infection to be accurately determined within the linear range of this quantitative assay. In this manner, the percentage of GFP^+ artery or vein cells (enumerated by flow cytometry) was used to calculate the multiplicity of infection, which was then multiplied by the number of artery or vein cells to yield the inferred number of pseudotyped lentivirus particles that were originally used to inoculate the artery or vein cells. Given that the same absolute *volume* of pseudotyped lentivirus was used to inoculate artery or vein cells, any differences in the inferred *number* of pseudotyped lentivirus particles for artery vs. vein cells must be attributable to differences in the *tropism* of the pseudotyped lentivirus for artery vs. vein cells. Finally, the inferred number of pseudotyped lentivirus particles used to inoculate artery cells was divided by the inferred number of pseudotyped lentivirus particles used to inoculate vein cells, thus calculating the *arteriovenous tropism* of Nipah- or VSV-pseudotyped lentiviruses.

Generating stocks of Nipah and Hendra viruses and viral quantification— Authentic Nipah and Hendra viruses are classified in Risk Group 4 (CDC and NIH, 2020). All experiments with Risk Group 4 viruses were conducted under maximum containment conditions in the biosafety level 4 (BSL4) laboratory of the Robert Koch Institute, in accordance with standard operating procedures institutionally approved by the Robert Koch Institute.

For this study, Nipah virus, Malaysia variant (Nipah virus/human/MY/1999/CDC) (Harcourt et al., 2000) and Hendra virus, Brisbane variant (Hendra virus/horse/AU/1994/Hendra) (Murray et al., 1995) were obtained from CDC Viral Special Pathogens Branch reference stocks. These viruses were then subsequently propagated on Vero E6 cells (Vero C1008 (Vero 76, clone E6, Vero E6), from the European Collection of Authenticated Cell Cultures (ECACC)) in DMEM + 2% FBS to generate archive stocks, which were frozen at −80°C. As needed, archive stocks were thawed and passaged once more on Vero E6 to generate working stocks of these viruses, which were frozen at −80°C. Working stocks of these viruses were used for all subsequent experiments.

These viral stocks were quantified using the tissue culture infectious dose 50% ($TCID_{50}$) assay. For viral quantitation, Vero E6 cells were seeded into 96-well tissue culture plates in DMEM containing 10% FBS, 2 mM glutamine, and 1% penicillin/streptomycin, at such a density that after overnight plating the cells became 95–100% confluent the following day. Separately, serial 10-fold dilutions of virus stocks were then diluted in DMEM. Then, the Vero E6 culture media was aspirated and 100 μL of viral supernatant was added to triplicate wells of Vero E6 cells. This was incubated for 1 hour at 37 °C, 5% CO_2. Subsequently, 100 μL of DMEM containing 4% FBS, 4 mM glutamine, and 2% penicillin/streptomycin was added to the wells (such that the final FBS concentration was 2%) and this was incubated for 4–5 days at 37 °C, 5% CO_2. The cells were then scored for the presence of cytopathic effects (CPE). The endpoint dilution of the viral stock in which 50% of the wells exhibited CPE was calculated using the Spearman-Karber method, therefore quantifying the viral dose present in the original viral stocks (expressed as $TCID_{50}$ units/mL). These titrated viral stocks were then used to infect hPSC-derived artery and vein ECs, as described below.

In certain experiments, Sendai virus, Cantell strain (Cantell and Hirvonen, 1981)—a paramyxovirus not known to cause disease (López et al., 2006; Yoshida et al., 2018)—was used as a control for Nipah and Hendra viruses, which are highly-lethal paramyxoviruses. Sendai virus is classified in Risk Group 2, but was handled in the BSL4 laboratory for consistency. Sendai virus, Cantell strain was obtained from ATCC (VR-907).

Infection of hPSC-derived artery and vein cells with Nipah or Hendra viruses

—Prior to viral infection, frozen stocks of hPSC-derived artery and vein ECs were thawed as described above and propagated on Geltrex-coated 24-well plates, 48-well plates or 8-well chamber slides (Ibidi, 80826) in their respective expansion media (EGM2 for artery ECs and EGM2 + RO4929097 + SB505124 for vein ECs) until they became fully confluent, at 4–5 days post-seeding. At that point, they were then transferred into BSL4 containment.

In each experiment, hPSC-derived artery or vein ECs were then inoculated with the same infectious quantity of a given virus. This enabled a side-by-side comparison of the responses of artery vs. vein ECs. Artery and vein ECs were inoculated with viruses for 1 hour (37°C, 5% CO_2) in EGM2 medium. Different amounts of virus (titrated as described above) were used in various experiments depending on the objective of the experiment:

- Visualization of syncytia formation at a fixed timepoint (Fig. 5a,b, Fig. S5e): 10^4 $TCID_{50}$ units of Nipah or Hendra virus were added per well of a 24-well plate

- Visualization of syncytia formation through live-imaging (Fig. 5c–e, Fig. S5h,i): 10^4 $TCID_{50}$ units of Nipah or Hendra virus were added per well of an 8-well chamber slide
- Quantification of viral replication kinetics (Fig. 6a, Fig. S6a): 5×10^3 $TCID_{50}$ units of Nipah or Hendra virus were added per well of a 48-well plate
- RNA-seq analysis of infected cells (Fig. 7a–d, Fig. S7a–c): 10^5 $TCID_{50}$ units of Nipah or Hendra virus, or 30 HA units of Sendai virus, were added per well of a 24-well plate
- IFNβ secretion by infected cells (Fig. 7e, Fig. S7d): 5×10^4 $TCID_{50}$ units of Nipah or Hendra virus, or 15 HA units of Sendai virus, were added per well of a 48-well plate

After 1 hour of incubation with virus, cells were washed twice in EGM2 to remove residual virus in the media. Infected artery and vein ECs were then cultured in their respective arterial or venous expansion media for various lengths of time, as described for each individual experiment. Media was changed every 24 hours.

Assessing cytopathic effects in virally-infected hPSC-derived artery and vein cells—To visualize cytopathic effects, Diff-Quik staining (Labor+Technik, LT 001) was performed on hPSC-derived ECs that had been infected with Nipah virus, Hendra virus or left uninfected for 24 hours. For each condition, 5 fields of view were randomly selected and imaged. In each image, the number of total nuclei as well as syncytia were quantified using ImageJ/Fiji. To count multinucleated cells, ImageJ/Fiji's cell counter was used to label and tally the total number of cells with 1 nucleus and ≥2 nuclei. To count the total number of cells, multiple ImageJ/Fiji plugins were used to process the images automatically. Images were converted to 8-bit format, and then thresholded, smoothened and filtered to remove noise (despeckled). In each image, overlapping objects were separated using the function "watershed" and finally, cells/particles were counted using the function "analyze particles". In summary, both *1*) the number of nuclei per cell and *2*) the frequency of multinucleated cells relative to total cell numbers were quantified.

Live imaging of Nipah and Hendra infection in BSL4 conditions—To visualize the kinetics and extent of Nipah and Hendra virus-induced cell fusion and cell death in real time, live imaging was performed under maximum containment in the BSL4 laboratory. To quantify cell fusion, GFP^+ ECs (obtained from the SUN004.1.9 hiPSC line) and wild-type ECs (obtained from the H1 hESC line) were cocultured at a 4:1 ratio, such that fusion between cells of these two genotypes would manifest as diffusion of GFP from one cell to the other.

To this end, frozen stocks of wild-type H1-derived and GFP^+ SUN004.1.9-derived artery and vein ECs were thawed and cocultured as described above, on Geltrex-coated 8-well chamber slides compatible with microscopy (Ibidi, 80826) in 200 μL of their respective arterial or venous expansion media. After infection with Nipah virus (10^4 $TCID_{50}$ units/well), Hendra virus (10^4 $TCID_{50}$ units/well) or a negative control (uninfected), live imaging of artery and vein ECs was performed on a spinning disk confocal microscope (CorrSight, FEI) for 24

hours, with a frame rate of 5 minutes, at 37°C, 5% CO_2, using a 5x objective lens. For these live imaging experiments, a high virus titer was used in order to rapidly induce cytopathic effects to visualize virally-induced cell fusion and death.

Computational analysis of virally-infected live imaging data—Time-lapse videos were imported into Fiji and then analyzed using Mastodon or Trackmate v6.0.2 (Tinevez et al., 2017). As described above, cocultures of wild-type and GFP^+ cells were used for live-imaging experiments. GFP^+ cells were identified as spots or blobs with an estimated blob/spot size of 20 pixels (using the Laplacian of Gaussian [LoG] filter). Then, the 20-pixel spots were filtered based on a quality score above 0.26–0.28. Next, the spots were then linked from frame to frame to build track segments and linking costs of the tracks were calculated (using LAP tracker, based on the Linear Assignment Problem mathematical framework). The parameters for frame-to-frame linking, track segment gap closing, and track segment merging were all set to a maximum distance of 15 pixels. The outputs of this analysis include the median velocity of spots and cell tracks. Cell tracks were exported as .xml files and imported into Icy (de Chaumont et al., 2012) to obtain images whereby cell tracks were overlaid over the microscope field. To compare the median velocities of infected artery vs. vein cells, the Mann Whitney non-parametric t-test was performed and two-tailed p-values calculated to determine statistical significance.

Quantification of viral replication—hPSC-derived artery and vein ECs were inoculated with Nipah and Hendra viruses for 1 hour and then washed twice in EGM2 to remove excess virus (as described above). After viral inoculation, both the extracellular levels of viral RNA (encompassing viral particles budding into the culture media) and the intracellular levels of viral RNA (encompassing intracellular viral replication) were quantified across different timepoints.

To quantify viral genomes present in the media, 140 μL of the culture media (i.e., supernatant) was placed in 560 μL of lysis buffer AVL (Qiagen QIAamp Viral RNA extraction kit, Qiagen, 52904), in addition to 560 μL of 100% ethanol, in order to inactivate it for transfer out of the BSL4 laboratory. Then, RNA was extracted following the manufacturer's instructions. To quantify intracellular viral genomes, RNA was first extracted from cellular monolayers as described below (in the section "Bulk-population RNA-seq of virally-infected cells"). Subsequently, qRT-PCR was performed using primers directed against the viral genome and the AgPath-ID™ One-Step RT-PCR Kit (Thermo Fisher, 4387391).

Bulk-population RNA-seq of virally-infected cells—H1 hPSC-derived and SUN004.1.9 hPSC-derived artery and vein ECs in 24-well plates were inoculated with Nipah virus (10^5 $TCID_{50}$ units/well), Hendra virus (10^5 $TCID_{50}$ units/well) or Sendai virus, Cantell strain (30 HA units/well) or left uninfected (negative control). For RNA-seq experiments, a high viral dose (multiplicity of infection [MOI] ≈ 5) was used in order to synchronize infection in a large proportion of cells. In the same experiment, hPSC-derived artery and vein ECs from two separate genetic backgrounds (H1 hESC-derived and SUN004.1.9 hiPSC-derived) were infected to ensure the consistency of any transcriptional changes that were identified. The timepoints of 5, 10 and 15 hours post-infection were

chosen because they encompassed viral entry, viral replication and virus-induced cell fusion prior to extensive cellular destruction at 24 hours post-infection induced by Nipah virus (at the viral dose used in this experiment). For each timepoint, Nipah-, Hendra- or Sendai-infected cells were transcriptionally compared against uninfected cells (negative control) harvested at the same timepoint.

Cells were harvested at 5 hours, 10 hours, and 15 hours post-infection; at each timepoint, cells were lysed in 350 μL of buffer RLT from the RNeasy Micro Kit (Qiagen, 74004) and then triturated with 350 μL of 70% ethanol to inactivate infectious material for transfer out of the BSL4 laboratory. Then, RNA was extracted as per the manufacturer's instructions. After quality control procedures, polyadenylated mRNA was enriched using oligo(dT) beads. The mRNA was then fragmented randomly in fragmentation buffer, followed by cDNA synthesis using random hexamers and reverse transcriptase. After first-strand synthesis, a second-strand synthesis buffer (Illumina) was added with dNTPs, RNase H and E. coli polymerase I to generate the second strand by nick-translation. The final cDNA library was then subjected to a round of purification, terminal repair, A-tailing, ligation of sequencing adapters, size selection and PCR enrichment. RNA-seq libraries were sequenced on an Illumina NovaSeq 6000 sequencer by Novogene.

After obtaining RNA-seq reads, quality control was performed using FastQC (Andrews, 2010) and Trim Galore (Krueger, 2012) as described above (section "Bulk-population RNA-seq of uninfected cells"). Trimmed and filtered reads from each individual library (which was originally sequenced on multiple lanes) were then merged into a single pooled file for each library.

RNA-seq profiles of virus-infected cells contained both human and viral reads. To analyze human (host cell) transcripts, reads were aligned to the GRCh38 (hg38) *Homo sapiens* reference genome and gene-level RNA-seq counts were quantified using Kallisto (Bray et al., 2016). These counts were imported into RStudio and differential gene expression analyses of these counts were performed using DESeq2 (Love et al., 2014). For all samples, regularized log transformation was performed on the counts to remove the dependence of variance on the mean.

To determine the overall percentage of viral reads within a given RNA-seq sample, Kallisto (Bray et al., 2016) was used to align reads to the reference genomes of Nipah virus (NCBI accession number NC_002728), Hendra virus (NCBI accession number NC_001906) or Sendai virus (NCBI accession number NC_001552). This enabled the detection of all viral reads within a given sample. Then the number of total viral counts was divided over the number of total human + viral counts to estimate what proportion of the cellular transcriptome comprised viral transcripts.

To quantify the expression of specific viral genes, Kallisto was used to align reads to the following viral genes:

- For Nipah virus, reads were aligned to Nipah F (NC_002728.1:6370–8706 nucleotides), Nipah G (NC_002728.1:8710–11255 nucleotides), Nipah L (NC_002728.1:11259–18213 nucleotides), Nipah M (NC_002728.1:5008–6366

nucleotides), Nipah N (NC_002728.1:56–2297 nucleotides) and Nipah P/V/W/C (otherwise known as Nvgp2; NC_002728.1:2301–5004 nucleotides).

- For Hendra virus, reads were aligned to Hendra F (NC_001906.3:6346–8676 nucleotides), Hendra G (NC_001906.3:8680–11243 nucleotides), Hendra P/V/W/C (otherwise known as Hvgp2; NC_001906.3:2283–4980 nucleotides), Hendra L (NC_001906.3:11247–18201 nucleotides), Hendra M (NC_001906.3:4984–6342 nucleotides) and Hendra N (NC_001906.3:56–2279 nucleotides).
- For Sendai virus, reads were aligned to Sendai F (NC_001552.1:4866–6563 nucleotides), Sendai HN (NC_001552.1:6693–8420 nucleotides), Sendai L (NC_001552.1:8556–15242 nucleotides), Sendai M (NC_001552.1:3669–4715 nucleotides), Sendai NP (NC_001552.1:120–1694 nucleotides) and Sendai P/V/W/C (NC_001552.1:1844–3550 nucleotides).

Quantification of IFNβ secretion by virally-infected cells—H1 hPSC-derived, SUN004.1.9 hPSC-derived and SUN004.2 hPSC-derived artery and vein ECs in 48-well plates were inoculated with Nipah virus (5×10^4 $TCID_{50}$ units/well), Hendra virus (5×10^4 $TCID_{50}$ units/well), Sendai virus (15 HA units/well), or left uninfected (negative control), for 1 hour. For this experiment, a high viral dose (multiplicity of infection [MOI] ≈ 5) was used in order to synchronize infection in a large proportion of cells.

After 1 hour of viral infection, cells were washed twice in EGM2 medium, and then artery and vein cells were cultured in their respective growth media in standard incubator conditions (37°C, 5% CO_2). 12 and 24 hours later, supernatants (culture media) were harvested, and stored at −80 °C. Media was then thawed, and the concentration of secreted interferon-β (IFNβ) protein in the undiluted media was quantified using ELISA (enzyme-linked immunosorbent assay), specifically using the Human IFNβ Quantikine QuicKit ELISA Kit (R&D Systems, QK410) following the manufacturer's instructions. Absorbance was quantified using a TECAN Sunrise plate reader (Tecan Trading AG, Switzerland) with a spectral filter. The concentration of IFNβ in the samples was calculated by comparing the absorbance to that of a standard curve generated with human IFNβ, after subtracting background absorbance, using TECAN Magellan software. Data shown represent the average of results from three separate cell lines (H1, SUN004.1.9 and SUN004.2 hPSCs).

Calculation of case fatality rates—The case fatality rates of both Nipah and Hendra viruses are currently estimated at ~57–59%, and are referred to as such in this manuscript.

- Nipah virus: In a recent review (Ang et al., 2018), Nipah virus was recognized to have caused 326 fatalities among 573 human cases in the following regions: Malaysia and Singapore (1998–1999), India and Bangladesh (2001–2012) and the Philippines (2014). Additionally, the World Health Organization has recognized 48 fatalities among 65 new human cases in Bangladesh (2013–2015) and India (2018) (https://web.archive.org/web/20180613144643/ http://www.searo.who.int/entity/emerging_diseases/links/morbidity-and-mortality-nipah-sear-2001–2018.pdf?ua=1). Taken together,

Nipah virus is currently recognized to have caused 374 fatalities among 638 human cases (~58.6% case fatality rate).

- Hendra virus: Hendra virus is currently recognized to have caused 4 fatalities among 7 human cases in Australia (~57.1% case fatality rate) (Mahalingam et al., 2012).

QUANTIFICATION AND STATISTICAL ANALYSIS

Throughout this study, all error bars represent the standard error of the mean (s.e.m.) and a two-tailed t test was employed to determine statistical significance. Statistical significance values (P values) were reported in the figures and accompanying main text. Throughout all figures in this manuscript, wherever asterisks are used to denote statistical significance, *P<0.05 and **P<0.01, as defined in the figure legends. Statistical tests were implemented in Microsoft Excel and GraphPad Prism.

For qPCR analyses of differentiated hPSCs, for each experimental condition, two wells of cells in the same cell culture plate were analyzed (representing biological replicates) and for each of these wells, qPCR was performed twice in two separate wells of a 384-well qPCR plate (representing technical replicates). The average (mean) of these four datapoints is reported in histograms, and error bars represent the standard error of the mean.

For Diff-Quik staining of virally-infected hPSC-derived artery and vein cells, for each experimental condition, microscope images of five randomly-selected fields-of-view were generated. The number of nuclei per cell was quantified to determine syncytia formation: the average (mean) of data obtained from these five fields-of-view is reported in histograms, and error bars represent the standard error of the mean.

For qPCR analyses of viral replication in wild-type hPSC-derived artery and vein cells, for each experimental condition, three independent wells of cells in the same cell culture plate were analyzed (representing biological replicates). The average (mean) of these three datapoints is reported in histograms, and error bars represent the standard error of the mean.

For RNA-seq analyses of gene expression in virally-infected hPSC-derived artery and vein cells, for each experimental condition, two independent wells of cells in the same cell culture plate were analyzed (representing biological replicates). The average (mean) of these two datapoints is reported in histograms and heatmaps, and error bars represent the standard error of the mean.

For interferon-β secretion from virally-infected hPSC-derived artery and vein cells, for each experimental condition, three independent wells of cells in the same cell culture plate were analyzed (representing biological replicates). The average (mean) of these three datapoints is reported in histograms and heatmaps, and error bars represent the standard error of the mean.

Supplementary Material

Refer to Web version on PubMed Central for supplementary material.

ACKNOWLEDGMENTS

We thank A. Elefanty, E. Stanley and E. Ng for *MIXL1-GFP* and *SOX17-mCherry* hPSCs; the CDC Viral Special Pathogens Branch and M. Nakanishi for viruses; B. Lee, J. Weissman, A. Smith and O. Witte for plasmids; P. Rios, T. Nishimura, N. Pek, S. Miao, M. Gu and M. Rabinovitch for contributing to preliminary experiments; and M. Nichane, M.R. Corces, A. Kershner, A. Chang, I. Williams, P. Beachy, R. Nusse, K. Davis, B. Azizoglu, R. Saunders, W. Allen, S. Zheng, M. Blewett, I. Weissman, A. McCarty and J. Choi for reagents and advice. Infrastructure support was provided by the Stanford Stem Cell FACS Core and Animal Facility, Stanford Diabetes Genomics Analysis Core Facility (NIH P30DK116074), C. Carswell-Crumpton, M. Alvarez and L. Dunkin-Hubby. This work was supported by NIH (DP5OD024558 and R01HL128503), JDRF Northern California Center of Excellence, Additional Ventures Innovation Fund, Stanford Ludwig and Beckman Centers, Stanford Maternal and Child Health Research Institute, A*STAR Industrial Alignment Fund (H18/01/a0/017), Robert Koch Institute intramural funds, and the Anonymous, Fickel and Weintz families. This work was also supported by CIRM Bridges Program TB1-01195 (A.C. and A.T.N.); NIH T32GM119995 (R.M.M., J.L.F.) and T32GM007365 (T.C.); NDSEG and Stanford Bio-X Fellowships (J.L.F.); and the Assar Gabrielsson Foundation and Swedish Research Council (20170034, J.B.). L.T.A. is a Siebel Investigator. K.R.H. is an HHMI Investigator. K.M.L. and C.C. are Human Frontier Science Program Young Investigators (RGY0069/2019). K.M.L. is a Packard Foundation Fellow, Pew Scholar, Baxter Foundation Faculty Scholar and The Anthony DiGenova Endowed Faculty Scholar.

REFERENCES

Aljofan M, Saubern S, Meyer AG, Marsh G, Meers J, and Mungall BA (2009). Characteristics of Nipah virus and Hendra virus replication in different cell lines and their suitability for antiviral screening. Virus research 142, 92–99. 10.1016/j.virusres.2009.01.014. [PubMed: 19428741]

Andrews S.(2010). FastQC: A Quality Control Tool for High Throughput Sequence Data. http://www.bioinformatics.babraham.ac.uk/projects/fastqc/.

Ang BSP, Lim TCC, and Wang L.(2018). Nipah Virus Infection. Journal of Clinical Microbiology 56, e01875–01817-01810. 10.1128/JCM.01875-17.

Aranguren XL, Agirre X, Beerens M, Coppiello G, Uriz M, Vandersmissen I, Benkheil M, Panadero J, Aguado N, Pascual-Montano A, et al. (2013). Unraveling a novel transcription factor code determining the human arterial-specific endothelial cell signature. Blood 122, 3982–3992. 10.1182/blood-2013-02-483255. [PubMed: 24108462]

Arunkumar G, Chandni R, Mourya DT, Singh SK, Sadanandan R, Sudan P, Bhargava B, and Group N.I.P.a.H.S. (2019). Outbreak Investigation of Nipah Virus Disease in Kerala, India, 2018. The Journal of infectious diseases 219, 1867–1878. 10.1093/infdis/jiy612. [PubMed: 30364984]

Augustin HG, and Koh GY (2017). Organotypic vasculature: From descriptive heterogeneity to functional pathophysiology. Science 357. 10.1126/science.aal2379.

Babicki S, Arndt D, Marcu A, Liang Y, Grant JR, Maciejewski A, and Wishart DS (2016). Heatmapper: web-enabled heat mapping for all. Nucleic Acids Research 44, W147–153. 10.1093/nar/gkw419. [PubMed: 27190236]

Baseler L, de Wit E, Scott DP, Munster VJ, and Feldmann H.(2015). Syrian hamsters (Mesocricetus auratus) oronasally inoculated with a Nipah virus isolate from Bangladesh or Malaysia develop similar respiratory tract lesions. Veterinary pathology 52, 38–45. 10.1177/0300985814556189. [PubMed: 25352203]

Becht E, McInnes L, Healy J, Dutertre C-A, Kwok IWH, Ng LG, Ginhoux F, and Newell EW (2018). Dimensionality reduction for visualizing single-cell data using UMAP. Nature Biotechnology 37, 38–44. 10.1038/nbt.4314.

Bonaparte MI., Dimitrov AS., Bossart KN., Crameri G., Mungall BA., Bishop KA., Choudhry V., Dimitrov DS., Wang L-F., Eaton BT., and Broder CC. (2005). Ephrin-B2 ligand is a functional receptor for Hendra virus and Nipah virus. Proceedings of the National Academy of Sciences 102, 10652–10657. 10.1073/pnas.0504887102.

Bray NL, Pimentel H, Melsted P, and Pachter L.(2016). Near-optimal probabilistic RNA-seq quantification. Nature Biotechnology 34, 525–527. 10.1038/nbt.3519.

Cantell K, and Hirvonen S.(1981). Preparation and assay of Sendai virus. Methods in enzymology 78, 299–301. 10.1016/0076-6879(81)78131-x. [PubMed: 6173605]

Carmeliet P.(2005). Angiogenesis in life, disease and medicine. Nature 438, 932–936. 10.1038/nature04478. [PubMed: 16355210]

Casie Chetty S, Rost MS, Enriquez JR, Schumacher JA, Baltrunaite K, Rossi A, Stainier DYR, and Sumanas S.(2017). Vegf signaling promotes vascular endothelial differentiation by modulating etv2 expression. Developmental Biology 424, 147–161. 10.1016/j.ydbio.2017.03.005. [PubMed: 28279709]

CDC, and NIH. (2020). Biosafety in Microbiological and Biomedical Laboratories—6th Edition (U.S. Department of Health and Human Services).

Chen EY, Tan CM, Kou Y, Duan Q, Wang Z, Meirelles GV, Clark NR, and Ma'ayan A (2013). Enrichr: interactive and collaborative HTML5 gene list enrichment analysis tool. BMC Bioinformatics 14, 128–114. 10.1186/1471-2105-14-128. [PubMed: 23586463]

Childs K, Stock N, Ross C, Andrejeva J, Hilton L, Skinner M, Randall R, and Goodbourn S.(2007). mda-5, but not RIG-I, is a common target for paramyxovirus V proteins. Virology 359, 190–200. 10.1016/j.virol.2006.09.023. [PubMed: 17049367]

Chong DC, Koo Y, Xu K, Fu S, and Cleaver O.(2011). Stepwise arteriovenous fate acquisition during mammalian vasculogenesis. Developmental Dynamics 240, 2153–2165. 10.1002/dvdy.22706. [PubMed: 21793101]

Chua KB, Bellini WJ, Rota PA, Harcourt BH, Tamin A, Lam SK, Ksiazek TG, Rollin PE, Zaki SR, Shieh W, et al. (2000). Nipah virus: a recently emergent deadly paramyxovirus. Science 288, 1432–1435. 10.1126/science.288.5470.1432. [PubMed: 10827955]

Ciancanelli MJ, Volchkova VA, Shaw ML, Volchkov VE, and Basler CF (2009). Nipah virus sequesters inactive STAT1 in the nucleus via a P gene-encoded mechanism. Journal of Virology 83, 7828–7841. 10.1128/JVI.02610-08. [PubMed: 19515782]

Ciau-Uitz A, Pinheiro P, Kirmizitas A, Zuo J, and Patient R.(2013). VEGFA-dependent and -independent pathways synergise to drive Scl expression and initiate programming of the blood stem cell lineage in Xenopus. Development 140, 2632–2642. [PubMed: 23637333]

Corada M, Orsenigo F, Morini MF, Pitulescu ME, Bhat G, Nyqvist D, Breviario F, Conti V, Briot A, Iruela-Arispe ML, et al. (2013). Sox17 is indispensable for acquisition and maintenance of arterial identity. Nature Communications 4, 2609. 10.1038/ncomms3609.

Coultas L, Chawengsaksophak K, and Rossant J.(2005). Endothelial cells and VEGF in vascular development. Nature 438, 937–945. 10.1038/nature04479. [PubMed: 16355211]

Cradick TJ, Qiu P, Lee CM, Fine EJ, and Bao G.(2014). COSMID: A Web-based Tool for Identifying and Validating CRISPR/Cas Off-target Sites. Mol Ther Nucleic Acids 3, e214. 10.1038/mtna.2014.64. [PubMed: 25462530]

Davis RP, Ng ES, Costa M, Mossman AK, Sourris K, Elefanty AG, and Stanley EG (2008). Targeting a GFP reporter gene to the MIXL1 locus of human embryonic stem cells identifies human primitive streak-like cells and enables isolation of primitive hematopoietic precursors. Blood 111, 1876–1884. [PubMed: 18032708]

de Chaumont F, Dallongeville S, Chenouard N, Herve N, Pop S, Provoost T, Meas-Yedid V, Pankajakshan P, Lecomte T, Le Montagner Y, et al. (2012). Icy: an open bioimage informatics platform for extended reproducible research. Nat Methods 9, 690–696. 10.1038/nmeth.2075. [PubMed: 22743774]

De Val S, and Black BL (2009). Transcriptional control of endothelial cell development. Dev Cell 16, 180–195. 10.1016/j.devcel.2009.01.014. [PubMed: 19217421]

DeBuysscher BL, de Wit E, Munster VJ, Scott D, Feldmann H, and Prescott J.(2013). Comparison of the pathogenicity of Nipah virus isolates from Bangladesh and Malaysia in the Syrian hamster. PLoS neglected tropical diseases 7, e2024. 10.1371/journal.pntd.0002024. [PubMed: 23342177]

Ditadi A., Sturgeo CM., Tobe J., Awon G., Kenned M., Yzaguirr AD., Azzol L., N ES., Stanle EG., Frenc DL., et al. . (2015). Human definitive haemogenic endothelium and arterial vascular endothelium represent distinct lineages. Nature Cell Biology 17, 580–591. 10.1038/ncb3161. [PubMed: 25915127]

Drubin DG, and Hyman AA (2017). Stem cells: the new “model organism”. Molecular Biology of the Cell 28, 1409–1411. 10.1091/mbc.E17-03-0183. [PubMed: 28559439]

Duarte A, Hirashima M, Benedito R, Trindade A, Diniz P, Bekman E, Costa L, Henrique D, and Rossant J.(2004). Dosage-sensitive requirement for mouse Dll4 in artery development. Genes & Development 18, 2474–2478. 10.1101/gad.1239004. [PubMed: 15466159]

Ellis EL, and Delbrück M.(1939). THE GROWTH OF BACTERIOPHAGE. The Journal of general physiology 22, 365–384. 10.1085/jgp.22.3.365. [PubMed: 19873108]

Elvert M, Sauerhering L, and Maisner A.(2020). Cytokine Induction in Nipah Virus-Infected Primary Human and Porcine Bronchial Epithelial Cells. The Journal of infectious diseases 221, S395–S400. 10.1093/infdis/jiz455. [PubMed: 31665348]

Erbar S, Diederich S, and Maisner A.(2008). Selective receptor expression restricts Nipah virus infection of endothelial cells. Virology journal 5, 142–146. 10.1186/1743-422X-5-142. [PubMed: 19036148]

Fang J, and Hirschi K.(2019). Molecular regulation of arteriovenous endothelial cell specification. F1000Research 8, 1208. 10.12688/f1000research.16701.1.

Fish JE, and Wythe JD (2015). The molecular regulation of arteriovenous specification and maintenance. Developmental Dynamics 244, 391–409. 10.1002/dvdy.24252. [PubMed: 25641373]

Fowler JL, Ang LT, and Loh KM (2019). A critical look: Challenges in differentiating human pluripotent stem cells into desired cell types and organoids. Wiley Interdisciplinary Reviews: Developmental Biology 113, 891–823. 10.1002/wdev.368.

Gage BK, Liu JC, Innes BT, MacParland SA, McGilvray ID, Bader GD, and Keller GM (2020). Generation of Functional Liver Sinusoidal Endothelial Cells from Human Pluripotent Stem-Cell-Derived Venous Angioblasts. Cell Stem Cell. 10.1016/j.stem.2020.06.007.

Gale NW, Dominguez MG, Noguera I, Pan L, Hughes V, Valenzuela DM, Murphy AJ, Adams NC, Lin HC, Holash J, et al. (2004). Haploinsufficiency of delta-like 4 ligand results in embryonic lethality due to major defects in arterial and vascular development. Proceedings of the National Academy of Sciences of the United States of America 101, 15949–15954. [PubMed: 15520367]

Geisbert TW, Daddario-DiCaprio KM, Hickey AC, Smith MA, Chan Y-P, Wang L-F, Mattapallil JJ, Geisbert JB, Bossart KN, and Broder CC (2010). Development of an acute and highly pathogenic nonhuman primate model of Nipah virus infection. PLoS ONE 5, e10690. 10.1371/journal.pone.0010690.

Goldstein AS, Drake JM, Burnes DL, Finley DS, Zhang H, Reiter RE, Huang J, and Witte ON (2011). Purification and direct transformation of epithelial progenitor cells from primary human prostate. Nature Protocols 6, 656–667. 10.1038/nprot.2011.317. [PubMed: 21527922]

Gomez Roman R, Tornieporth N, Cherian NG, Shurtleff AC, L'Azou Jackson M, Yeskey D, Hacker A, Mungai E, and Le TT (2021). Medical countermeasures against henipaviruses: a review and public health perspective. Lancet Infect Dis. 10.1016/S1473-3099(21)00400-X.

Hafemeister C, and Satija R.(2019). Normalization and variance stabilization of single-cell RNA-seq data using regularized negative binomial regression. Genome Biology, 1–15. 10.1186/s13059-019-1874-1.

Halaidych OV, Freund C, van den Hil F, Salvatori DCF, Riminucci M, Mummery CL, and Orlova VV (2018). Inflammatory Responses and Barrier Function of Endothelial Cells Derived from Human Induced Pluripotent Stem Cells. Stem Cell Reports 10, 1642–1656. 10.1016/j.stemcr.2018.03.012. [PubMed: 29657098]

Harcourt BH, Tamin A, Ksiazek TG, Rollin PE, Anderson LJ, Bellini WJ, and Rota PA (2000). Molecular characterization of Nipah virus, a newly emergent paramyxovirus. Virology 271, 334–349. 10.1006/viro.2000.0340. [PubMed: 10860887]

Harschnit O., and Stude L. (2021). Human stem cell models to study host-virus interactions in the central nervous system. Nature Reviews Immunology, 1–13. 10.1038/s41577-020-00474-y.

Hong CC, Peterson QP, Hong J-Y, and Peterson RT (2006). Artery/vein specification is governed by opposing phosphatidylinositol-3 kinase and MAP kinase/ERK signaling. Curr Biol 16, 1366–1372. [PubMed: 16824925]

Iwano S, Sugiyama M, Hama H, Watakabe A, Hasegawa N, Kuchimaru T, Tanaka KZ, Takahashi M, Ishida Y, Hata J, et al. (2018). Single-cell bioluminescence imaging of deep tissue in freely moving animals. Science 359, 935–939. 10.1126/science.aaq1067. [PubMed: 29472486]

Kälin RE, Kretz MP, Meyer AM, Kispert A, Heppner FL, and Brändli AW (2007). Paracrine and autocrine mechanisms of apelin signaling govern embryonic and tumor angiogenesis. Developmental Biology 305, 599–614. 10.1016/j.ydbio.2007.03.004. [PubMed: 17412318]

Kalucka J, de Rooij LPMH, Goveia J, Rohlenova K, Dumas SJ, Meta E, Conchinha NV, Taverna F, Teuwen L-A, Veys K, et al. (2020). Single-Cell Transcriptome Atlas of Murine Endothelial Cells. Cell, 1–37. 10.1016/j.cell.2020.01.015.

Kidoya H, Naito H, Muramatsu F, Yamakawa D, Jia W, Ikawa M, Sonobe T, Tsuchimochi H, Shirai M, Adams RH, et al. (2015). APJ Regulates Parallel Alignment of Arteries and Veins in the Skin. Developmental Cell 33, 247–259. 10.1016/j.devcel.2015.02.024. [PubMed: 25920569]

Krebs LT, Shutter JR, Tanigaki K, Honjo T, Stark KL, and Gridley T.(2004). Haploinsufficient lethality and formation of arteriovenous malformations in Notch pathway mutants. Genes & Development 18, 2469–2473. 10.1101/gad.1239204. [PubMed: 15466160]

Krueger F.(2012). Trim Galore. https://www.bioinformatics.babraham.ac.uk/projects/trim_galore/.

Kuleshov MV, Jones MR, Rouillard AD, Fernandez NF, Duan Q, Wang Z, Koplev S, Jenkins SL, Jagodnik KM, Lachmann A, et al. (2016). Enrichr: a comprehensive gene set enrichment analysis web server 2016 update. Nucleic Acids Research 44, W90–97. 10.1093/nar/gkw377. [PubMed: 27141961]

Kurian L, Sancho-Martinez I, Nivet E, Aguirre A, Moon K, Pendaries C, Volle-Challier C, Bono F, Herbert J-M, Pulecio J, et al. (2012). Conversion of human fibroblasts to angioblast-like progenitor cells. Nature methods.

Kurokawa YK, Yin RT, Shang MR, Shirure VS, Moya ML, and George SC (2017). Human Induced Pluripotent Stem Cell-Derived Endothelial Cells for Three-Dimensional Microphysiological Systems. Tissue engineering. Part C, Methods 23, 474–484. 10.1089/ten.tec.2017.0133. [PubMed: 28622076]

Labun K, Montague TG, Krause M, Torres Cleuren YN, Tjeldnes H, and Valen E.(2019). CHOPCHOP v3: expanding the CRISPR web toolbox beyond genome editing. Nucleic Acids Res 47, W171–W174. 10.1093/nar/gkz365. [PubMed: 31106371]

Law CW, Chen Y, Shi W, and Smyth GK (2014). voom: Precision weights unlock linear model analysis tools for RNA-seq read counts. Genome Biol 15, R29. 10.1186/gb-2014-15-2-r29. [PubMed: 24485249]

Lawson ND, Scheer N, Pham VN, Kim CH, Chitnis AB, Campos-Ortega JA, and Weinstein BM (2001). Notch signaling is required for arterial-venous differentiation during embryonic vascular development. Development 128, 3675–3683. [PubMed: 11585794]

Lawson ND, Vogel AM, and Weinstein BM (2002). sonic hedgehog and vascular endothelial growth factor act upstream of the Notch pathway during arterial endothelial differentiation. Developmental Cell 3, 127–136. [PubMed: 12110173]

Lian X, Bao X, Al-Ahmad A, Liu J, Wu Y, Dong W, Dunn KK, Shusta EV, and Palecek SP (2014). Efficient Differentiation of Human Pluripotent Stem Cells to Endothelial Progenitors via Small-Molecule Activation of WNT Signaling. Stem Cell Reports 3, 804–816. 10.1016/j.stemcr.2014.09.005. [PubMed: 25418725]

Lin F-J, Tsai M-J, and Tsai SY (2007). Artery and vein formation: a tug of war between different forces. EMBO Rep 8, 920–924. [PubMed: 17906673]

Lin Y, Gil C-H, and Yoder MC (2017). Differentiation, Evaluation, and Application of Human Induced Pluripotent Stem Cell-Derived Endothelial Cells. Arteriosclerosis, Thrombosis, and Vascular Biology, ATVBAHA.117.309962. 10.1161/ATVBAHA.117.309962.

Lo MK, Miller D, Aljofan M, Mungall BA, Rollin PE, Bellini WJ, and Rota PA (2010). Characterization of the antiviral and inflammatory responses against Nipah virus in endothelial cells and neurons. Virology 404, 78–88. 10.1016/j.virol.2010.05.005. [PubMed: 20552729]

Loh KM, Ang LT, Zhang J, Kumar V, Ang J, Auyeong JQ, Lee KL, Choo SH, Lim CYY, Nichane M, et al. (2014). Efficient Endoderm Induction from Human Pluripotent Stem Cells by Logically Directing Signals Controlling Lineage Bifurcations. Cell Stem Cell 14, 237–252. [PubMed: 24412311]

Loh KM., Chen A., Koh PW., Deng TZ., Sinha R., Tsai JM., Barkal AA., Shen KY., Jain R., Morganti RM., et al. . (2016). Mapping the Pairwise Choices Leading from Pluripotency to Human Bone, Heart, and Other Mesoderm Cell Types. Cell 166, 451–467. 10.1016/j.cell.2016.06.011. [PubMed: 27419872]

López CB, Yount JS, Hermesh T, and Moran TM (2006). Sendai virus infection induces efficient adaptive immunity independently of type I interferons. Journal of Virology 80, 4538–4545. 10.1128/JVI.80.9.4538-4545.2006. [PubMed: 16611914]

Love MI, Huber W, and Anders S.(2014). Moderated estimation of fold change and dispersion for RNA-seq data with DESeq2. Genome Biology 15, 550. 10.1186/s13059-014-0550-8. [PubMed: 25516281]

Lu X, le Noble F, Yuan L, Jiang Q, De Lafarge B, Sugiyama D, Bréant C, Claes F, De Smet F, Thomas J-L, et al. (2004). The netrin receptor UNC5B mediates guidance events controlling morphogenesis of the vascular system. Nature 432, 179–186. 10.1038/nature03080. [PubMed: 15510105]

Mahalingam S, Herrero LJ, Playford EG, Spann K, Herring B, Rolph MS, Middleton D, McCall B, Field H, and Wang LF (2012). Hendra virus: an emerging paramyxovirus in Australia. Lancet Infect Dis 12, 799–807. 10.1016/S1473-3099(12)70158-5. [PubMed: 22921953]

Martin RM, Ikeda K, Cromer MK, Uchida N, Nishimura T, Romano R, Tong AJ, Lemgart VT, Camarena J, Pavel-Dinu M, et al. (2019). Highly Efficient and Marker-free Genome Editing of Human Pluripotent Stem Cells by CRISPR-Cas9 RNP and AAV6 Donor-Mediated Homologous Recombination. Cell Stem Cell 24, 821–828.e825. 10.1016/j.stem.2019.04.001. [PubMed: 31051134]

Masaki H, Kato-Itoh M, Takahashi Y, Umino A, Sato H, Ito K, Yanagida A, Nishimura T, Yamaguchi T, Hirabayashi M, et al. (2016). Inhibition of Apoptosis Overcomes Stage-Related Compatibility Barriers to Chimera Formation in Mouse Embryos. Cell Stem Cell 19, 587–592. 10.1016/j.stem.2016.10.013. [PubMed: 27814480]

Mathieu C, Guillaume V, Sabine A, Ong KC, Wong KT, Legras-Lachuer C, and Horvat B.(2012). Lethal Nipah virus infection induces rapid overexpression of CXCL10. PLoS ONE 7, e32157. 10.1371/journal.pone.0032157.

McCracken IR, Taylor RS, Kok FO, de la Cuesta F, Dobie R, Henderson BEP, Mountford JC, Caudrillier A, Henderson NC, Ponting CP, and Baker AH (2019). Transcriptional dynamics of pluripotent stem cell-derived endothelial cell differentiation revealed by single-cell RNA sequencing. European Heart Journal 385, 9963117. 10.1093/eurheartj/ehz351.

Mehand MS, Al-Shorbaji F, Millett P, and Murgue B.(2018). The WHO R&D Blueprint: 2018 review of emerging infectious diseases requiring urgent research and development efforts. Antiviral research 159, 63–67. 10.1016/j.antiviral.2018.09.009. [PubMed: 30261226]

Metzger T, Gache V, Xu M, Cadot B, Folker ES, Richardson BE, Gomes ER, and Baylies MK (2012). MAP and kinesin-dependent nuclear positioning is required for skeletal muscle function. Nature 484, 120–124. 10.1038/nature10914. [PubMed: 22425998]

Monaghan P, Green D, Pallister J, Klein R, White J, Williams C, McMillan P, Tilley L, Lampe M, Hawes P, and Wang L-F (2014). Detailed morphological characterisation of Hendra virus infection of different cell types using super-resolution and conventional imaging. Virology journal 11, 1–12. 10.1186/s12985-014-0200-5. [PubMed: 24393133]

Murray K, Selleck P, Hooper P, Hyatt A, Gould A, Gleeson L, Westbury H, Hiley L, Selvey L, and Rodwell B.(1995). A morbillivirus that caused fatal disease in horses and humans. Science 268, 94–97. 10.1126/science.7701348. [PubMed: 7701348]

Nakatsu MN, Davis J, and Hughes CCW (2007). Optimized fibrin gel bead assay for the study of angiogenesis. Journal of visualized experiments : JoVE, 186. 10.3791/186.

Negrete OA., Chu D., Aguilar HC., and Lee B. (2007). Single amino acid changes in the Nipah and Hendra virus attachment glycoproteins distinguish ephrinB2 from ephrinB3 usage. Journal of Virology 81, 10804–10814. 10.1128/JVI.00999-07. [PubMed: 17652392]

Negrete OA, Levroney EL, Aguilar HC, Bertolotti-Ciarlet A, Nazarian R, Tajyar S, and Lee B.(2005). EphrinB2 is the entry receptor for Nipah virus, an emergent deadly paramyxovirus. Nature 436, 401–405. 10.1038/nature03838. [PubMed: 16007075]

Ng AHM, Khoshakhlagh P, Rojo Arias JE, Pasquini G, Wang K, Swiersy A, Shipman SL, Appleton E, Kiaee K, Kohman RE, et al. (2020). A comprehensive library of human transcription factors for cell fate engineering. Nature Biotechnology 51, 987. 10.1038/s41587-020-0742-6.

Nguyen J, Lin Y-Y, and Gerecht S.(2021). The next generation of endothelial differentiation: Tissue-specific ECs. Cell Stem Cell 28, 1188–1204. 10.1016/j.stem.2021.05.002. [PubMed: 34081899]

Nguyen MTX, Okina E, Chai X, Tan KH, Hovatta O, Ghosh S, and Tryggvason K.(2016). Differentiation of Human Embryonic Stem Cells to Endothelial Progenitor Cells on Laminins in Defined and Xeno-free Systems. Stem Cell Reports 7, 802–816. 10.1016/j.stemcr.2016.08.017. [PubMed: 27693424]

Nishimura K, Ohtaka M, Takada H, Kurisaki A, Tran NVK, Tran YTH, Hisatake K, Sano M, and Nakanishi M.(2017). Simple and effective generation of transgene-free induced pluripotent stem cells using an auto-erasable Sendai virus vector responding to microRNA-302. Stem Cell Research 23, 13–19. 10.1016/j.scr.2017.06.011. [PubMed: 28666145]

Nishimura K, Sano M, Ohtaka M, Furuta B, Umemura Y, Nakajima Y, Ikehara Y, Kobayashi T, Segawa H, Takayasu S, et al. (2011). Development of defective and persistent Sendai virus vector: a unique gene delivery/expression system ideal for cell reprogramming. The Journal of biological chemistry 286, 4760–4771. 10.1074/jbc.M110.183780. [PubMed: 21138846]

Olmer R, Engels L, Usman A, Menke S, Malik MNH, Pessler F, Göhring G, Bornhorst D, Bolten S, Abdelilah-Seyfried S, et al. (2018). Differentiation of Human Pluripotent Stem Cells into Functional Endothelial Cells in Scalable Suspension Culture. Stem Cell Reports 10, 1657–1672. 10.1016/j.stemcr.2018.03.017. [PubMed: 29681541]

Ouyang JF, Kamaraj US, Cao EY, and Rackham OJL (2021). ShinyCell: Simple and sharable visualisation of single-cell gene expression data. Bioinformatics. 10.1093/bioinformatics/btab209.

Paik DT, Tian L, Lee J, Sayed N, Chen IY, Rhee S, Rhee J-W, Kim Y, Wirka RC, Buikema JW, et al. (2018). Large-Scale Single-Cell RNA-Seq Reveals Molecular Signatures of Heterogeneous Populations of Human Induced Pluripotent Stem Cell-Derived Endothelial Cells. Circulation Research. 10.1161/CIRCRESAHA.118.312913.

Palomares K, Vigant F, Van Handel B, Pernet O, Chikere K, Hong P, Sherman SP, Patterson M, An DS, Lowry WE, et al. (2013). Nipah virus envelope-pseudotyped lentiviruses efficiently target ephrinB2-positive stem cell populations in vitro and bypass the liver sink when administered in vivo. Journal of Virology 87, 2094–2108. 10.1128/JVI.02032-12. [PubMed: 23192877]

Park MA, Kumar A, Jung HS, Uenishi G, Moskvin OV, Thomson JA, and Slukvin II (2018). Activation of the Arterial Program Drives Development of Definitive Hemogenic Endothelium with Lymphoid Potential. Cell Reports 23, 2467–2481. 10.1016/j.celrep.2018.04.092. [PubMed: 29791856]

Patsch C, Challet-Meylan L, Thoma EC, Urich E, Heckel T, O'Sullivan JF, Grainger SJ, Kapp FG, Sun L, Christensen Ket al. . (2015). Generation of vascular endothelial and smooth muscle cells from human pluripotent stem cells. Nature Cell Biology 17, 994–1003. 10.1038/ncb3205. [PubMed: 26214132]

Poduri A, Chang AH, Raftrey B, Rhee S, Van M, and Red-Horse K.(2017). Endothelial cells respond to the direction of mechanical stimuli through SMAD signaling to regulate coronary artery size. Development 144, 3241–3252. 10.1242/dev.150904. [PubMed: 28760815]

Potente M, and Mäkinen T.(2017). Vascular heterogeneity and specialization in development and disease. Nature Reviews Molecular Cell Biology 18, 477–494. 10.1038/nrm.2017.36. [PubMed: 28537573]

Prescott J., DeBuysscher BL., Feldmann F., Gardner DJ., Haddock E., Martellaro C., Scott D., and Feldmann H. (2015). Single-dose live-attenuated vesicular stomatitis virus-based vaccine protects African green monkeys from Nipah virus disease. Vaccine 33, 2823–2829. 10.1016/j.vaccine.2015.03.089. [PubMed: 25865472]

Rafii S, Butler JM, and Ding B-S (2016). Angiocrine functions of organ-specific endothelial cells. Nature 529, 316–325. 10.1038/nature17040. [PubMed: 26791722]

Red-Horse K, and Siekmann AF (2019). Veins and Arteries Build Hierarchical Branching Patterns Differently: Bottom-Up versus Top-Down. BioEssays 41, e1800198. 10.1002/bies.201800198.

Reich M, Liefeld T, Gould J, Lerner J, Tamayo P, and Mesirov JP (2006). GenePattern 2.0. Nature Genetics 38, 500–501. 10.1038/ng0506-500. [PubMed: 16642009]

Ritchie ME, Phipson B, Wu D, Hu Y, Law CW, Shi W, and Smyth GK (2015). limma powers differential expression analyses for RNA-sequencing and microarray studies. Nucleic Acids Res 43, e47. 10.1093/nar/gkv007. [PubMed: 25605792]

Robinson MD, McCarthy DJ, and Smyth GK (2010). edgeR: a Bioconductor package for differential expression analysis of digital gene expression data. Bioinformatics 26, 139–140. 10.1093/bioinformatics/btp616. [PubMed: 19910308]

Rodriguez JJ, Parisien J-P, and Horvath CM (2002). Nipah virus V protein evades alpha and gamma interferons by preventing STAT1 and STAT2 activation and nuclear accumulation. Journal of Virology 76, 11476–11483. 10.1128/jvi.76.22.11476-11483.2002. [PubMed: 12388709]

Rosa S, Praça C, Pitrez PR, Gouveia PJ, Aranguren XL, Ricotti L, and Ferreira LS (2019). Functional characterization of iPSC-derived arterial- and venous-like endothelial cells. Scientific Reports 9, 3826–3815. 10.1038/s41598-019-40417-9. [PubMed: 30846769]

Sakamoto Y, Hara K, Kanai-Azuma M, Matsui T, Miura Y, Tsunekawa N, Kurohmaru M, Saijoh Y, Koopman P, and Kanai Y.(2007). Redundant roles of Sox17 and Sox18 in early cardiovascular development of mouse embryos. Biochem Biophys Res Commun 360, 539–544. [PubMed: 17610846]

Schindelin J, Arganda-Carreras I, Frise E, Kaynig V, Longair M, Pietzsch T, Preibisch S, Rueden C, Saalfeld S, Schmid B, et al. (2012). Fiji: an open-source platform for biological-image analysis. Nat Methods 9, 676–682. 10.1038/nmeth.2019. [PubMed: 22743772]

Schountz T, Campbell C, Wagner K, Rovnak J, Martellaro C, DeBuysscher B, Feldmann H, and Prescott J.(2019). Differential Innate Immune Responses Elicited by Nipah Virus and Cedar Virus Correlate with Disparate In Vivo Pathogenesis in Hamsters. Viruses 11, 291–211. 10.3390/v11030291. [PubMed: 30909389]

Shalaby F, Rossant J, Yamaguchi TP, Gertsenstein M, Wu XF, Breitman ML, and Schuh AC (1995). Failure of blood-island formation and vasculogenesis in Flk-1-deficient mice. Nature 376, 62–66. [PubMed: 7596435]

Shaw AE, Hughes J, Gu Q, Behdenna A, Singer JB, Dennis T, Orton RJ, Varela M, Gifford RJ, Wilson SJ, and Palmarini M.(2017). Fundamental properties of the mammalian innate immune system revealed by multispecies comparison of type I interferon responses. PLoS Biology 15, e2004086. 10.1371/journal.pbio.2004086.

Shin JW, Huggenberger R, and Detmar M.(2008). Transcriptional profiling of VEGF-A and VEGF-C target genes in lymphatic endothelium reveals endothelial-specific molecule-1 as a novel mediator of lymphangiogenesis. Blood 112, 2318–2326. 10.1182/blood-2008-05-156331. [PubMed: 18614759]

Simoneau CR, and Ott M.(2020). Modeling Multi-organ Infection by SARS-CoV-2 Using Stem Cell Technology. Cell Stem Cell 27, 859–868. 10.1016/j.stem.2020.11.012. [PubMed: 33275899]

Sriram G, Tan JY, Islam I, Rufaihah AJ, and Cao T.(2015). Efficient differentiation of human embryonic stem cells to arterial and venous endothelial cells under feeder- and serum- free conditions. Stem Cell Research & Therapy, 1–17. 10.1186/s13287-015-0260-5. [PubMed: 25559585]

Stuart T, Butler A, Hoffman P, Hafemeister C, Papalexi E, Mauck WM, Hao Y, Stoeckius M, Smibert P, and Satija R.(2019). Comprehensive Integration of Single-Cell Data. Cell 177, 1888–1902.e1821. 10.1016/j.cell.2019.05.031. [PubMed: 31178118]

Tai-Nagara I., Yoshikawa Y., Numata N., Ando T., Okabe K., Sugiura Y., Ieda M., Takakura N., Nakagawa O., Zhou B., et al. . (2017). Placental labyrinth formation in mice requires endothelial FLRT2/UNC5B signaling. Development 144, 2392–2401. 10.1242/dev.149757. [PubMed: 28576770]

Takashima Y, Guo G, Loos R, Nichols J, Ficz G, Krueger F, Oxley D, Santos F, Clarke J, Mansfield W, et al. (2014). Resetting Transcription Factor Control Circuitry toward Ground-State Pluripotency in Human. Cell 158, 1254–1269. 10.1016/j.cell.2014.08.029. [PubMed: 25215486]

Tinevez JY, Perry N, Schindelin J, Hoopes GM, Reynolds GD, Laplantine E, Bednarek SY, Shorte SL, and Eliceiri KW (2017). TrackMate: An open and extensible platform for single-particle tracking. Methods 115, 80–90. 10.1016/j.ymeth.2016.09.016. [PubMed: 27713081]

Travaglini KJ, Nabhan AN, Penland L, Sinha R, Gillich A, Sit RV, Chang S, Conley SD, Mori Y, Seita J, et al. (2020). A molecular cell atlas of the human lung from single-cell RNA sequencing. Nature 587, 619–625. 10.1038/s41586-020-2922-4. [PubMed: 33208946]

Virtue ER, Marsh GA, and Wang LF (2011). Interferon Signaling Remains Functional during Henipavirus Infection of Human Cell Lines. Journal of Virology 85, 4031–4034. 10.1128/JVI.02412-10. [PubMed: 21289115]

Wang HU, Chen ZF, and Anderson DJ (1998). Molecular distinction and angiogenic interaction between embryonic arteries and veins revealed by ephrin-B2 and its receptor Eph-B4. Cell 93, 741–753. [PubMed: 9630219]

Wang K, Lin R-Z, Hong X, Ng AH, Lee CN, Neumeyer J, Wang G, Wang X, Ma M, Pu WT, et al. (2020). Robust differentiation of human pluripotent stem cells into endothelial cells via temporal modulation of ETV2 with modified mRNA. Science Advances 6, eaba7606. 10.1126/sciadv.aba7606.

Wickham H.(2016). ggplot2: Elegant Graphics for Data Analysis (Springer-Verlag New York).

Wickham H, Averick M, Bryan J, and Chang W.(2019). Welcome to the Tidyverse. The Journal of Open Source Software. 10.21105/joss.01686.

Wickham H, François R, Henry L, and Müller K.(2022). dplyr: A Grammar of Data Manipulation. https://dplyr.tidyverse.org.

Wong KT, Shieh W-J, Kumar S, Norain K, Abdullah W, Guarner J, Goldsmith CS, Chua KB, Lam SK, Tan CT, et al. (2002). Nipah virus infection: pathology and pathogenesis of an emerging paramyxoviral zoonosis. The American Journal of Pathology 161, 2153–2167. 10.1016/S0002-9440(10)64493-8. [PubMed: 12466131]

Xu C, Hasan SS, Schmidt I, Rocha SF, Pitulescu ME, Bussmann J, Meyen D, Raz E, Adams RH, and Siekmann AF (2014). Arteries are formed by vein-derived endothelial tip cells. Nature Communications 5, 5758. 10.1038/ncomms6758.

Yoshida A, Kawabata R, Honda T, Sakai K, Ami Y, Sakaguchi T, and Irie T.(2018). A Single Amino Acid Substitution within the Paramyxovirus Sendai Virus Nucleoprotein Is a Critical Determinant for Production of Interferon-Beta-Inducing Copyback-Type Defective Interfering Genomes. Journal of Virology 92. 10.1128/JVI.02094-17.

Zeng Y, He J, Bai Z, Li Z, Gong Y, Liu C, Ni Y, Du J, Ma C, Bian L, et al. (2019). Tracing the first hematopoietic stem cell generation in human embryo by single-cell RNA sequencing. Cell Research, 1–14. 10.1038/s41422-019-0228-6. [PubMed: 30514898]

Zhang J, Chu L-F, Hou Z, Schwartz MP, Hacker T, Vickerman V, Swanson S, Leng N, Nguyen BK, Elwell A, et al. (2017). Functional characterization of human pluripotent stem cell-derived arterial endothelial cells. Proceedings of the National Academy of Sciences of the United States of America, 201702295. 10.1073/pnas.1702295114.

Zheng GXY., Terry JM., Belgrader P., Ryvkin P., Bent ZW., Wilson R., Ziraldo SB., Wheeler TD., McDermott GP., Zhu J., et al. . (2017). Massively parallel digital transcriptional profiling of single cells. Nature Communications 8, 14049. 10.1038/ncomms14049.

HIGHLIGHTS

- Efficient, rapid generation of >90% pure human artery and vein cells in 3–4 days
- Precisely inducing artery cells by blocking vein-specifying cues and *vice versa*
- Nipah and Hendra viruses preferentially infect artery (rather than vein) cells
- Human pluripotent stem cells provide a new platform for biosafety-level-4 virology

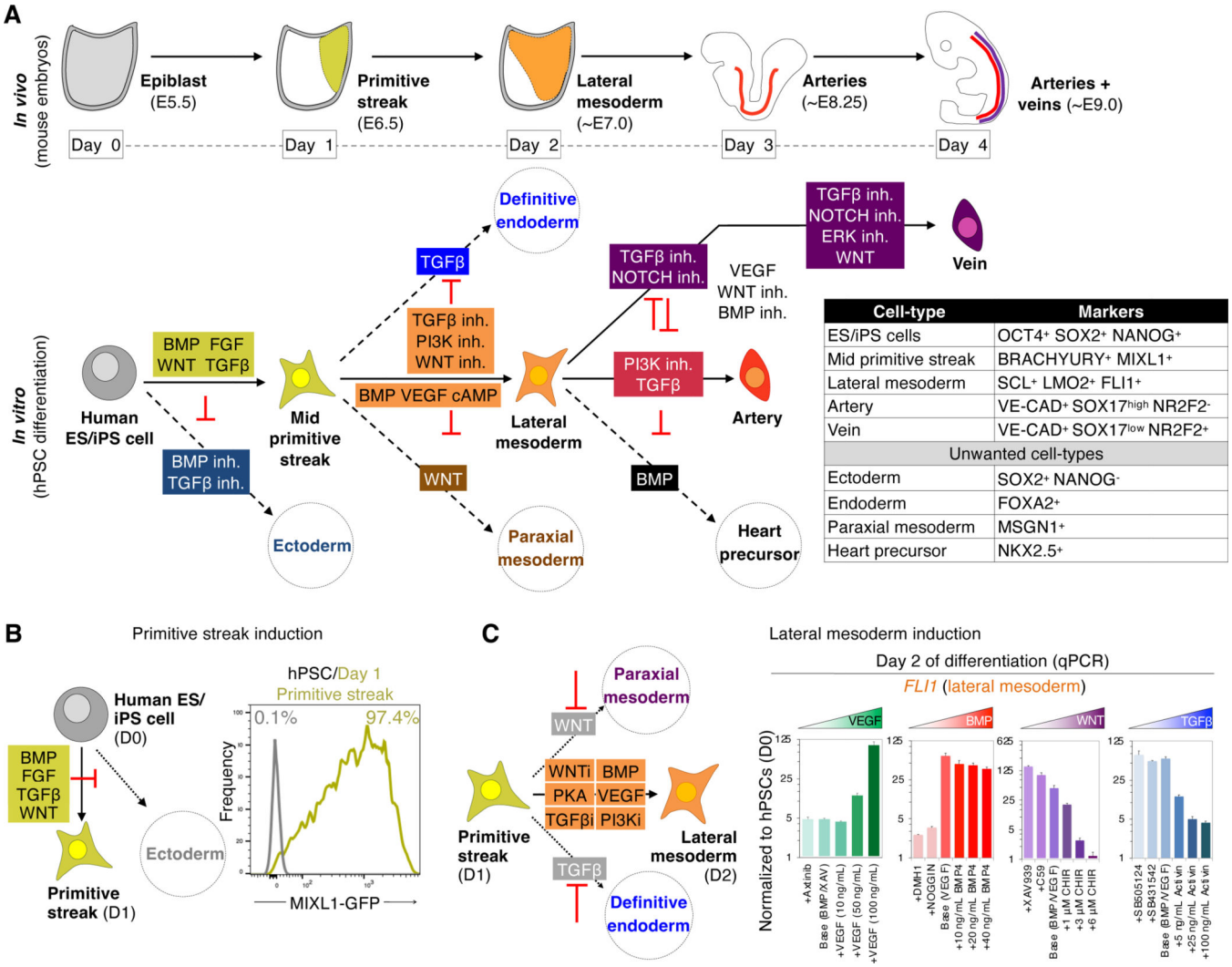

Figure 1: Efficient generation of human primitive streak and lateral mesoderm from hPSCs within 1 and 2 days, respectively

A) Artery and vein development

B) Generating MIXL1^{+} mid primitive streak within 24 hours of hPSC differentiation (Loh et al., 2016), assayed by flow cytometry of *MIXL1-GFP* hPSCs (Davis et al., 2008)

C) VEGF and BMP specify, whereas TGFβ and WNT repress, day 2 lateral mesoderm. Day 1 hPSC-derived primitive streak was treated with the indicated signals (concentrations indicated, and 10 nM Axitinib; 200 ng/mL NOGGIN; 1 μM DMH1, XAV939 and C59; 2 μM SB505124 and SB431542; base conditions contained 10 ng/mL BMP4 and/or 100 ng/mL VEGF) for 24 hours; qPCR was performed on day 2.

See also Figure S1 and Table S5

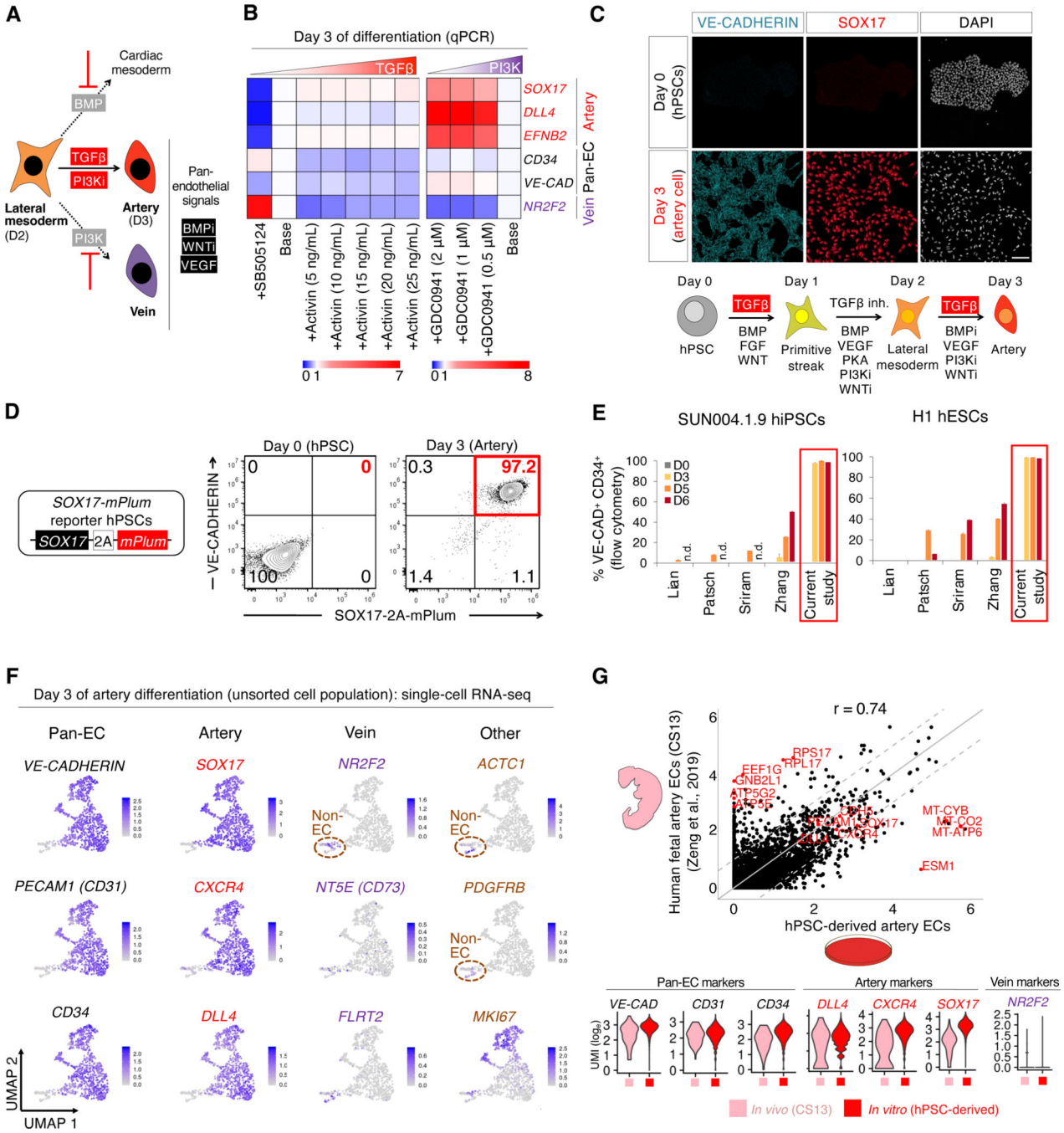

Figure 2: Efficient generation of human artery endothelial cells from hPSCs within 3 days

A) Summary of present work

B) TGFβ promotes, while PI3K inhibits, day 3 artery formation. Day 2 hPSC-derived lateral mesoderm was treated with the indicated signals, including TGFβ agonist (Activin, 5–25 ng/mL), TGFβ inhibitor (SB505124, 2 μM) or PI3K inhibitor (GDC0941, 0.5–2 μM), for 24 hours; qPCR was performed on day 2 (base media: GDC0941+VEGF+XAV939+AA2P+TTNPB [*left*] and

VEGF+XAV939+AA2P+TTNPB+Activin [*right*]). Gene expression was normalized to the base media lacking TGFβ or PI3K modulators.

C) Immunostaining of H1 hPSCs either before or after differentiation into day 3 artery ECs; scale = 100 μm

D) Flow cytometry of *SOX17–2A-mPlum* hPSCs before or after differentiation into day 3 artery ECs

E) H1 and SUN004.1.9 hPSC lines differentiated using the present artery EC induction method or 4 prevailing EC differentiation protocols (Lian et al., 2014; Patsch et al., 2015; Sriram et al., 2015; Zhang et al., 2017); flow cytometry was performed on days 0, 3, 5 and 6 of differentiation; n.d. = not determined

F) scRNAseq of H1 hPSCs differentiated towards artery ECs; the entire day 3 cell population was harvested without pre-selecting ECs; gene expression in $\log_e$ UMI units

G) scRNAseq comparison of hPSC-derived day 3 artery ECs vs. Carnegie Stage 13 (CS13) human fetal artery ECs (Zeng et al., 2019); 6000 variable genes (*top*, each dot = 1 gene) or selected genes (*bottom*) shown

See also Figure S2 and Tables S1 and S5

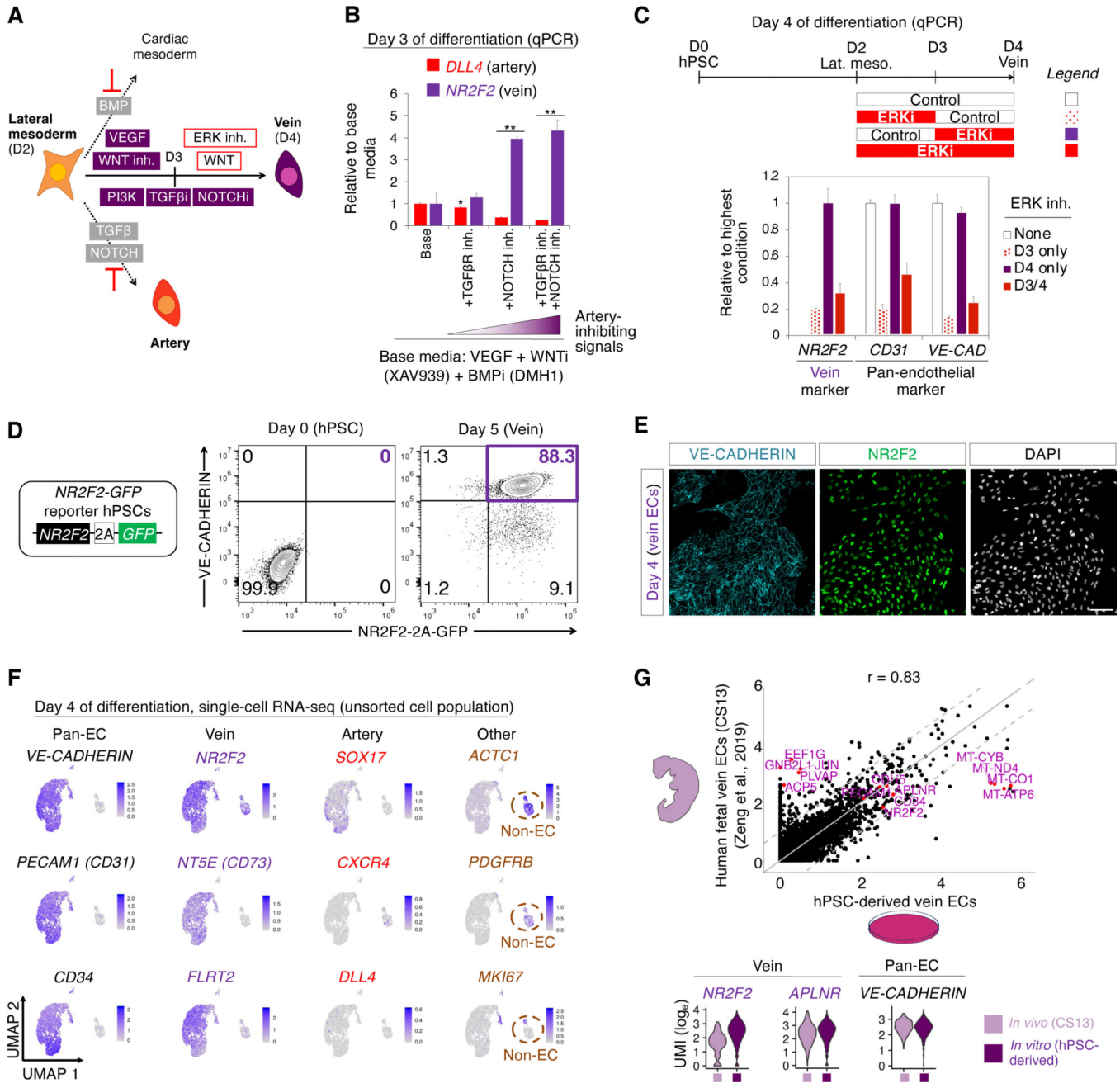

Figure 3: Efficient generation of human vein endothelial cells from hPSCs within 4 days

A) Summary of present work

B) Dually inhibiting TGFβ and NOTCH promotes day 3 vein gene expression. Day 2 hPSC-derived lateral mesoderm was further differentiated for 24 hours with the indicated signals, including TGFβ inhibitor (SB505124, 2 μM) and/or NOTCH inhibitor (RO4929097, 1 μM); qPCR performed on day 3; *P<0.05; **P<0.01

C) VEGF/ERK activation followed by inhibition is critical for vein formation. Day 2 hPSC-derived lateral mesoderm was further differentiated for 48 hours in the presence or absence

of ERK inhibitor (PD0325901, 100 nM) for the indicated durations; qPCR performed on day 4 (base media: VEGF+SB505124+RO4929097+XAV939+DMH1+AA2P for days 3–4)

D) Flow cytometry of H1 *NR2F2–2A-GFP* hPSCs before or after differentiation into day 5 vein ECs

E) NR2F2 and VE-CADHERIN immunostaining of H1 hPSC-derived day 4 vein ECs; scale = 100 μm

F) scRNAseq of H1 hPSCs differentiated towards vein ECs; the entire day 4 cell population was harvested without pre-selecting ECs; gene expression in $\log_e$ UMI units

G) scRNAseq comparison of hPSC-derived day 4 vein ECs vs. Carnegie Stage 13 (CS13) human fetal vein ECs (Zeng et al., 2019); 6000 variable genes (*top*, each dot = 1 gene) or selected genes (*bottom*) shown

See also Figure S3 and Tables S2 and S5

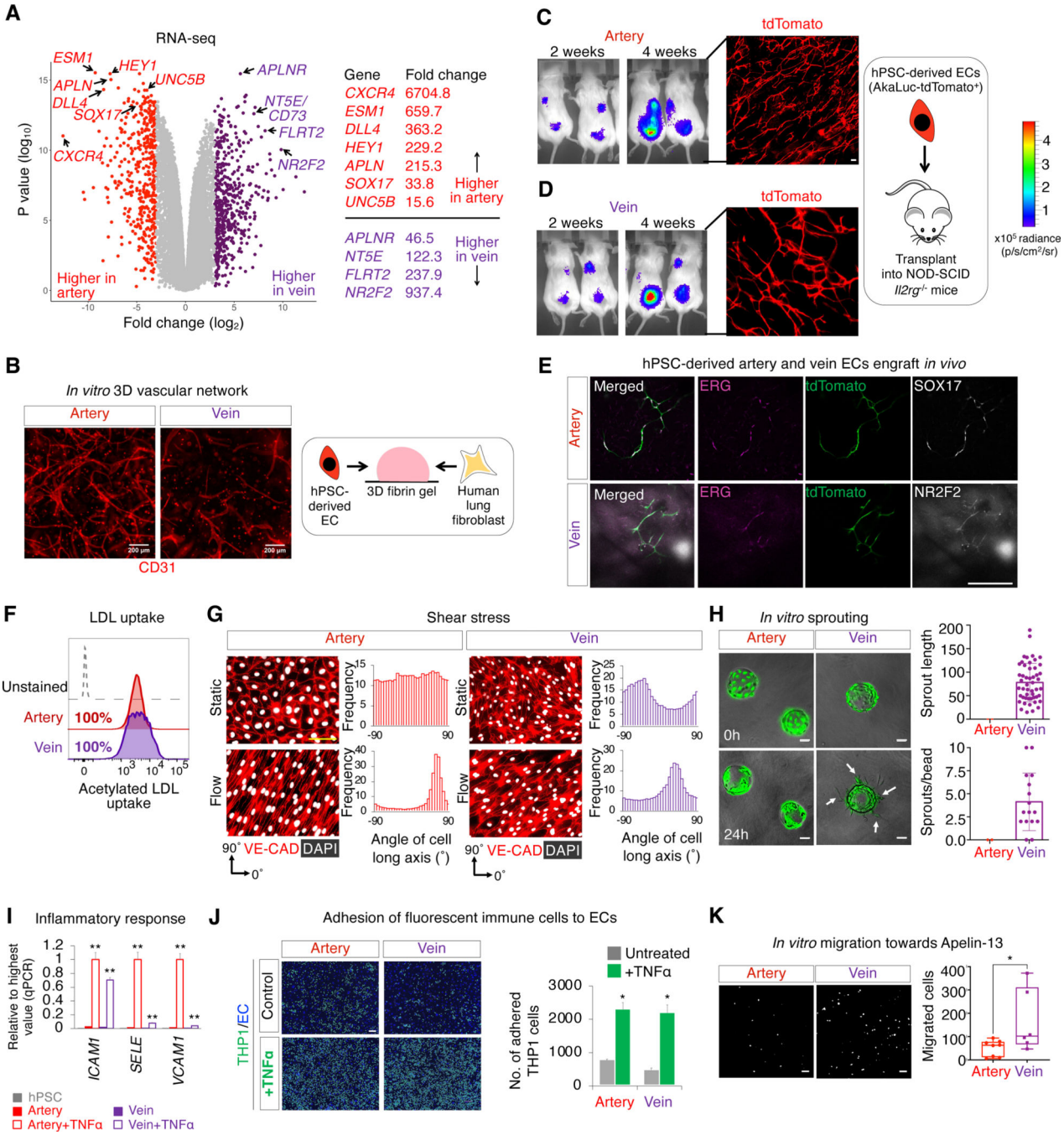

Figure 4: Transcriptional and functional differences between hPSC-derived artery and vein endothelial cells

A) Bulk-population RNA-seq of H1 hPSC-derived day 3 artery vs. day 4 vein ECs ($CD144^+$ FACS sorted), each dot = 1 gene

B) 3D vascular networks formed by H1 hPSC-derived artery and vein ECs cocultured with fibroblasts in fibrin gel for 1 week (Kurokawa et al., 2017); scale = 200 μm

C-E) Subcutaneous transplantation of *CAG-AkaLuciferase-tdTomato*$^+$ SUN003.1 hPSC-derived artery and vein ECs, monitored by intravital imaging (to assess cell proliferation) and microscopy (4 weeks post-transplant); scale = 150 μm

F) Flow cytometry of fluorescently-labelled, acetylated LDL uptake by H1 hPSC-derived artery and vein ECs within 4 hours

G) SUN004.1.9 hPSC-derived artery and vein ECs exposed to shear stress or static conditions for 24 hours align to the direction of fluid flow, quantified by the angle of the long axis of CD144$^+$ cell membranes; scale = 100 μm

H) Beads coated with *CAG-GFP*$^+$ SUN004.1.9 hPSC-derived vein ECs preferentially form vascular sprouts after embedding in 3D fibrin gel for 1 day, as opposed to artery EC-coated beads; scale = 100 μm

I) H1 hPSC-derived artery and vein ECs were expanded for 5 days, and then treated with TNFα (10 ng/mL) or left untreated for 4 hours, followed by qPCR to assess TNFα-induced upregulation of immune cell adhesion molecules; **P<0.01

J) H1 hPSC-derived artery and vein ECs were expanded for 6 days, and then were treated with TNFα (10 ng/mL) or left untreated for 4 hours, prior to addition of fluorescent THP1 cells for 30 minutes; scale = 100 μm; *P<0.05

K) In Transwell assay, *CAG-GFP*$^+$ SUN004.1.9 hPSC-derived vein ECs preferentially migrate towards Apelin-13; images of migrated cells situated on the bottom membrane surface; scale = 100 μm; *P<0.05

See also Figure S4 and Tables S3 and S5

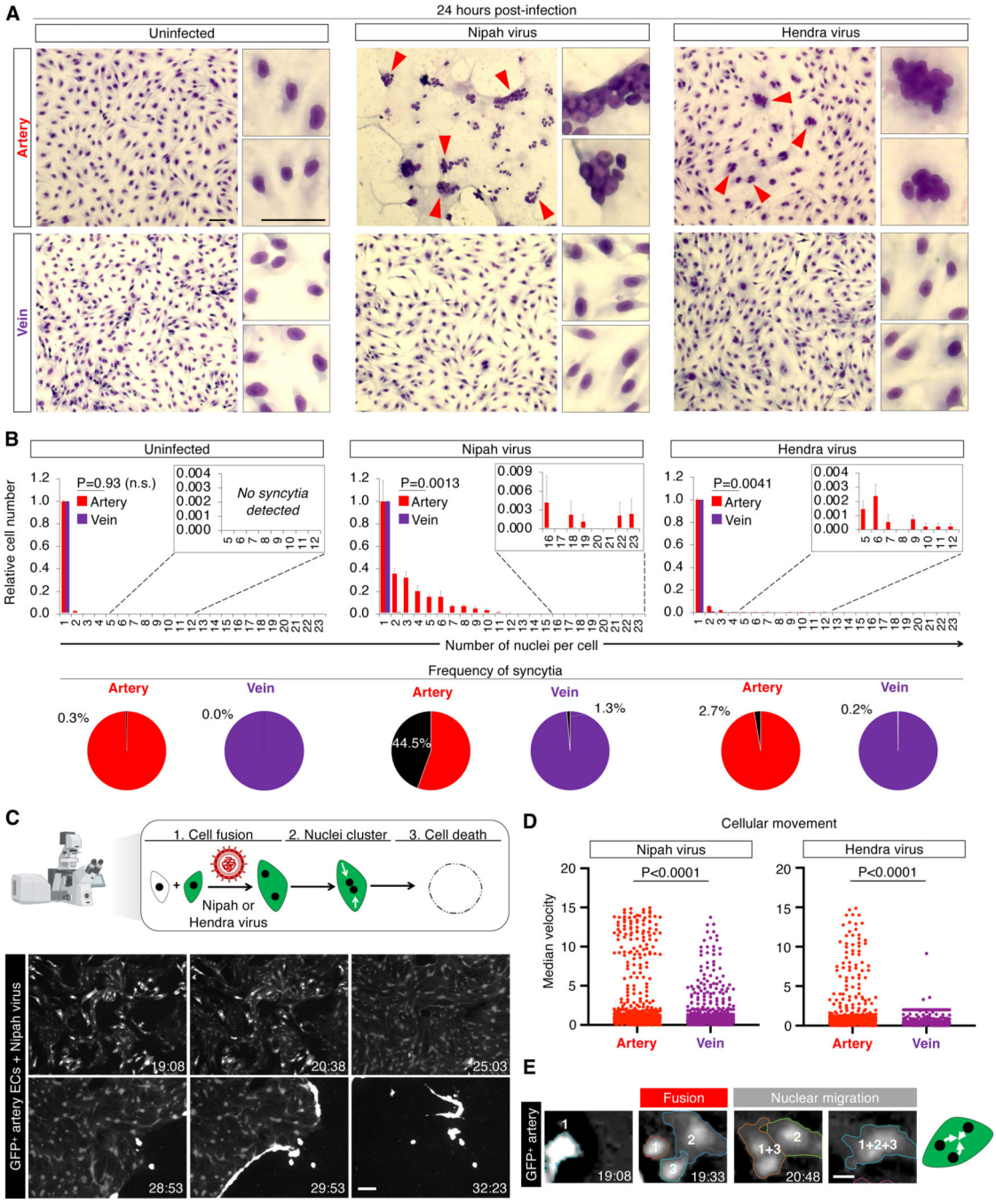

Figure 5: Nipah and Hendra viruses target artery cells

A) Syncytia (arrows) in H1 hPSC-derived artery and vein ECs inoculated with Nipah or Hendra viruses for 24 hours; scale = 25 μm

B) Numbers of nuclei per cell after inoculation with Nipah or Hendra viruses for 24 hours (*top*); syncytia frequency (≥3 nuclei/cell; *bottom*)

C) Live imaging of cocultured SUN004.1.9 GFP$^+$ and H1 wild-type artery ECs infected with Nipah virus, tracking cell fusion into GFP$^+$ syncytia, followed by death (scale = 200 μm, timestamp: hours:minutes)

D) Live imaging showed Nipah- and Hendra-infected artery ECs displayed significantly greater median velocity (a measure of cell fusion) than vein ECs

E) Fusion and GFP diffusion between 3 Nipah-infected artery ECs, followed by aggregation of their nuclei (scale bar = 20 μm, timestamp: hours:minutes)

See also Figure S5 and Movie S1

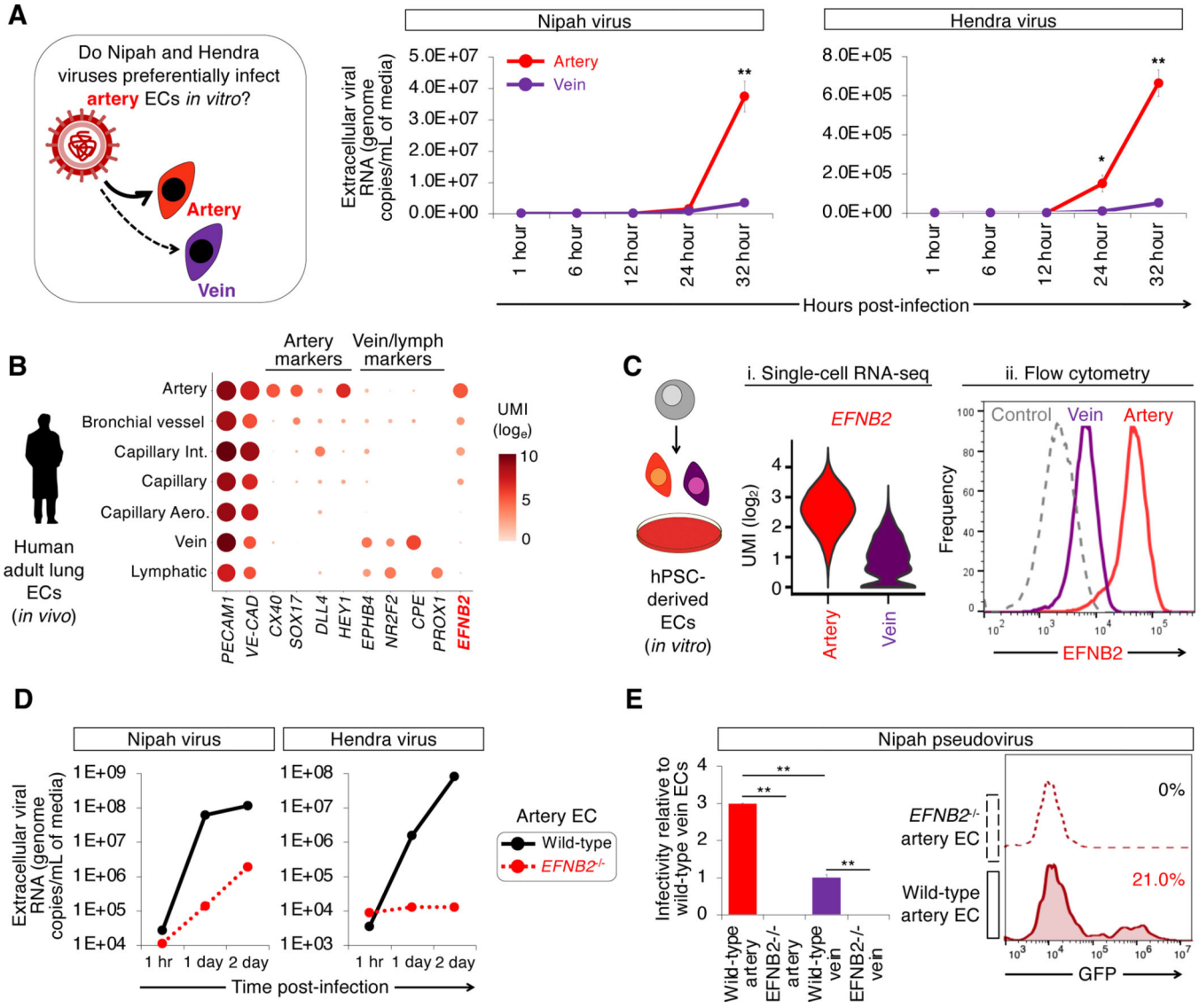

Figure 6: Artery cells express higher levels of EFNB2, the Nipah and Hendra virus receptor

A) Nipah and Hendra viral RNA replication in H1 hPSC-derived artery and vein ECs, as quantified by qPCR of culture media; *P<0.05; **P<0.01

B) scRNAseq of human adult lung ECs (Travaglini et al., 2020)

C) Higher EFNB2 levels in hPSC-derived artery ECs relative to vein ECs, as shown by *i*) scRNAseq of day 3 artery vs. day 4 vein ECs and *ii*) flow cytometry for surface EFNB2 protein expression on artery vs. vein ECs, 4 days post-expansion

D) Nipah or Hendra viral RNA replication in H1 and *EFNB2*$^{-/-}$ hPSC-derived artery and vein ECs, as assayed by qPCR of culture media

E) H1 and *EFNB2*$^{-/-}$ hPSC-derived artery and vein ECs inoculated with *GFP*-encoding Nipah pseudovirus (Palomares et al., 2013); **P<0.01

See also Figure S6 and Table S5

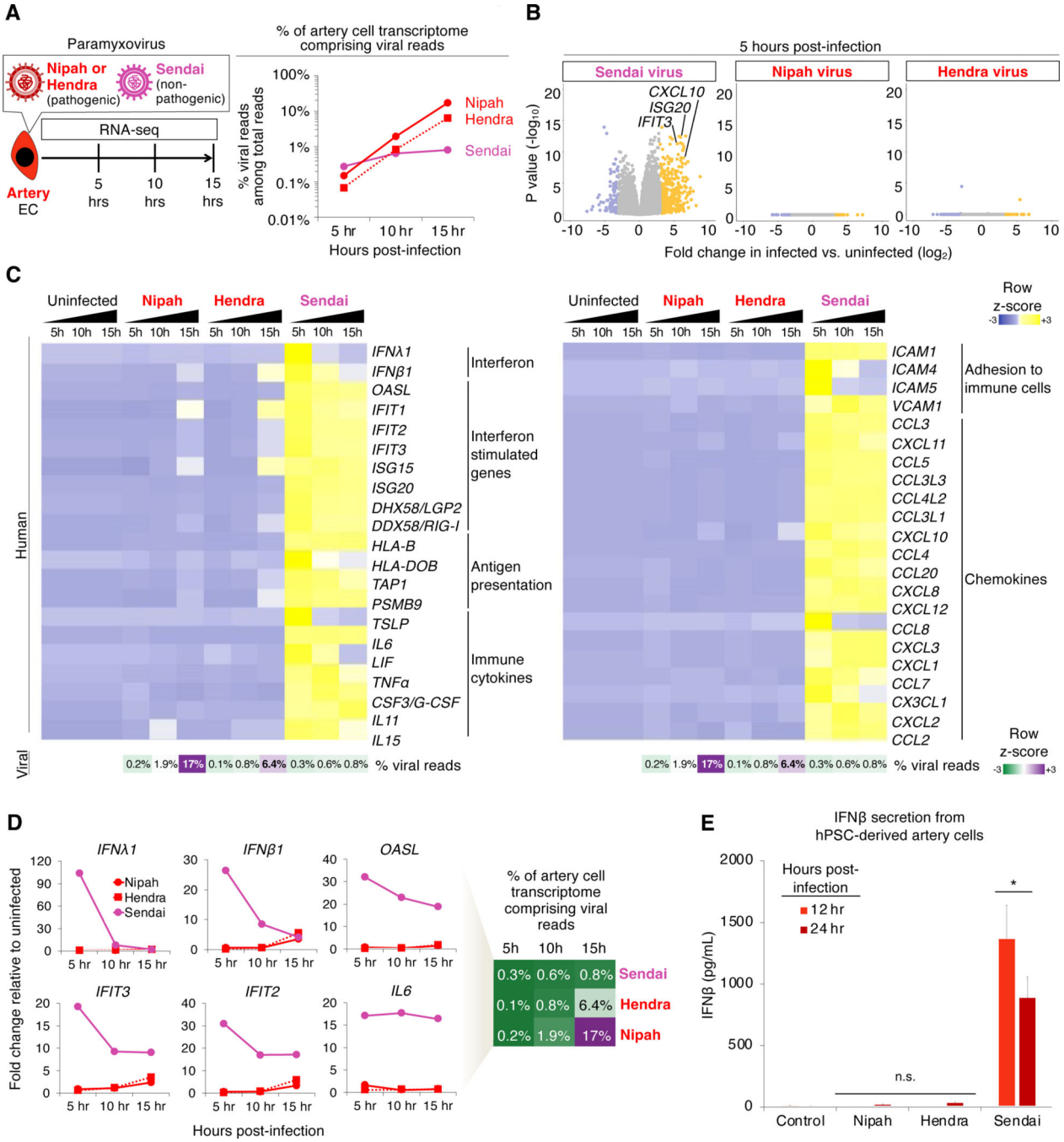

Figure 7: Nipah and Hendra viruses elicit minimal transcriptional changes in artery endothelial cells, despite extensive viral replication and cell fusion

A) Percentage of hPSC-derived artery EC transcriptome comprising viral reads, as quantified by RNA-seq; averaged from H1 and SUN004.1.9 hPSCs

B) Transcriptome-wide differences between infected vs. uninfected artery ECs by RNA-seq; averaged from H1 and SUN004.1.9 hPSCs

C,D) RNA-seq of infected hPSC-derived artery ECs, including viral read percentage in transcriptome; averaged from H1 and SUN004.1.9 hPSCs

E) IFNβ secretion by hPSC-derived artery ECs; averaged from H1, SUN004.1.9 and SUN004.2 hPSCs; *P<0.05; n.s. = not significant
See also Figure S7 and Table S4

KEY RESOURCES TABLE

Reagent or Resource	Source	Identifier
Antibodies		
anti-CD144 Alexa Fluor 647 antibody	BD	561567
anti-human CD73 (Ecto-5'-nucleotidase) PE	Biolegend	344004
anti-human Delta-like protein 4 (DLL4) APC	Biolegend	346508
Anti-NR2F2 antibody	Abcam	ab211777 (1:100)
Anti-SOX17 antibody	R&D Systems	AF-1924 (1:1000)
Anti-CD31	BD Biosciences	555444
Anti-ERG (ETS related gene)	Abcam	ab92513 (1:500)
Mouse Anti-Human CD144 (VE-Cad)	BD Bioscience	555661 (1:500)
Anti-EFNB2	R&D Systems	AF496 (1:5)
APC Donkey Anti-Goat	R&D Systems	F0108 (1:10)
Alexa Fluor 568 Donkey Anti-rabbit	Thermo Fisher Scientific	1:250
Alexa Fluor 647 Donkey Anti-mouse	Thermo Fisher Scientific	1:250
Bacterial and viral strains		
Nipah virus (Malaysia variant): Nipah virus/human/MY/1999/ CDC	Centers for Disease Control and Prevention, Viral Special Pathogens Branch	(Harcourt et al., 2000)
Hendra virus (Brisbane variant): Hendra virus/horse/AU/1994/ Hendra	Centers for Disease Control and Prevention, Viral Special Pathogens Branch	(Murray et al., 1995)
Sendai virus (Cantell strain)	ATCC	VR-907
Sendai virus (recombinant, replication-defective, encoding *KLF4/ OCT4/SOX2/MYC* and *miR-302* target site)	Dr. Mahito Nakanishi, National Institute of Advanced Industrial Science and Technology	(Nishimura et al., 2017)
NEB® Stable Competent *E. coli*	New England BioLabs	C3040H
Chemicals, peptides and recombinant proteins		
mTesR Plus medium	STEMCELL Technologies	#100–0276
Penicillin/streptomycin	Thermo Fisher Scientific	15–140-122
KnockOut Serum Replacement	Thermo Fisher Scientific	10828028
MEM Non Essential Amino Acids Solution (100X)	Thermo Fisher Scientific	11–140-050
Geltrex LDEV-Free, hESC-Qualified, Reduced Growth Factor Basement Membrane Matrix	Thermo Fisher Scientific	A1413302
Recombinant Human Vitronectin Protein, Truncated (VTN-N)	Gibco	A14700
Matrigel Matrix GFR Phenol RF	BD Biosciences	356231
Gelatin Solution	Sigma	ES-006-B
Versene solution	Thermo Fisher Scientific	15040066
Trypsin-EDTA, 0.05%	Thermo Fisher Scientific	25300054 or 25300062
Accutase - Enzyme Cell Detachment Medium	Thermo Fisher Scientific	00–4555-56
TrypLE Express Enzyme (1X)	Thermo Fisher Scientific	12604013
Fetal Bovine Serum Premium Select	Atlanta Biologicals	S11550H
2-mercaptoethanol	Gibco	21985023

Reagent or Resource	Source	Identifier
RPMI 1640 Medium, GlutaMAX	Thermo Fisher Scientific	61870036
DMEM	Sigma	D6429
DMEM/F12 + GlutaMAX	Gibco	10565042
IMDM + GlutaMAX	Thermo Fisher	31980–097
F12 + GlutaMAX	Thermo Fisher	31765–092
Polyvinyl alcohol	Sigma	P8136–250G
Chemically defined lipid concentrate	Thermo Fisher	11905–031
1-thioglycerol	Sigma	M6145–100ML
Recombinant human insulin	Sigma	11376497001
Recombinant human VEGF	R&D Systems	293-VE-0500
Recombinant human FGF2	R&D Systems	233-FB-01M
Human transferrin	Sigma	10652202001
Recombinant human BMP4	R&D Systems	314-BP-050
Penicillin/streptomycin	Thermo Fisher	15070–063
Recombinant Activin	R&D Systems	338-AC-500/CF
GDC-0941	Cellagen Technology	C4321–25
Forskolin	Tocris	1099
Thiazovivin	Tocris	3845
XAV939	Tocris	3748
Ascorbic acid-2-phosphate	Sigma	49752–10G
DMH1	Tocris	4126
SB505124	Tocris	3263
RO4929097	Cellagen Technology	C7649–10
CHIR99201	Tocris	4423
PD0325901	Tocris	4192
PIK90	Calbiochem	528117
8-bromo-cAMP	Tocris	1140
KT5720	Calbiochem	420320
GM-CSF	Peprotech	100–11
IL-3	Peprotech	200–03
IL-6	Peprotech	200–06
FLT3L	Peprotech	300–19
TPO	R&D Systems	288-TP-005/CF
SCF	Peprotech	300–07
Endothelial Cell Growth Medium 2 (EGM2)	Lonza	CC-3162
Endothelial Cell Growth Basal Medium 2 (EBM2)	Lonza	CC-3156
Fibroblast Growth Medium 2 (FGM2)	Lonza	CC-3132
Fibrinogen solution	Sigma Aldrich	F8630
Thrombin	Sigma Aldrich	T3399

Reagent or Resource	Source	Identifier
Cytodex-3 beads	Sigma Aldrich	C3275
Apelin-13	Tocris	2420
Transwell polycarbonate membrane cell culture inserts, 6.5 mm Transwell with 8.0 μm pore polycarbonate membrane insert, 24-well	Corning	3422
Lipofectamine 3000	Thermo Fisher Scientific	L3000001
Low-density lipoprotein Dylight 550	Cayman Chemical	10011125
Acetylated Alexa Fluor 488 conjugate low-density lipoprotein	Thermo Fisher Scientific	L-23380
Recombinant Human TNFα	R&D Systems	210-TA-020
FuGENE® HD Transfection Reagent	Promega	E2311
Poly-L-lysine	R&D Systems	3438–200-01
LV-MAX Lentiviral Production System	GibcoGibco	A35684
Bovine serum albumin (BSA)	Sigma	A2153
Tween-20	Sigma	P9416
10% Formalin	Sigma	F5554
Fibrinogen	Sigma-Aldrich	F8630
Thrombin	Sigma-Aldrich	T4648
Vectashield	Vector Labs	H-100
Glutamax	Gibco	35050061
STEMdiff™ APEL™	StemCell Technologies	05270
CP21R7	Selleckchem	S7954
Neurobasal medium	Thermo Fisher Scientific	21103049
B27	Thermo Fisher Scientific	17504044
N2	Thermo Fisher Scientific	17502001
StemPro-34 SFM medium	Thermo Fisher Scientific	10639011
Essential 8 media	Thermo Fisher Scientific	A1517001
SB431542	Tocris	1614
Resveratrol	R&D Systems	1418/100
L690	R&D Systems	0682/5
Poly(I:C) sodium salt	Sigma	P1530
Critical commercial assays		
Human IFNβ Quantikine QuicKit ELISA	R&D Systems	QK410
RNeasy Plus Mini Kit	Qiagen	10010049
QIAamp Viral RNA kit	Qiagen	52904
RNeasy Micro kit	Qiagen	74004
High-Capacity cDNA Reverse Transcription Kit	Applied Biosystems	4368814
AgPath-ID™ One-Step RT-PCR Kit	Thermo Fisher	4387391
SYBRGreen	Thomas Scientific	BIO-94050
10x Genomics Chromium single cell 3’ GEM reagent kit (v3)	10x Genomics	1000075
Chromium Chip B Single Cell Kit 48rxns	10x Genomics	1000073
LEGENDScreen PE-Conjugated Human Antibody Plates	Biolegend	700007

Reagent or Resource	Source	Identifier
Magnetically Activated Cell Sorting (MACS)	Miltenyi Biotec	130–046-703
MACS LS column	Miltenyi Biotech	130–042-401
Fc blocking reagent	Miltenyi Biotec	130–046-703
Triton X-100	Sigma	X100–500ML
PBS, pH 7.4	Thermo Fisher	10010049
DPBS without ions	Thermo Fisher	14190144
Diff-Quik stain	Labor+Technik	LT 001
8-well chambered coverslip for live imaging	Ibidi	80826
CellTrace CFSE Cell proliferation kit	Thermo Fisher Scientific	C34554
Molecular Probes DAPI (4',6 Diamidino 2 Phenylindole, Dihydrochloride)	Thermo Fisher Scientific	D1306
Experimental models: cell lines		
H1 hESCs	WiCell	WiCell, WA01
H7 hESCs	WiCell	WiCell, WA07
H9 hESCs	WiCell	WiCell, WA09
H1 *NR2F2–2A-GFP* knock-in reporter hESCs	This study	N/A
H1 *SOX17–2A-mPlum* knock-in reporter hESCs	This study	N/A
H9 *SOX17*-mCherry knock-in reporter hESCs	This study	(Loh et al., 2014)
SUN004.1.9 *CAG-GFP* hiPSCs	This study	N/A
SUN004.2 *CAG-tdTomato* hiPSCs	This study	N/A
SUN003.1 *CAG-AkaLuciferase-tdTomato* hiPSCs	This study	N/A
Human umbilical artery endothelial cells (HUAEC)	Sigma-Aldrich	202–05N
Human umbilical vein endothelial cells (HUVEC)	Sigma-Aldrich	200–05N
Normal human lung fibroblast cells (NHLF)	Lonza	CC-2512
THP-1 cells	ATCC	TIB-202
HEK 293T/17 cells	ATCC	CRL-11268
Vero C1008 (Vero 76, clone E6, Vero E6)	ECACC	85020206
Experimental models: organisms/strains		
Mus musculus (mouse): NOD-SCID *Il2rg*$^{-/-}$ strain	The Jackson Laboratory	005557
Oligonucleotides		
Primers	See Table S5	
Recombinant DNA		
pCAGGS-coNiV-G-HA	Shreyas Kowdle and Benhur Lee, Icahn School of Medicine at Mount Sinai	(Palomares et al., 2013)
pcDNA3.1+coNiV-F T5F-AU1	Shreyas Kowdle and Benhur Lee, Icahn School of Medicine at Mount Sinai	(Palomares et al., 2013)
pCAGGS-coHeV-G-HA	Shreyas Kowdle and Benhur Lee, Icahn School of Medicine at Mount Sinai	(Negrete et al., 2007)
pCAGGS-coHeV-F-AU1	Shreyas Kowdle and Benhur Lee, Icahn School of Medicine at Mount Sinai	(Negrete et al., 2007)
pVSV-G	Owen Witte, University of California Los Angeles	(Goldstein et al., 2011)

Reagent or Resource	Source	Identifier
pMDL	Owen Witte, University of California Los Angeles	(Goldstein et al., 2011)
pREV	Owen Witte, University of California Los Angeles	(Goldstein et al., 2011)
pRS348 *EF1A-GFP; mU6-CD34 sgRNA*	Reuben Saunders and Jonathan Weissman, Whitehead Institute/MIT	N/A
PiggyBac *CAG-GFP* donor plasmid	Austin Smith, University of Cambridge	(Takashima et al., 2014)
CMV-PBase plasmid	Austin Smith, University of Cambridge	(Takashima et al., 2014)
pCS-CAG-mScarlet lentiviral plasmid	This study	N/A
pCS-CAG-AkaLuciferase-tdTomato lentiviral plasmid	This study	N/A
Software and algorithms		
ImageJ/Fiji	(Schindelin et al., 2012)	https://imagej.net/software/fiji/
Seurat v3	(Stuart et al., 2019)	https://satijalab.org/seurat/
Ggplot2	(Wickham, 2016)	https://ggplot2.tidyverse.org/
Tidyverse	(Wickham et al., 2019)	https://www.tidyverse.org/
Dplyr	(Wickham et al., 2022)	https://dplyr.tidyverse.org/
Limma	(Ritchie et al., 2015)	https://bioconductor.org/packages/release/bioc/html/limma.ht
Voom	(Law et al., 2014)	https://rdrr.io/bioc/limma/man/voom.html
EdgeR	(Robinson et al., 2010)	http://bioconductor.org/packages/release/bioc/html/edgeR.html
RStudio	RStudio Team	https://www.rstudio.com/
Icy	(de Chaumont et al., 2012)	http://icy.bioimageanalysis.org/
Kallisto	(Bray et al., 2016)	https://pachterlab.github.io/kallisto/
Cell Ranger	10x Genomics	https://support.10xgenomics.com/single-cell-geneexpression/software/pipelines/latest/what-is-cell-ranger
DESeq2	(Love et al., 2014)	https://github.com/mikelove/DESeq2
SCTransform	(Hafemeister and Satija, 2019)	https://github.com/satijalab/sctransform
Enrichr	(Chen et al., 2013; Kuleshov et al., 2016)	https://maayanlab.cloud/Enrichr/

Reagent or Resource	Source	Identifier
FastQC	(Andrews, 2010)	http://www.bioinformatics.babraham.ac.uk/projects/fastqc/
Trim Galore	(Krueger, 2012)	http://www.bioinformatics.babraham.ac.uk/projects/trim_galore/
Trackmate v6.0.2	(Tinevez et al., 2017)	https://imagej.net/plugins/trackmate/
ShinyCell	(Ouyang et al., 2021)	https://github.com/SGDDNB/ShinyCell